MARMARA UNIVERSITY
INSTITUTE FOR GRADUATE STUDIES
IN PURE AND APPLIED SCIENCES

SMART POLYMER NANOSTRUCTURES FROM RENEWABLE RESOURCES FOR BIOMEDICAL APPLICATIONS

ELİF IŞIKÇI KOCA

Ph.D. THESIS

Department of Bioengineering

Thesis Supervisor

Prof. Dr. Dilek KAZAN

Thesis CO- Supervisor

Assist. Prof. Dr. Pınar ÇAKIR HATIR

ISTANBUL, 2020

MARMARA UNIVERSITY
INSTITUTE FOR GRADUATE STUDIES
IN PURE AND APPLIED SCIENCES

SMART POLYMER NANOSTRUCTURES FROM RENEWABLE RESOURCES FOR BIOMEDICAL APPLICATIONS

ELİF IŞIKÇI KOCA

(724214002)

Ph.D. THESIS

Department of Bioengineering

Thesis Supervisor

Prof. Dr. Dilek KAZAN

Thesis CO- Supervisor

Assist. Prof. Dr. Pınar ÇAKIR HATIR

ISTANBUL, 2020

ACKNOWLEDGEMENTS

First of all, I would like to say a very big thank you to my PhD supervisors Prof. Dr. Dilek KAZAN and Assist. Prof. Dr. Pınar ÇAKIR HATIR for all supports, encouragements, guidance in the light of their extensive knowledge in the field.

I would like to express my appreciation to Assoc. Prof. Dr. Gökhan ÇAYLI for his valuable advice and suggestions throughout the study.

I would like to thank the members of the BIOFUNLAB and Gülnihal BOZDAĞ for her supports and advices.

I want to mention my gratefulness to my dear friends for their help and support during the preparation of this study.

I would like to express my appreciation to Marmara University Bioengineering Department faculty members, Istanbul Arel University Biomedical Engineering Department faculty members and Istanbul Arel University POTKAM members for their supports.

Financial support provided by Marmara University, Scientific Research Projects Committee (BAPKO) FEN-C-DRP-170118-0011 is gratefully acknowledged.

Finally, I would like to thank my parents, I am notably thankful to my mom, dad and brother for their endless understanding and patience during my all life.

I want to thank my husband, Hüsnü KOCA, for his support, being with me all the time and giving me courage.

My endless love, my son, Umut Ali, so glad that I have you. Thank you very much for your patience and for always giving me happiness and joy.

ELİF IŞIKÇI KOCA

TABLE OF CONTENTS

ACKNOWLEDGEMENTS i
TABLE OF CONTENTS ii
ÖZET vi
ABSTRACT vii
CLAIM FOR ORIGINALITY viii
SYMBOLS ix
ABBREVIATIONS x
LIST OF FIGURES xii
LIST OF TABLES xv
1. INTRODUCTION 1
1.1. Polymers 1
1.1.1. Classifications of polymers 1
1.1.2. Polymerization methods 3
1.1.2.1. Anionic polymerization 3
1.1.2.2. Cationic polymerization 4
1.1.2.3. Free-radical polymerization 4
1.1.3. Characterization of polymers 7
1.1.3.1. Chemical characterization of polymers 8
1.1.3.2. Thermal characterization of polymers 9
1.1.3.3. Morphologic characterization of polymers 11
1.2. Functional Smart Polymers 12
1.2.1. Thermoresponsive hydrogels 12
1.2.2.1. N-isopropylacrylamide based thermoresponsive hydrogels 14
1.2.2. Functional smart polymers based on PNIPAAm 15
1.2.2.1. Hydrophilic monomers 16
1.2.2.2. Hydrophobic monomers 18
1.2.2.3. Natural materials 19
1.2.2.4. Nanomaterials 22
1.2.3. Biomedical applications of functional smart polymers 23
1.2.3.1. Drug delivery systems 23

1.2.3.2. Gene delivery....24
1.2.3.3. Tissue engineering....25
1.2.3.4. Biosensors....26
1.2.3.5. Medical devices....27
1.2.3.6. Cell therapy....28
2. MATERIAL AND METHOD....29
2.1. Materials....29
2.1.1. Laboratory equipment....29
2.1.2. Chemicals....30
2.1.3. Buffers and solutions.....31
2.1.4. Natural materials....31
2.2. Methods....31
2.2.1. Preparation of quercetin solution....31
2.2.1.1. The stability of quercetin....31
2.2.1.2. The solubility of quercetin....32
2.2.1.3. Loading capacities....32
2.2.1.4. Release behaviors....33
2.2.2. Synthesis of the hydrogels....34
2.2.2.1. Synthesis of the hydrogels using BDC as a photoinitiator....34
2.2.2.2. Synthesis of the hydrogels with varied molar ratios of NIPAM....34
2.2.2.3. Synthesis and comparison of EBAM and EGDMA based hydrogels....35
2.2.2.4. Synthesis of plant oil based hydrogels using acrylate methyl ricinoleate (AMR)....35
2.2.2.5. Synthesis of CO and BC based hydrogels....38
2.2.2.6. Synthesis of hydrogels with varied molar ratios of BC....39
2.2.3. Swelling and deswelling studies....41
2.2.4. Characterization of hydrogels....42
2.2.5. Cytotoxicity analyzes....42
3. RESULTS AND DISCUSSION....44
3.1. Synthesis of Thermoresponsive Hydrogels by Using Conventional Monomers....44
3.1.1. The stability of quercetin....44
3.1.2. The solubility of quercetin....46

3.1.3. Synthesis of Thermoresponsive Hydrogels 53
3.1.3.1. Loading capacities 54
3.1.3.2. Factors on release performances.....55
Temperature effects on release profiles.....55
pH effects on release behaviors.....56
The effects of NIPAM ratio on release performances 59
The effects of different crosslinker types on release behaviors.....61
3.1.3.3. Swelling behaviors 64
3.1.3.4. Characterization of hydrogels.....66
3.2. Synthesis of Thermoresponsive Hydrogels by Using Renewable Monomers 70
3.2.1. Characterization of renewable monomers 70
3.2.2. Synthesis and characterization of AMR based thermoresponsive hydrogels 72
3.2.2.1. Characterization of the hydrogels.....73
3.2.2.2. Release behaviors 75
3.2.2.3. Swelling performances 77
3.2.3. CO based thermoresponsive hydrogels 79
3.2.3.1. Characterization of the hydrogels.....80
Structural characterization of CO based hydrogels.....80
Thermal characterization of CO based hydrogels 83
SEM analyzes of CO based hydrogels.....84
3.2.3.2. Swelling and deswelling performances 87
3.2.4. BC and CO based thermoresponsive hydrogels 89
Evaluation of crosslinker effects on structural characteristics.....89
3.2.4.1. Characterization of the hydrogels.....91
Characterization of hydrogels with and without MBAM 93
3.2.4.2. Release behaviors 95
3.2.4.3. Swelling and deswelling performances.....97
Swelling behaviors of hydrogels with and without MBAM 100
3.2.4.4. Cytotoxicity analyzes 101
4. CONCLUSION 104
REFERENCES 107
CURRICULUM VITAE .....

ÖZET

BİYOMEDİKAL UYGULAMALAR İÇİN YENİLENEBİLİR KAYNAKLARDAN AKILLI POLİMER NANOYAPILAR

Sıcaklığa duyarlı hidrojeller, ilaç salım sistemlerinde aktif olarak rol alan polimerik yapılardır. Bu hidrojellerin sentezinde genellikle kimyasal kökenli materyaller kullanılmaktadır. Ancak ilaç salım sistemlerinin vücutta kontrollü ilaç salımı sağlayabilmesi için biyouyumlu ve biyobozunur özellikler taşıması gerekmektedir. Ekonomik sürdürülebilirlik kapsamında yenilenebilir kaynakların kullanımı büyük önem taşımaktadır. Kullanılan materyallerin çevre döngüsünde yer alabilmesi için hidrojellerin yenilenebilir kaynaklardan elde edilen materyallerden sentezlenmesi, bu tezin asıl amacını oluşturmaktadır. Sıcaklığa duyarlı hidrojellerin bakteriyel selüloz, hint yağı ve türevlerinin kullanılarak sentezlenmesi, karakterizasyonu, ilaç yükleme ve salım performanslarının değerlendirilmesi, in vitro şişme davranışlarının ve sitotoksisite testlerinin incelenmesi, bu çalışmanın temel bölümlerini oluşturmaktadır. Hidrojel sentezinde bitkisel ve mikrobiyal materyallerin kullanımı ile biyouyumluluk ve biyobozunurluk özelliklere sahip ilaç salım sistemlerinin elde edilmesi mümkün kılınmıştır. Model ilaç molekülü olarak kuersetin kullanılmıştır. Kuersetinin sulu çözeltilerde var olan çözünürlük problemlerinin çözümüne yönelik çalışmalar gerçekleştirilmiştir. Hidrojellerin ilaç salım oranları irdelenerek ilaç salımına etki eden parametreler öne çıkarılmıştır. Şişme denemeleri ile hidrojellerin dayanıklılığı irdelenirken sitotoksisite çalışmaları ile de hidrojellerin ve kullanılan bileşiklerin hücrelerle uyumu araştırılmıştır. Yenilenebilir kaynaklardan sentezlenen hidrojellerin özellikleri ile kimyasal kökenli materyallerden elde edilen hidrojellerin performansları karşılaştırıldığında elde edilen sonuçlar, yenilenebilir kaynaklı materyallerin sıcaklığa duyarlı hidrojel sentezinde aktif olarak yer alabileceğini göstermiştir. Bu çalışma, bitki ve bakteri kökenli ham maddelerin biyomedikal uygulamalar için önemini vurgulayan öncü bir çalışmadır.

Anahtar Kelimeler: Hidrojel, Sıcaklığa duyarlı hidrojel, Biyomedikal, Yenilenebilir kaynak, Akıllı polimer

İstanbul, 2020 **Elif IŞIKÇI KOCA**

ABSTRACT

SMART POLYMER NANOSTRUCTURES FROM RENEWABLE RESOURCES FOR BIOMEDICAL APPLICATIONS

Thermoresponsive hydrogels are polymeric structures that play an active role in drug delivery systems. Conventional raw materials are generally used in the synthesis of the hydrogels. They should have biocompatible and biodegradable properties to be employed in the body as controlled drug release systems. The use of renewable resources has great importance within the scope of economic sustainability. For that reason, the synthesis of the thermoresponsive hydrogels with renewable sources is the main purpose of this thesis. So, the materials used in the hydrogel synthesis can be involved in the environmental cycle.

Synthesis of temperature-sensitive hydrogels using bacterial cellulose, castor oil and derivatives, evaluation of drug loading and release performances, examination of in vitro swelling behaviors, and cytotoxicity trials are the main parts of this study. It is possible to obtain drug release systems with high biocompatibility and biodegradability characters by using plant and microbial based materials in hydrogel synthesis. Quercetin was used as a model drug molecule. The studies on the dissolution problems of quercetin were performed.

Drug release ratios of hydrogels were investigated and the parameters that affect drug release characters were highlighted. The durability of the hydrogels was examined by swelling performances. The biocompatibility of hydrogels and starting materials was investigated by cytotoxicity tests.

According to the results, novel thermoresponsive hydrogels were successfully synthesized with renewable resources. This study is a pioneering study that highlights the importance of plant and bacteria based materials for biomedical applications.

Keywords: Hydrogel, Thermoresponsive hydrogel, Biomedical, Renewable resource, Smart polymer

Istanbul, 2020 **Elif ISIKCI KOCA**

CLAIM FOR ORIGINALITY

This study includes the use of the materials from renewable resources to synthesize the hydrogels for biomedical applications. Plant and microbial based materials such as bacterial cellulose and castor oil were used to synthesize thermoresponsive hydrogels. The first part of the thesis focuses on the synthesis of novel thermoresponsive hydrogels. Castor oil and derivatives were examined to obtain thermoresponsive hydrogels. In addition, bacterial cellulose and castor oil were used together for the synthesis of thermoresponsive hydrogels. Thus, it was ensured that sustainable materials were applied in the biomedical field.

In the second part, the properties of the developed hydrogels were evaluated. Their drug loading/release capacities and swelling/deswelling properties were investigated. According to the results, their behaviors at body temperatures were tried to be predicted. Their features were compared with hydrogels based on chemical materials. Following the results, renewable materials based hydrogels showed similar loading/release performances with conventional material based ones. In addition, the effects of the types of raw materials on polymerizations were examined. Their biocompatibility was examined with cytotoxicity tests. It was observed that the materials obtained from renewable resources have higher biocompatibility. These results proved that the materials obtained from renewable resources can be used for biomedical applications. In this context, this study can be considered as the adaptation of the green chemistry field to health studies in terms of sustainability. Moreover, this study is one of the earliest studies showing that castor oil and its derivatives can be included in biomedical applications.

The combination of castor oil with bacterial cellulose is a novel study showing that biodegradable materials of different origins can function together. Experiments based on this point of view show that the combinations of different renewable resources can have successful and innovative results in the biomedical field.

Assist. Prof. Dr. Pınar ÇAKIR HATIR
Prof. Dr. Dilek KAZAN
Elif IŞIKÇI KOCA
Istanbul, 2020

SYMBOLS

°C : Celsius

H : Hour

mg : Miligram

min : Minutes

µM : Mikromolar

mM : Milimolar

M : Molar

L : Liter

T : Sıcaklık (°C)

ABBREVIATIONS

AA : Acrylic acid

ACN : Acetonitrile

AMR : Plant oil acrylate methyl ricinoleate

BC : Bacterial cellulose

BDC : Benzyl-n,n-dimethyl dithiocarbamate

CDRS : Controlled drug release systems

COS-7 : African green monkey kidney fibroblast-like cell line

DMA : Dynamic mechanical analysis

DMEM : Dulbecco's Modified Eagle Medium

IR : Infrared

DMF : Dimethylformamide

DMPA : 2,2-Dimethoxy-2-phenylacetophenone

DMSO : Dimethyl Sulfoxide

DSC : Differential scanning calorimetry

EAA : 2-ethylacrylic acid

EbAM : N,N′-Ethylenebis (acrylamide)

EGDMA : Ethylene glycol dimethacrylate

EtOH : Ethanol

FTIR : Fourier-transformed Infrared Spectroscopy

LCST : Lower critical solution temperature

MAA : Methacrylic acid

MBAM : N,N′-methylenebis (acrylamide)

MDI : 4,4’-diphenylmethane diisocyanate

MeOH : Methanol

MTT : (3-(4,5-Dimethylthiazol-2-yl)-2,5-diphenyltetrazolium bromide

NIPAM : *N*-isopropylacrylamide

NMR : Nuclear magnetic resonance spectroscopy

PBS : Phosphate buffer solution

PNIPAM : poly (*N*-isopropylacrylamide)

RA : Ricinoleic acid

RT : Room temperature

SEM : Scanning electron microscopy

TEM : Transmission electron microscopy

TGA : Thermogravimetric analysis

TMA : Thermomechanical analysis

UV-Vis : Ultraviolet and visible light

LIST OF FIGURES

Figure 1.1 Classification of polymers 3
Figure 1.2 DMPA is activated by UV light (Polymer Properties Database) 6
Figure 1.3 Thermal initiator VA 044 is activated by heat (Wilems et al., 2017) 7
Figure 1.4 Growing of EGDMA radical chains with a photoinitiator (DMPA) (Ramelow, 2010) 7
Figure 1.5 The response of a smart hydrogel to external stimulants 12
Figure 1.6 LCST behaviors of thermoresponsive hydrogels 13
Figure 1.7 Functionalization of PNIPAM hydrogels through the addition of monomers 16
Figure 1.8 Scaffold formations with thermoresponsive hydrogels 26
Figure 1.9 Basic elements of a biosensor 27
Figure 2.1 The appearances of the solutions before and after loading 33
Figure 2.2 Wet and dry BC 41
Figure 3.1 1.0 mM of quercetin solutions in different solvents 45
Figure 3.2 The solubility of quercetin in different solvents respect to time (A. Quercetin in MeOH; B. Quercetin in EtOH; C. Quercetin in DMF; D. Quercetin in DMSO; E. Quercetin in ACN) 46
Figure 3.3 The stability of quercetin in various organic solvent: buffer (50:50) (A. MeOH:Buffer; B. EtOH:Buffer; C. DMF:Buffer; D. DMSO:Buffer; E. ACN: Buffer) 48
Figure 3.4 The solubility of quercetin in various EtOH:Buffer solutions 50
Figure 3.5 The calibration curve of quercetin 50
Figure 3.6 Quercetin loading ratio (%) with various concentrations 54
Figure 3.7 Quercetin release behavior of Hydrogel_01 at RT and 37°C 56
Figure 3.8 Quercetin release profiles of Hydrogel_01 at RT and 37°C 56
Figure 3.9 Quercetin release profiles of Hydrogel_01 at various temperatures 57
Figure 3.10 Quercetin release profiles of Hydrogel_01 at pH 4 and pH 9 58
Figure 3.11 Quercetin release profiles of Hydrogel_01 at pH 4 and pH 7.4 59
Figure 3.12 Quercetin release profiles of H-N1, H-N3, and H-N10 at RT 60
Figure 3.13 Quercetin release profiles of H-N1, H-N3, and H-N10 at 37°C 60
Figure 3.14 Quercetin loading ratio (%) of EbAM and EGDMA based hydrogels 62
Figure 3.15 Quercetin release profiles of EGDMA and EbAM based hydrogels 63

Figure 3.16 Swelling performances of EGDMA and EbAM based hydrogels 65
Figure 3.17 FTIR bands of EbAM and EGDMA based hydrogels (A. 1% EbAM and EGDMA; 10% EbAM and EGDMA; 25% EbAM and EGDMA)..... 68
Figure 3.18 FTIR bands of hydrogels based on two different crosslinker groups (A. EGDMA based hydrogels; B. EbAM based hydrogels)..... 69
Figure 3.19 FTIR spectra of starting materials; CO (A), BC (B), MDI (C), and NIPAM (D)..... 71
Figure 3.20 Thermoresponsive behavior of AMR0.01..... 73
Figure 3.21 FTIR bands of AMR based hydrogels based 74
Figure 3.22 Release profiles of AMR based hydrogels at RT..... 75
Figure 3.23 Release profiles of AMR based hydrogels at 37 °C..... 76
Figure 3.24 Release profiles of AMR0.25 and 25% EGDMA..... 77
Figure 3.25 A. The swelling procedure, swelling behavior of the AMR0.01 in water (t=0), B. Swelling behavior of the hydrogel in the water at t=10 min (left) and t=24 hours (right)..... 78
Figure 3.26 The swelling data of AMR based hydrogels..... 79
Figure 3.27 FTIR spectra of CO based thermoresponsive hydrogels (A. H-COT and H-WCO; B. H-NCOT and H-NCO)..... 82
Figure 3.28 DSC curves of H-WCOT and H-NCOT 83
Figure 3.29 TGA curves of CO based hydrogels A. H-WCOT; B. H-NCOT..... 85
Figure 3.30 SEM images of H-WCOT (A, B) and H-NCOT (C, D)..... 86
Figure 3.31 The swelling ratio of H-WCOT and H-NCOT..... 87
Figure 3.32 Deswelling performances of hydrogels H-WCOT and H-NCOT..... 88
Figure 3.33 Physical appearances of H-BC1, H-BC2, and H-BC3 before and after introducing NIPAM..... 90
Figure 3.34 Physical appearances of H-NC and H-WC 91
Figure 3.35 FTIR spectra of BC based hydrogels 92
Figure 3.36 FTIR spectra of hydrogels of H-BC1/H-BC1N (A), H-BC2/H-BC2N (B), and H-BC3/H-BC3N (C)..... 94
Figure 3.37 FTIR spectra of hydrogels with and without crosslinker..... 95
Figure 3.38 Release ratio (%) of BC based hydrogels at RT..... 96
Figure 3.39 Release values (%) of BC based hydrogels at 37°C 96

Figure 3.40 Swelling (at RT) and deswelling (at 40°C) performances of BC based hydrogels 97
Figure 3.41 Swelling (at RT) performances of BC based hydrogels over time 98
Figure 3.42 Swelling (at RT) data of BC based hydrogels over time..... 99
Figure 3.43 Deswelling (at 40°C) ratio of BC based hydrogels vs time 100
Figure 3.44 Swelling (at 40°C) data of BC based hydrogels over time 101
Figure 3.45 Cell viability values of the monomers (A) and thermoresponsive hydrogels (B) 103

LIST OF TABLES

Table 1.1 Transition temperatures of conventional polymers (Qureshi et al., 2019) 14
Table 2.1 Laboratory equipment and suppliers..... 29
Table 2.2 Chemicals and Suppliers..... 30
Table 2.3 Buffers used in the study 31
Table 2.4 Natural materials and suppliers..... 31
Table 2.5 Reagents used in the synthesis of BDC based hydrogels 34
Table 2.6 Reagents used for the synthesis of the hydrogels with varied molar ratios of NIPAM 35
Table 2.7 Synthesis of EGDMA and EbAM based hydrogels in H_2O 36
Table 2.8 Synthesis of AMR based and EGDMA based hydrogels 37
Table 2.9 Reagents used for CO based hydrogels 39
Table 2.10 Reagents used in the synthesis of BC based hydrogels 40
Table 2.11 Hydrogels with/without MBAM..... 41
Table 3.1 The pH values of quercetin in various aqueous solvents..... 49
Table 3.2 Three different hydrogels with the varied molar ratio of NIPAM..... 59
Table 3.3 FTIR spectra of the EbAM and EGDMA based hydrogels..... 67
Table 3.4 FTIR spectra of the starting materials used for the synthesis..... 70
Table 3.5 AMR based thermoresponsive hydrogels..... 73
Table 3.6 FTIR spectra of the AMR based hydrogels 74
Table 3.7 The code of CO based hydrogels..... 80
Table 3.8 FTIR spectra of the CO based hydrogels..... 81
Table 3.9 Thermal features of H-WCOT and H-NCOT 84
Table 3.10 BC ratio of hydrogels..... 89
Table 3.11 Hydrogels with and without MBAM..... 90

1. INTRODUCTION

1.1. Polymers

Greek roots *poly* (many) and *meros* (part) create the term "polymer". A polymer is a macromolecule, which has from hundreds to millions of monomers. Numerous small molecules, called monomers**,** come together to form polymer chains. The complete polymer chain is usually produced by the repetition of identical small molecules, called repeating units. The structure of repeating units depends on the type of monomer, which takes place in the formation of the polymer (Fakirov, 2017). Some polymers consist of a few repeating units, called oligomers, and they are often produced as a product of polymer syntheses (Braun et al., 2005).

If a polymer has only one type of monomer, it is called a homopolymer. If there is more than one type of monomer in the polymer structure, this macromolecule is called a copolymer. A copolymer has a minimum of several hundred covalently linked atoms. Its molar mass is clearly above 10^3 g/mol. Studies generally focus on high-molecular-weight molecules that have long linear chains and high molar masses. Two essential terms are usually used to define the characteristics of the copolymers. They are the degree of polymerization, *P*, and the molecular weight, *M*. *P*, indicates how many monomer units are linked in the polymer chain while *M* is the measure of the sum of the atomic weight values of the atoms in a molecule (Fakirov, 2017; Braun et al., 2005).

1.1.1. Classifications of polymers

There are various ways for the classification of polymers. As seen in **Figure 1.1**, polymers can be categorized according to their origins as *natural*, *modified natural*, and *synthetic*. Natural polymers are generally found in plants and animals. Starch, cellulose, DNA, RNA, proteins, and polysaccharides are the members of this group. They also play a crucial role in the life cycle. The modified natural ones are altered by chemical ways of natural polymers. Cellulose nitrate, cellulose derivatives may be given as an example to this group. Generally, these polymers have commercial importance. Synthetic polymers are created/synthesized by researchers in a lab. They are typically produced for human necessities by industries. Plastics, polyethylene, and nylon may be given as examples for synthetic polymers. Besides, polymers can also be classified into

three different groups, *organic, organometallic, or hybrid, inorganic polymers*, based on their chemical compositions. The organic ones have a carbon backbone, while backbones of inorganic polymers are constituted by elements other than carbon. Organometallic polymers include both organic and metallic compounds. They have a metal-containing moiety in the polymer chain. Moreover, polymers can be classified according to their structures of the monomer chains; *linear, branched, crosslinked* (**Figure 1.1**). The monomers are joined together linearly in a linear form while branched polymers branches originating at random points from a linear chain. Monomers joined together to have various branches in different lengths. These polymers cannot closely be packed together due to the branches. Their low density having low melting points is a result of their branched structures. In crosslinked polymers, they have strong covalent bonds to have bi or trifunctional structures in nature. Interconnections between chains in 3D, a network polymer structure, can be provided by crosslinked bonds.

In addition to these classified groups, polymers can be categorized according to their thermal response properties, *thermoplastic* and *thermosetting polymers*. Thermoplastic polymers are known as thermosoftening plastics that can be softened and melted by the application of heat and solidified again as they are cooled. Generally, intermolecular forces such as Van der Waals forces play an important role. Polyolefin, nylons, and linear polyesters are examples of this class. Thermosetting polymers act irreversibly according to temperature changes. A three-dimensional structure is formed by the application of heat. It becomes rigid when heated. Resins, urea, diene rubbers, and phenolic belong to thermosetting polymers (Wang et al., 2018).

Besides these classifications (**Figure 1.1**), polymers can be divided into two groups depending on their usages, such as *structural polymers* and *functional polymers* (Braun et al., 2005). Structural polymers are used as construction materials and also have excellent mechanical, thermal, and chemical properties. Therefore they can be used as construction materials for metals and ceramics. Moreover, they can be employed in wood applications such as fibers, plastics, elastomers. Fibers, films, elastomers, foams, and adhesives can be given as an example for metals, ceramics, or wood applications (Braun et al., 2005).

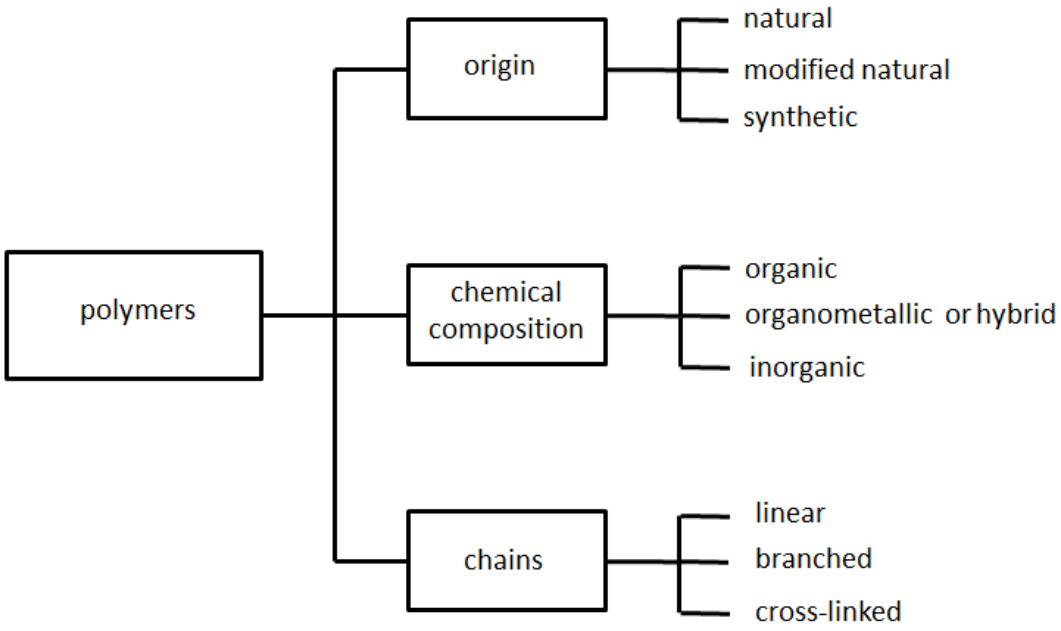

Figure 1.1 Classification of polymers

Functional polymers are also members of polymers and have some unique properties, for example, special electrical, optical, or biological properties. This difference in macromolecules is responsible for the presence of chemical functional groups in their structures and their differences from the main skeletal structure. If there is one reactive group in an organic compound, one linkage in the intended reaction occurs. If there are more than one reactive group, bi-, tri-, or oligo-functional are named for two, three, or more groups, respectively. They are employed in devices for microelectronic, biomedical applications, analytics, hygiene, synthesis, and cosmetics areas by their specific chemical or physical functions (Braun et al., 2005; Schulz et al., 1998).

1.1.2. Polymerization methods

1.1.2.1. Anionic polymerization

Anionic polymerization is a form of chain-growth polymerization. It includes anionic initiator transfers. The formation of an anion radical, named carbanion, can be occurred by transferring an electron from a donor molecule to the vinyl monomer. The electron donors (or initiators) contain alkali metals, while covalent or ionic metal amides, alkoxides, hydroxides, amines, phosphines, cyanides, and organometallic compounds are

membres of strong nucleophilic initiators. Initiation, polymerization, and termination are the main steps of the kinetics of anionic polymerization. Anionic polymerization is one of the most controlled methods for the direct introduction of functionality. This polymerization can proceed without any chain transfer and termination and applied for both chain-end (telechelic) and in-chain functional polymers (Schulz et al., 1998).

1.1.2.2. Cationic polymerization

Cationic polymerization is a type of chain-growth polymerization. It contains cationic initiator transfers that charge to a monomer, and then it becomes reactive. After that, it goes on to react similarly with other monomers to form a polymer. Monomers, including isobutylene, styrene, alpha-methyl styrene, butadiene, and vinyl alkyl ethers have abilities for enhancing the electron-sharing ability of the double bond of the vinyl monomers. Constant reaction condition cannot be maintained for cationic polymerization; therefore, it proceeds at high rates both at high and (very) low temperatures. For the synthesis of various polymers such as polyisobutylene (PIB), polybutene (low molecular weight copolymers of isobutylene (IB) and other butenes, mostly 1-butene), butyl rubber (a copolymer of IB with isoprene), polystyrene-block-polyisobutylene-block-polystyrene (SIBS), poly(vinyl ether)s (PVEs), etc., cationic polymerization is preferred (Roy et al., 2016).

Cationic polymerization was believed to be insufficient on the synthesis of well-defined functional polymers due to inter- or intra-molecular transfer or rearrangement. However, control of initiation, propagation, and termination to allow the synthesis of functional polymers has been provided in recent years when several monomers have been applied. Some physical properties such as low molecular weights, less toxicity, and low melt viscosities give great opportunities to both telechelic and macromonomers for converting them to chain extended polymers, networks, graft copolymers, and blocks, etc. (Schulz et al., 1998).

1.1.2.3. Free-radical polymerization

Free-radical polymerization is a polymerization method that requires polymer formation by the successive addition of free radical building blocks. Free radical polymerization is widely used for the most synthetic polymers. This method can be defined as one of the

most important ones from a commercial point of view. The technique is rapid and can be realized by thermal, catalytical, or photochemical decomposition of initiators. Cleavage of covalent bonds homolytically is the reason for production of initiators in free radical polymerizations. The formation of free radicals can be affected by the presence of weak covalent bonds or high-energy forces. Free-radical polymerization requires three main steps as initiation, propagation, and termination (Carraher et al., 2003).

Initiation: This is known as the first step and involves the formation of radicals followed by a radical reaction. Free radical initiation can realize by application of heat, light, ionization, redox reagents, electricity, etc., these processes create essential free radicals.

Initiation by radiation: The decomposition of the initiator is caused by light or another source of radiation. UV and visible light can affect the bonds forming free radicals. Electrons can be added or removed based on certain conditions where molecules are exposed to higher frequency light. In addition, higher energy and shorter wavelength are the conditions for electron transfers (Carraher et al., 2003). Polymerization at room temperature is one of the the advantages of photochemical initiations. **Figure 1.2** shows the photoinitiation of 2,2-Dimethoxy-2-phenylacetophenone (DMPA).

Thermal initiation: In this process, the decomposition of the initiator is caused by the application of heat. One of the critical points in these reactions is to know the decomposition temperature of the initiators. Generally, bond decomposition energies are between 100-170 kJ/mol, and compounds containing O-O, S-S, and N-O bonds have the appropriate bond decomposition energy. Various types of peroxy compounds are the most used ones (Pabuccuoğlu, S). **Figure 1.3** shows the thermal initiation of a thermal initiator.

Propagation: This step requires the addition of monomers to grow polymer chains. It is a repetitive process in which the physical chain of the polymer is formed. Since the monomer is reacted to the reactive polymer chain, the double bond of successive monomers is opened, and it is a rapid and continuously step. The example for this step can be seen in **Figure 1.4** that simulated with ethylene glycol dimethacrylate (EGDMA) and DMPA (Ramelow et al., 2010).

Termination: This step is related to the deactivation of the growing active polymer chain, usually by combination or coupling of the radicals of two growing polymer chains or by

disproportionation. It continues until all monomers are consumed. The termination of growing polymer chains mostly depends on the mechanism of the chain transfer to the initiator (Braun, 2009).

Free-radical polymerization has some disadvantages, such as broad polydispersity, which is an indication of its quality concerning the size distribution. Besides, control of end groups and chain architecture can be achieved poorly by free radical polymerization. The reason for this is the polymerization process being highly affected by termination or chain transfer. The branching of the growing polymer can be affected by termination or chain transfer mechanisms. Terminal reactions between the growing radical species can be suppressed by decreasing the instantaneous concentration of the activated form when the rapid and reversible interchange equilibrium (Danaei et al., 2018; Schulz et al., 1998).

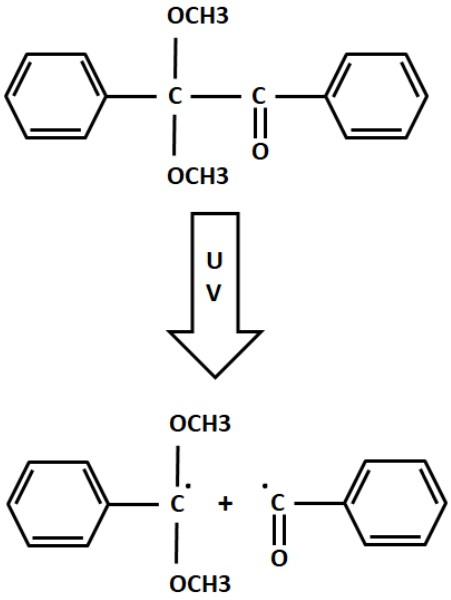

Figure 1.2 DMPA is activated by UV light (Polymer Properties Database)

Free-radical polymerization technique has cost advantages. Besides, it is easy and can be readily performed in bulk or suspension form. When it is compared with other polymerization methods, free radical polymerization can tolerate numerous reactive functional groups, unlike others that cannot incorporate a wide range of functional groups. Therefore well-defined polymers with low polydispersity can be obtained by free-radical polymerization (Schulz et al., 1998).

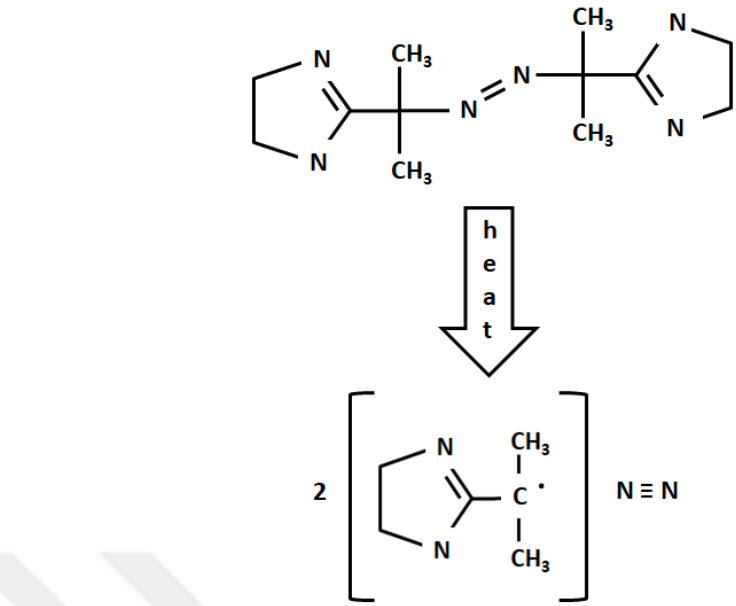

Figure 1.3 Thermal initiator VA 044 is activated by heat (Wilems et al., 2017)

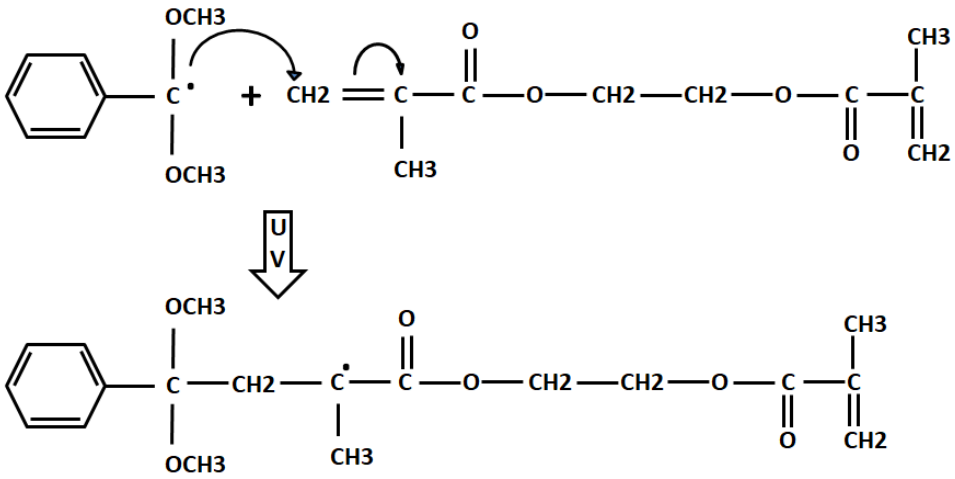

Figure 1.4 Growing of EGDMA radical chains with a photoinitiator (DMPA) (Ramelow, 2010)

1.1.3. Characterization of polymers

Characterization of polymers is a complicated process because of high intermolecular forces, obtained unavailable of structurally and molecularly uniform forms. Some elemental analyses, such as solubility, viscosity, molecular weight distribution, and

degree of crystallinity, must be determined for characterization. Besides, small variations in the molecular structures can affect the properties of polymers.

1.1.3.1. Chemical characterization of polymers

Infrared Spectroscopy

The infrared (IR) range includes the range of wavelengths closest to the red end of the visible light spectrum and extents this region to the microwave region at the lower frequencies. This energy region is corresponding to molecular interactions that involve vibrational modes. Polymer structures can be identified by infrared spectroscopy that is one of the conventional spectroscopic techniques. If the frequency of the radiation of a particular vibration is the same as the frequency of a particular molecular vibration, the radiation is absorbed by the molecule. The structure of molecules, the symmetry of the skeleton of molecules, and its electron distribution affect the intensity of interaction between IR radiation and molecules. The dipole moment of the molecules changes during vibration motion that affects the IR radiation.

Many IR instruments are rapid scan with Fourier-transformed (FTIR). IR spectroscopy can be used for identification of many monomers and polymers by evaluating molecular vibrations. This technique is very sensitive. Thus, it can allow analyses for structural features such as chain constitutions, functional and end groups, and copolymer compositions of molecules. Besides, it is a useful method to determine the crystallinity of solid polymer structures and components and compositions of modified polymeric structures. Despite the advantages of this technique, it is important to prepare the samples very carefully and homogeneously (Braun et al., 2005; Carraher et al., 2003).

Ultraviolet Spectroscopy

Similar to the IR spectroscopy method, ultraviolet/ visible light (UV-Vis) spectroscopy is one of the crucial methods for the characterization of polymers. From 185 nm to 760 nm wavelengths related to unpolarized light is used in standard spectroscopic analyses with UV-Vis spectroscopy (Braun et al., 2005). This method is not widely used, such as IR spectroscopy. Still, it is preferred to detect aromatics like polystyrene and appropriate additives as antioxidants that give characteristic absorption in the UV region (Carraher et al., 2003).

Nuclear Magnetic Resonance Spectroscopy

Nuclear magnetic resonance spectroscopy (NMR) is a powerful tool to identify the structures of polymers correlated with steric configuration and give detailed information about chain conformation, association, aggregation, and supramolecular self-organization behavior of macromolecular structures. The basis of NMR depends on transitions between energy states related to certain isotopes. These isotopes have two or more energy states, and these states are available if a magnetic field is applied. The nuclei activated magnetically have a property named *spin*, and these nuclei have magnetic moment as a consequence this spin and angular momentum. This technique is sensitive to nuclei with a nuclear spin different from zero. The magnetic field can be used to align the NMR-active nuclei or it can be aligned against the field, low energy state, and high-energy state. Usually, the lower energy state has more nuclei than the higher energy state at RT, but when magnetic energy is applied, some nuclei that have lower energy state, move to the high-energy state due to energy absorption. This reactions can be detected as NMR spectra. The strength of the external magnet is a factor that can affect the difference between the two energy states. The use of the instruments that have larger magnetic fields is better to obtain spectra (Braun et al., 2005; Carraher et al., 2003).

1.1.3.2. Thermal characterization of polymers

Thermogravimetric analysis

Thermogravimetric analysis (TGA) can be used in various applications such as environmental, food, pharmaceutical, and petrochemical areas. TGA depends on the monitorization of the mass of a substance as a function of temperature or time. The basis of TGA relies on decompositions of various components of the sample while the sample is being heated. Common sample size changes between 0.1 mg to 10 g, and the range of heating rates are from 0.1 to 50°C/min. Changes in the physical and chemical properties of materials can be monitored with TGA. The measurements are realized with constant heating rates (as a function of increasing temperature) or constant temperature and/or constant mass loss (as a function of time). Physical phenomena of materials are measured, such as vaporization, desorption, purity, sublimation, absorption, and reaction rate, identification, activation energy, solvent retention, and heat of reaction by TGA

results. Also, TGA supplies information about the chemical phenomena of materials such as solid-gas reactions (oxidation or reduction), chemisorption, dehydration, and decomposition. TGA is commonly preferred for studies of degradation mechanisms and reaction kinetics, determination of organic and inorganic contents of samples (Carraher et al., 2003; Pa'e et al., 2018).

Differential scanning calorimetry

Differential scanning calorimetry (DSC) analyzes thermal transitions of polymer materials. The samples are heated or cooled under an inert atmosphere. The results of DSC can supply information about melting, glass transition, crystallization, the specific heat capacity of samples. The measurement is a function of time or temperature in DSC for the temperature differences between the sample and a reference. Besides, this technique is related to the difference in the amount of heat required to increase the temperature that involves endothermic or exothermic processes. The measurement processes are relatively easy due to easy sample preparation. It can be applied for a wide range of temperature and its analysis time is short. Besides that, it can be applied for both liquid and solid samples and also shows excellent quantitative capability (Braun et al., 2005; Pa'e et al., 2018).

Thermomechanical analysis

Thermomechanical analysis (TMA) is correlated with measurements of the mechanical responses of the polymers. These reponses are expressed as a function of temperature. Information about thermal expansion and the thermal shrinkage can be obtained by TMA. Besides, TMA provides infromations about the glass transition and curing reaction. Penetration or expansion modes of this technique can supply information for the measurement of dimensional changes, even in thin films and coatings. Composition, structure, production conditions of materials that include hydrogels can be obtained by TMA analyses. Probe selection for TMA measurements should be made according to the purpose. Probes can be categorized into three groups: expansion/compression probe that is responsible for measurement of the deformation by the thermal expansion and the transition of the sample under the compressed force is applied; penetration probe that is related to softening temperature; tension probe that can supply information about thermal expansion and the thermal shrinkage of the sample such as the film and the fiber

(Carraher et al., 2003; Pa'e et al., 2018).

Dynamic Mechanical Analysis

Dynamic Mechanical Analysis (DMA) can measure the modulus (stiffness) and damping (energy dissipation) of materials when deformed under periodic stress. The basis of this technique depends on the monitoring of material modulus at different applied frequencies, thus provides simultaneous control. This method provides to analyze the natural-based hydrogels that are under effects of time, frequency, and temperature. Glass transition, softening and viscosity can be measured by DMA. Besides, this method can be used for obtaining degree of cure, and stress relaxation (Pa'e et al., 2018).

1.1.3.3. Morphologic characterization of polymers

Scanning electron microscopy

Scanning electron microscopy (SEM), is one of the conventional methods to investigate the surface of samples. This principle of SEM depends on the scanning of reflected electron beam or collecting of a back-scattered electron beams, displaying them by cathode-ray with tube screen. The behaviors of electrons give information about materials, some electrons may be reflected without any energy losses, and sometimes electrons can be absorbed and give rise to secondary electrons of deficient energy or absorbed and give rise to the emission of visible light. All of these actions produce images of materials. Besides, the contrast in the images is a factor in determining the sample morphology. The critical point for SEM of polymers, samples must be coated with a conductive material because the surface must be conductive for SEM (Braun et al., 2005; Carraher et al., 2003).

Transmission electron microscopy

Transmission electron microscopy (TEM), is one of the popular methods for surface characterization. An electron beam passes through the samples to determine the internal microstructures of the samples in this technique. The contrast in the images about structures that occurred by several concentrations of different elements can be observed at the atomic level. This method is very sensitive toward the internal structure of samples such as shape, size, etc. and also crystallinity properties and compositions (Braun et al., 2005; Carraher et al., 2003).

1.2. Functional Smart Polymers

Smart polymers can respond to external stimuli by changing their structures and properties in response to external chemical and physical stimuli in a controlled and reproducible manner. These materials are also known as “intelligent” materials and named as “stimuli-responsive” polymers. Smart polymers can be categorized according to their stimulants, such as temperature, pH, ionic strength, light, electric, magnetic field-sensitive, humidity, and redox reactions (Liu et al., 2017). Researchers have focused significantly on the synthesis and applicability of stimuli-responsive polymers over the past few decades. These smart advanced materials can be employed for several fields, especially biomedical and environmental areas (Huang, et al., 2019; Ward et al., 2011).

Figure 1.5 shows the behaviors of smart hydrogels under environmental effects. The smart hydrogel is defined as the polymer network able to respond to external stimuli. For instance, if the hydrogel has thermoresponsive properties, it will be unswollen form at high temperatures.

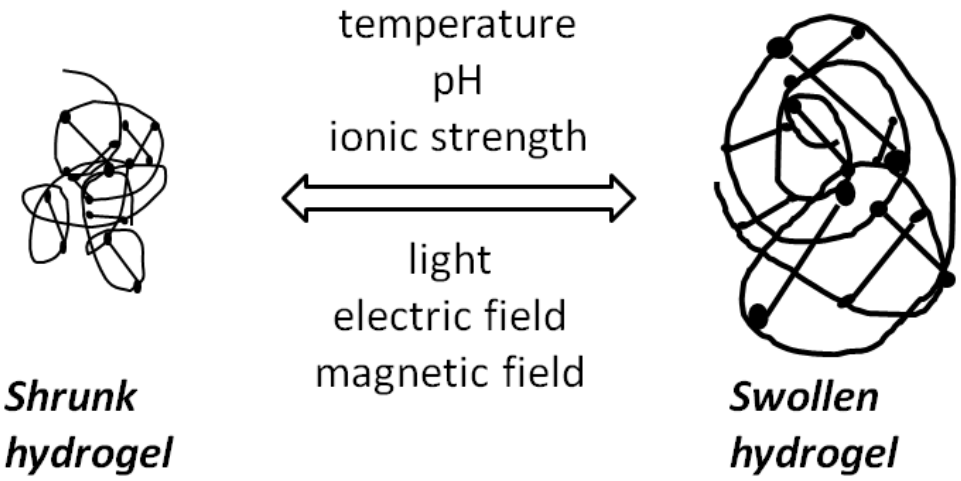

Figure 1.5. The response of a smart hydrogel to external stimulants

1.2.1. Thermoresponsive hydrogels

Hydrogels are known as three-dimensional polymeric networks and have hydrophilic characters; therefore they can absorb a considerable amount of water in their structures.

Hydrogels can give a rapid and strong response to external stimuli. Thanks to their high elasticity and strength characteristics, they can be used for several applications. If the hydrogels are sensitive to temperature changes, it is defined as thermoresponsive hydrogels (Klouda, 2015; Liu et al., 2017). Nowadays, researchers focus on thermoresponsive hydrogels for biomedical applications due to their conformational changes that can be triggered by ambient and physiological temperatures.

Thermoresponsive hydrogels are the most widely employed smart polymers. The term "lower critical solution temperature (LCST)" is crucial for thermoresponsive hydrogels (**Table 1.1**). If the temperature is below the LCST, the appearance of the hydrogel solution is transparent, but if the temperature increases, the appearance is opaque. The reason for this action is that phase separation is energetically more favorable, and the principles of their behaviors depend on Gibbs equation $\Delta G = \Delta H - T\Delta S$ (G: Gibbs free energy, H: enthalpy and S: entropy). The entropy of water is the main driving force. That when the polymer is not in solution, the water is less ordered and has higher entropy. This is also called the "hydrophobic effect". Besides that, when the temperature below LCST, the hydrogen bonds predominate between the hydrogel amide groups and the water molecules. If the temperature increases, hydrogen bonds will be broken, and as a result of this (**Figure 1.6**), the hydrogel removes water molecules and dehydrates (Almeida et al., 2012; Vihola et al., 2005; Ward et al., 2011). **Figure 1.6** shows the behaviors of thermoresponsive hydrogels while the temperature is under and above the LCST.

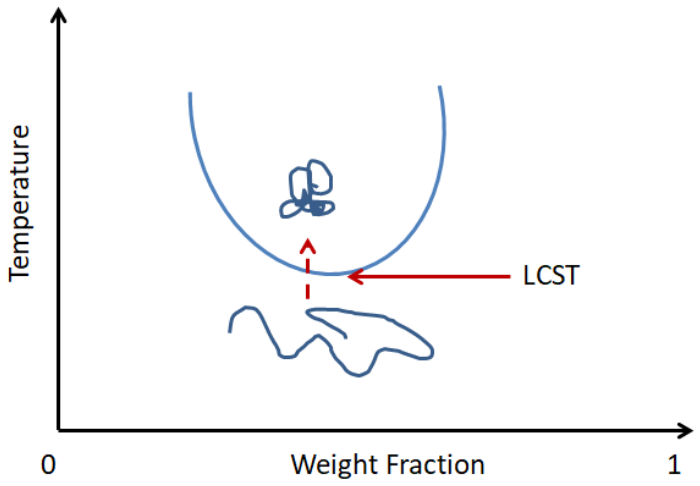

Figure 1.6 LCST behaviors of thermoresponsive hydrogels

Table 1.1 Transition temperatures of conventional polymers (Qureshi et al., 2019)

Name of the polymer	Transition temperature
Poly(N-isopropyl acrylamide) (PNIPAM)	32–34°C
Poly(N,N-diethyl acrylamide) (PDEAM)	25–32°C
Poly(methylvinylether) (PMVE)	37°C
Poly(N-vinylcaprolactam) (PNVCL)	32–34°C
Poly(N-cyclopropylacrylamide)	58°C
Poly(N-ethylacrylamide)	74°C
Poly(oligo ethylene glycol methacrylate) (POEGMA)	26–90°C
Elastin-like peptides	0–100°C (depending upon the composition)

1.2.2.1. *N*-isopropyl acrylamide based thermoresponsive hydrogels

N-isopropyl acrylamide (NIPAM) based thermoresponsive hydrogels are known as poly (*N*-isopropyl acrylamide) (PNIPAM). PNIPAM is the most common one because its LCST value is 32°C (Liu et al., 2017) that is a crucial temperature that is close to the body temperature (37°C) for biomedical applications. The determination of the LCST value is related to the hydrogen bond between the functional units of the PNIPAM hydrogel and water molecules. PNIPAM is from the family of poly (*N*-substituted acrylamide) is a synthetic temperature-sensitive polymer. As a different feature, it is soluble in water at room temperature, because of this feature; PNIPAM is most studied and most used for biomedical applications such as drug delivery systems and biomaterials (Almeida et al., 2012).

PNIPAM also has some attractive properties; this hydrogel allows the addition of comonomers or nanoparticles, so, the functionality of the hydrogel can be designed or modified. Besides, the synthesis of copolymers and nanocomposites is relatively easier than chemical methods. The incorporation of co-functionality can affect the LCST value of the hydrogels, and this helps to obtain a material with the desired properties for the purpose. Through to the multifunctional features of PNIPAM, its usage in the biomedical field is very common. For instance, controlled drug release systems

(CDRS), tissue engineering, self-healing materials, etc. are examples in biomedical applications (Frazar et al., 2019).

In literature, there are many studies concerning thermoresponsive hydrogels. For instance, Cao and coworkers studied mixed thermoreversible gels to fabricate a thermosensitive hydrogel by using PNIPAM to fibrillary nanostructures self-assembled from a short peptide I3K (Cao et al., 2019). Similar to this one, three-dimensional thermoresponsive P(NIPAM-co-BA) hydrogels synthesized with free radical polymerization reported by Park and coworkers. They used NIPAM, butyl acrylate, and N,N′-methylenebis (acrylamide) (MBAM) as the monomer, comonomers, and crosslinking agent, respectively. According to their results, the crosslinked P(NIPAM-co-BA) hydrogels have a huge potential as smart materials for biomedical issues (Park et al., 2019). Qureshi's team also reported CDRS applications with thermoresponsive hydrogels and LCST values of different monomers (Qureshi et al., 2019). Biocompatibility and biodegradability properties of 3D polymeric network structures of hydrogels were investigated in Onaciu's study. They analyzed the controlled release profiles of these hydrogels (Onaciu et al., 2019). Poly(N-vinyl caprolactam) based thermoresponsive hydrogels were developed as microgels by Etchenausia and coworkers, and the drug delivery carrier potential of these hydrogels was investigated (Etchenausia et al., 2019). A similar study was performed by Isikver. They worked on NIPAM, methacrylic acid, and MBAM based thermoresponsive hydrogels and investigated their thermal behaviors and swelling characters (Isikver et al., 2019). Poly(N-vinylcaprolactam)-grafted-aminated alginate was used to develop thermosensitive polymers by Durkut and coworkers; they analyzed the materials for in vitro cytotoxicity and hemocompatibility (Durkut et al., 2019).

1.2.2. Functional smart polymers based on PNIPAM

Most of the thermoresponsive hydrogels were prepared mostly with PNIPAM and copolymers. In clinical applications, some limits occur for poor biodegradability of PNIPAM hydrogel. For solving these biodegradability problems, several strategies were developed, like introducing biodegradable monomers, crosslinkers, or natural polymers or nanomaterials. Besides the biodegradability problems, polymeric materials have to be supported by chemical modification and functionalization to enhance their

characteristics like stability and mechanical/chemical properties. Therefore researches focus on the synthesis of new monomers and the (co-) polymerization of monomers (Kim et al., 2017). Comonomers are divided into two main groups as *hydrophilic* and *hydrophobic* comonomers, which can affect the LCST value of hydrogels. Frazar and coworkers reported that hydrophilic comonomers can shift the LCST to a higher temperature while hydrophobic ones shift the value to down (Frazar et al., 2019).

One of the leading features of NIPAM is that it allows different groups to integrate its structure, as shown in **Figure 1.7**. Incorporation of co-functionality by introducing different monomers can change the LCST value of the polymer so that new materials can be developed depending on the desired application (Lanzalaco et al., 2017).

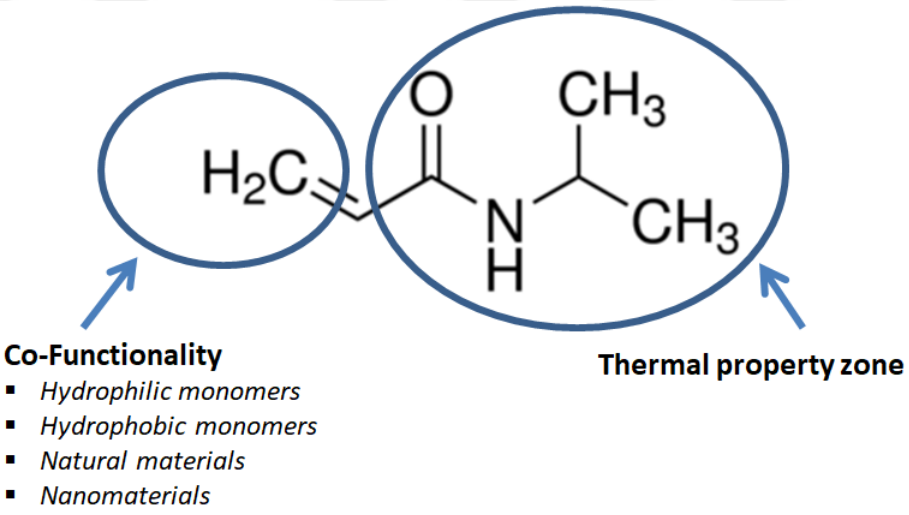

Figure 1.7. Functionalization of PNIPAM hydrogels through the addition of monomers

1.2.2.1. Hydrophilic monomers

Hydrophilic monomers can increase the LCST to a higher temperature. PNIPAM copolymers, including hydrophilic and ionic monomers, are generally developed as multi responsive systems. They are pH and thermoresponsive systems so that they can be employed in drug delivery applications. (Frazar et al., 2019).

Fundueanu and coworkers reported that they synthesized an appealing pH/thermo-responsive copolymer by using Poly(*N*-isopropyl acrylamide-co-maleic acid) (poly(NIPAAm-co-MAc). In their study, both carboxylic groups of MAc in copolymer

were ionized form while physiological conditions were at pH = 7.4 and T = 36°C in phosphate buffer solution (PBS). In these conditions, copolymer had more hydrophilic properties, so that the copolymer lost its thermosensitive property. However, if the carboxylate groups of the polymer are protonated or interacted ionically by positively-charged compounds with hydrophobic character, the polymer can have back thermosensitive properties at physiological conditions. In line with these explanations, the researchers observed that the polymers swell at physiological conditions. After, it was also observed that when ionic interactions with hydrophobic compounds occurred, the polymers shrink (Fundueanu et al., 2017).

Another temperature and pH-responsive based copolymers were studied by Li and coworkers. They improved temperature and pH-responsive poly(*N*-isopropyl acrylamide-co-N,N-dimethyl acrylamide-b-lactide) and poly(*N*-isopropyl acrylamide-co-N,N-dimethyl acrylamide-b-e-caprolactone) diblock copolymers for focusing on high temperature and low pH of tumor tissue. They investigated the structural properties and characterizations that were realized by NMR, TEM. Also, in vitro cytotoxicity assays were tested, cellular uptake and drug release behaviors were examined (Li et al., 2011). Liu and coworkers studied on thermoresponsive hydrogels due to their structural and mechanical properties. They synthesized a semi-interpenetrating copolymer networks based poly (N-isopropyl acrylamide-co-hydroxyethyl methacrylate) p(NIPAM-HEMA) chains. FTIR, NMR, SEM, DSC were used for characterization in their study. Besides that, the equilibrium swelling ratio and dynamic deswelling were investigated. They indicate that their copolymer system can be a useful platform for regenerative medicine and tissue engineering (Liu et al., 2017).

In 2016, Zhang's team reported that an injectable and self-healable hydrogel was synthesized. Glycol chitosan and a dibenzaldehyde terminated copolymer poly(N-isopropyl acrylamide)-co-poly(acrylic acid) were the compositions of the hydrogel. Besides, the hydrogel also has dual pH and temperature-responsive characters like Li's works (Li et al., 2011). They examined drug loading and release behaviors. This team observed that the developed hydrogel systems could successfully be applied for 3D cell cultivation of L929 cells (Zhang et al., 2016).

1.2.2.2. Hydrophobic monomers

Hydrophobic monomers can decrease the LCST to lower temperatures. PNIPAM-based polymers are very suitable for separation processes because polymers that have hydrophobic comonomers have lower LCST value near ambient temperature to reduce energy input for the transition. (Tang et al., 2017). Azobenzene-containing methacrylate is one of the hydrophobic monomers. Feng synthesized a novel amphiphilic diblock copolymer that had dual responsiveness to heat and light. Diblock copolymer contained a hydrophilic poly (ethylene oxide) block and a hydrophobic block. Temperature affected the sizes of micelles and encapsulated substances in hydrophobic regions. The release process was also influenced by temperature changes. In this study, it was reported that a reversible change to respond to light provided by the hydrophobicity of the micellar cores (Feng et al., 2010).

Similar to Fundueanu's study (Fundueanu et al., 2017), pH and temperature-sensitive copolymers obtained by Lu and coworkers. They synthesized a series of homo- and copolymers through 2-alkyl acrylic acids such as acrylic acid (AA), methacrylic acid (MAA), or 2-ethyl acrylic acid (EAA) to increase hydrophobicity. Swelling behaviors and pH responsiveness were investigated. According to their results, molecular/cellular adhesion can be controlled, and the systems can be used for biomedical applications (Lu et al., 2013).

Wang and coworkers focused on the lack of identified binding sites for drugs and the limits on the degradation of PNIPAM for CDRS. The poly (Maleic anhydride-β-cyclodextrin-co-NIPAAm) hydrogels based on maleic anhydride-β-cyclodextrin, one of the hydrophobic comonomers, were synthesized against the limits on the degradation of PNIPAM. These hydrogels also have a dual response to pH and temperature. The swelling/deswelling behaviors and drug loading/release properties were analyzed. Furthermore, researchers reported that these hydrogels have biodegradability in the presence of α-amylase so that these hydrogel systems can be used as an effective oral drug system (Wang et al., 2018).

1.2.2.3. Natural materials

Studies about renewable, sustainable, and greener materials are attracting increased interest instead of petroleum-based materials (Garcia-Valdez et al., 2018). They have biocompatible and biodegradable properties and generally low cost due to renewability. In this context, the utilization of PNIPAM for CDRS and tissue engineering applications gain importance because of their biocompatibility and potential biodegradability. Additionally, the viscoelastic behavior of PNIPAM polymers gives advantages to interactions with living tissues. Mechanical properties of PNIPAM can be improved with sustainable and naturally occurring materials such as cellulose, alginates, chitosan, cellulose, starches, and dextran. They have biocompatible and nontoxic properties. Additionally, they are suitable for biomedical applications, environmental applications like sorbent development for water treatment, and remediation (Bawa et al., 2009; Petrusic et al., 2013).

Plant-derived cellulose is one of the renewable materials. However, it requires complicated and unhealthy chemical processes to obtain it from a plant under mild conditions, as lignin and hemicellulose like plant-derived cellulose branches. Bacterial cellulose (BC) production has gained importance in recent years due to these poor conditions. Muhlethalerin described the BC microfibrils firstly in 1949 and also observed that plant-derived cellulose are about 100 times bigger than these fibrils. Well-arranged three-dimensional nanofibers are formed by the fibrous network of BC, and also β-D glucopyranose units. Surface area of BC was large and BC has a porous hydrogel structure due to this arrangement (Esa et al., 2014). A high degree of polymerization and crystallization, high purity and biological adaptation are some of the fundamental properties of BC (Lin et al., 2014). Besides these available features, it also has the capacity for a chemical modification that is especially important for biomedical applications. Moreover, high water retention capacity is one of the important characteristics of BC. It is believed that BC is one of the ideal material for hydrogel synthesis due to its flexibility, elasticity, (Czaja et al., 2007; Akoğlu et al., 2010) and biodegradability (Kucinska-Lipka et al., 2015).

Vegetable oils (VOs) are the triglycerides of fatty acids and often known as renewable raw materials that can be used for polymer synthesis. VOs have many features that can

be useful in biomedical applications such as low toxicity, biodegradable properties. Besides that, they have multi structural characteristics that provide them superiority in their use (Das et al., 2017). Their low cost gives them the chance to be used instead of petroleum-based compounds. Easily hydrolyzable bonds can be obtained by chemical modifications of fatty acids (Kunduru et al., 2015). After polyol functionalization, they can be used as monomers for polymerization reactions. They can be divided into two groups as saturated and unsaturated depending on the presence of double bonds in their structures. Unsaturated fatty acids have at least one double bond, such as oleic/linoleic/ricinoleic acid, while saturated ones do not have any double bonds like stearic/palmitic. Forming of bio-based polyols, especially unsaturated ones, are more suitable due to different reactions that can be carried out with their bonds (Anastas et al., 2010; Das et al., 2017).

Castor oil (CO) is known as a member of the non-volatile (VOs) and also belonges to the Euphorbiaceae family. It can be used in the synthesis of different biodegradable polymers. Ricinoleic acid (RA-12-hydroxy-cis-9-octadecenoic acid) has a hydroxyl contained fatty acid. These acid groups have chain lengths that include 18 and 20 carbon atoms. Additionally, CO is known as a glycerol triester of RA, and its ratio in CO is approximately 90%. This feature distinguishes it from other vegetable oils and gives it superiority for polymer synthesis. As a result of these, flexible structures can be obtained with CO/RA-based hydrophobic polymers. CO has low toxicity so it is known as an excellent renewable agricultural resource. Furthermore, since ancient days, its medicinal value has been known (Kunduru et al., 2015; Salmiah et al., 2015). Modification processes do not require the synthesis of polyols with CO, because CO is only commercially available natural VO; it has natural hydroxyl groups and can be obtained directly from plants. The chemical modification is necessary for other materials in VOs groups to have polyols (Das et al., 2017).

In this thesis, acrylated methyl ricinoleate (AMR) was used to synthesize new hydrogels. AMR is one of the plant-based monomers. It can be used as a renewable material for biomedical applications to developed a green approach to the synthesis of thermoresponsive hydrogels. It is obtained from CO. Methyl ricinoleate and boric acid are used to obtain AMR. A detailed synthesis method was described by Cakir Hatir and coworkers (Cakir Hatir et al., 2019).

BC and CO are known as commonly used renewable materials for biomedical applications. In this thesis, experiments were realized with CO and BC to synthesize of thermoresponsive hydrogels. In the literature, a number of studies have been reported on the synthesis of hydrogels from renewable materials and their use in biomedical applications. For instance, PNIPAM brushes were grafted by wet BC sheets in Alosmanov's study (Alosmanov et al., 2017). They observed that the swelling and drying behaviors of BC were affected by PNIPAM with wet BC. Similarly, Wang's team reported that BC was modified by 4,4'-diphenylmethane diisocyanate (MDI). In their study, the impacts of the molar ratio of MDI and glucose unit of BC was examined, and also the new composite form was evaluated if it had any property for use in artificial muscles (Wang et al., 2018).

Some studies include more than one type of natural materials, for example, Arikibe and coworkers studied on chitosan combined BC. BC/Chitosan-based hydrogels were investigated about performances related swelling profiles and drug release behaviors under pH effects (Arikibe, et al., 2019). Similar to Arikibe's study, Li and coworkers studied on chitosan and BC-based scaffold for cartilage tissue engineering applications (Li et al., 2017). In another study reported by Basu et al. (2019), BC was filled with calcium phosphate. Then this material was used to have hydrogel based scaffolds, so swelling and rheological properties were investigated (Basu et al., 2019). This study was very crucial for biomedical areas such as bone tissue engineering and bone tissue regeneration applications.

Similar to BC-based studies, CO-based studies are also very attractive for researchers. In this context, we can analyze the Salmiah's studies focused on designing of CO-based polyurethane polymer electrolytes (Salmiah et al., 2015). CO can also be used with other natural/synthetic materials. For instance, Uscátegui et al. (2019) reported that they improved polyurethanes by using polyols derived from CO and their thermal and mechanical characters were tested. Moreover, they introduced and added polycaprolactonediol and chitosan to their CO-based system. As a result of that, they had biocompatible polymers and investigated them for biomedical devices. Besides that, CO can also be employed in tissue enginerring applications such as wound dressing (Uscátegui et al., 2019). Another study focused on obtaining CO/citric acid-based

biocompatible polymers (Hernandez et al., 2019). Tan's team reported that they obtained bio-polyurethane by using glycerol and CO whereas Mark's team expressed bio-polyurethane as siliconized epoxy-terminated (Mathew et al., 2018; Tan et al., 2017). Besides that, there are some studies about CO and new CO-based polyurethane forms to be employed for biomedical applications that were reported by Alquichire and coworkers (Alquichire et al., 2018).

1.2.2.4. Nanomaterials

Composite materials have synergistic interactions occurred by interactions with inorganic or carbon nanomaterials and thermoresponsive polymers. As a result of this, structures are more complex and robust than individual pieces. Usage of PNIPAM polymers and nanomaterial systems are very popular, especially for biomedical and environmental applications. The use of polymeric systems individually involves some disadvantages due to the insufficiency in their structure. For instance, simple polymers do not have very complex structures. Thus their mechanical and biological properties are not sufficient for tissue engineering applications. Hydrophilic and hydrophobic interactions can provide durability to polymers for maintaining medical applications. By adding nanoparticles to polymeric systems, the structure is strengthened, and different properties are gained. In this way, the disadvantages resulting from individual use are eliminated (Frazar et al., 2019; Zhao et al., 2015).

Currently, one of the fastest-growing areas in science is *nanotechnology (*Botterhuis, 2008). Nanostructures are known generally as nanoparticles whose sizes can change between 1-100 nm. There are different chemical or biological methods for the synthesis of nanoparticles. Because of their small size, high surface area, and efficiency, nanostructures are preferred for many biomedical applications, especially for controlled drug release and targeting drug delivery systems (Hasan, 2015). Nanostructures designed from polymers have many advantages such as biocompatibility, biodegradable nature, and suitable surface, mechanical and physical structures. Additionally, polymer nanostructures may have micro and nanopore sizes so that they can be modified easily with different functional groups for better-controlled drug release. Polymers can have ionic, covalent bonds, and hydrogen interactions depending on their structures. All of these interactions and bonds play an essential role in designing nanostructures. For

example, hydrogen interactions between the urea groups can be used for having nanofiber structures. The nanofibers provide reversible crosslinks to the polymer. These interactions are also responsible for the thermoplastic and elastomeric behavior of polymers (Botterhuis, 2008).

One of the medical applications of nanotechnology is nanomedicine, for example, CDRS and tissue engineering applications (Goldberg et al., 2007). Polymers are attractive materials for these applications due to their biocompatible, biodegradable, mechanical, chemical, and surface properties; besides, their sizes can be modified for purposes of usage. It can be achieved by functionalization with the interaction of the functional group for successful CDRS (Botterhuis, 2008).

For instance, when *gold nanoparticles* are integrated into structures of thermoresponsive polymers, optoelectrical and external stimuli-responsive properties can be gained. Furthermore, it was reported by Frazar and coworkers that gold nanoparticles have biocompatible properties (Frazar et al., 2019; Luo et al., 2016).

Carbon nanomaterials such as carbon nanotubes and graphene oxide are other groups that can be used with hydrogels. For instance, it was reported that in recent studies, graphene oxide was used in hydrogel systems due to its flexible architecture and electrochemical properties (Wang et al., 2015).

Iron oxide nanoparticles are other groups that have the features of being applied in many areas, such as biomedical applications, catalysis, and environmental fields (Gutierrez et al., 2017).

1.2.3. Biomedical applications of functional smart polymers

1.2.3.1. Drug delivery systems

Drug delivery is a method of administering the drug molecule to achieve a therapeutic effect in humans or animals. The right region, the right time, and the right concentration are essential parameters for drug delivery. Low solubility, environmental or enzymatic degradation of drugs can affect the success of drug delivery. Moreover, a fast clearance rate from the body is a critical factor for drug delivery. Besides, their inability to cross the biological barriers can also affect the success of drug release. They had non-specific

toxicity (Ward et al., 2011). The ideal drug delivery should respond to metabolic states and physiological variations of the body. Notably, effective drug delivery systems rely on drug distribution on a specific target and temporal drug modulation according to physiological needs.

Functional smart polymers are very suitable structures for drug delivery thanks to their sensitivity to external stimulants. They can exhibit an active response to small signals from environments and change their microstructures according to stimuli following the principles of effective drug delivery systems (Almeida et al., 2012). Smart polymers are active materials for drug delivery systems due to their responses to the stimulus are reversible. When the external factors disappear, smart polymers behave according to initial conditions. Thermoresponsive hydrogels are one of the most studied polymers in drug delivery systems. Especially, the LCST value is the most beneficial issue in drug delivery systems. When the temperature is below LCST, the hydrogels swell, and the drug molecules can be loaded or mixed with materials that have thermoresponsive properties. Then it can be injectable to the human body. At this time, the temperature will increase above the LCST (human body temperature is approximately 37°C), the hydrogels will give a response to increased temperature and shrink. As a result of this behavior, the release of the drug molecule is achieved. This kind of pharmaceutical system can provide controlled delivery of the drugs. These CDRS are very important for chemotherapeutic agents in solid tumors. Local stimulation can be provided by the application of heat, ultrasounds, and light to tumor cells (Almeida et al., 2012; Sponchioni et al., 2019).

1.2.3.2. Gene delivery

Gene delivery is related to the treatment of many genetic diseases caused by defective genes. The principles of this method base on regulating, repairing, or replacing the defective genes with a therapeutic gene (DNA). DNA is one of the hydrophilic molecules and also negatively charged. So that it is not feasible for transferring it to cell and nucleus from the membrane, because of these reasons, gene delivery carriers must be developed. In this context, polymers based carriers also have been studied because they are cheaper and easier than for production. For having a useful polymeric carrier, some steps are essential, like complexation of DNA and polymer, the addition of

DNA/polymer complex onto cells during transfection, successful removing complex from cells, and incubation time until obtaining of results. Thermoresponsive hydrogels also can be preferred for the successful carrying of DNAs, because they can enhance the transfection when the temperature changes during the complexation and the incubation or transfection period (Pattanashetti et al., 2017; Ward et al., 2011).

1.2.3.3. Tissue engineering

Tissue engineering is a multidisciplinary area that aims to repair or regenerate biological damaged, diseased tissue, or organs. The topics of tissue engineering include improving tissue functions. The basic principles depend on the usage of a biocompatible scaffold that has the 3D structure for giving mechanical, physical, chemical, support, and provides nutrients and growth factors for growing the cells. Scaffolds are known as porous solid biomaterials, and their assignments are promoting cell-biomaterial interactions, cell adhesion, and extracellular matrix deposition, and also they can biodegrade at a controllable rate, and besides, it has to have a minimum *in vivo* toxicity (Pattanashetti et al., 2017).

Thermoresponsive polymers are very favorite ones for tissue engineering applications thanks to their abilities to regulate the behaviors of the cells. They can be used as a suitable material for repeated cell culture due to attachment and detachment functions of the cells from a surface. Another application that includes thermoresponsive hydrogels is the production of the encapsulated cells in 3D structures as they are in the body. The thermoresponsive hydrogels are mixed with cells at RT then injected to the body. In the body, temperature increases to 37°C. Thus, the mixture will form a physical gel. As a result, the cells are encapsulated by the gel that have 3D structure (Pattanashetti et al., 2017; Ward et al., 2011).

Figure 1.8 shows the behaviors of the thermoresponsive hydrogels in tissue engineering applications. If the temperature is lower than LCST, the hydrogel has a swollen form. If the temperature increases, the hydrogel shrinks to encapsulate the cells.

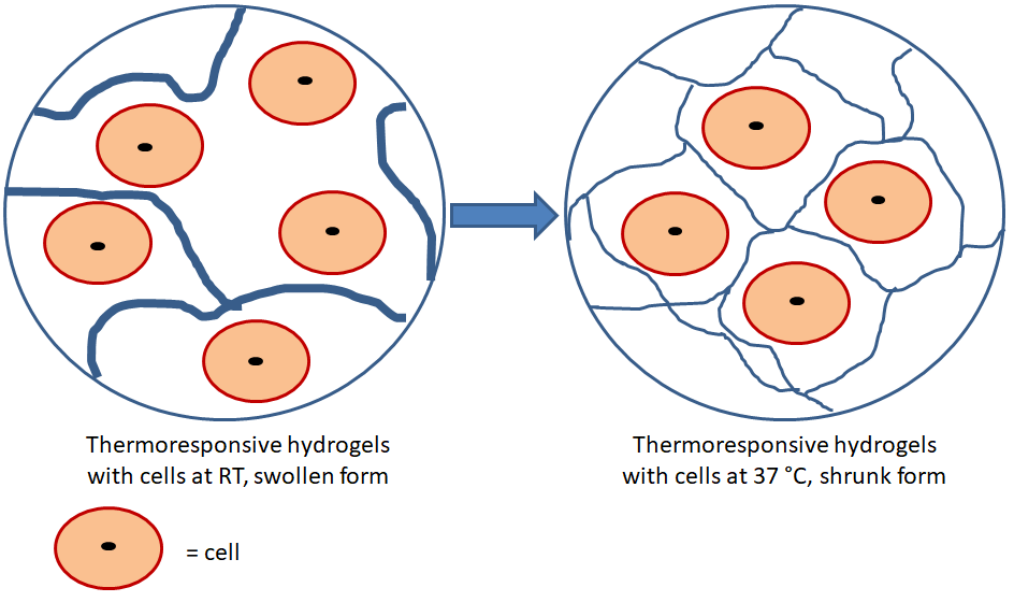

Figure 1.8. Scaffold formations with thermoresponsive hydrogels

1.2.3.4. Biosensors

A biosensor is one of the analytical devices which detect the biological changes such as genetic abnormalities, pathogens, viruses, toxins, and biological markers of disease. Moreover, it can measure the presence or concentration of biological molecules. The interactions between the surface of biosensors and quantifiably measured materials can provide information. They can be used for healthcare, environmental monitoring, food quality monitoring, and biosecurity due to their valuable properties (Aydemir, et al., 2016).

The basic elements of a biosensor can be seen in **Figure 1.9**. The first interactions occur with the analytes and receptors. For biosensor, the receptors are usually biological in origin, such as an enzyme, antibody, etc. in which their selectivity is high for analytes. In the second step must be related to the transducer to obtain measurable physical change about binding events. The third step contains the information collected by the transducer as useful information that can be presented by computer, etc. (Davis et al., 2007).

Nano biosensor architecture can be improved with incorporated polymers in fabrication processes. Polymers have some advantages in biosensor applications due to their surface characteristics. Furthermore, they can be used for biological and diagnostic researches due to their biocompatibility and biodegradability properties. To their potential for

biomedical applications, they can be employed for analytical protein detection techniques to measure quantitatively and qualitatively of proteins (Hahm, 2011).

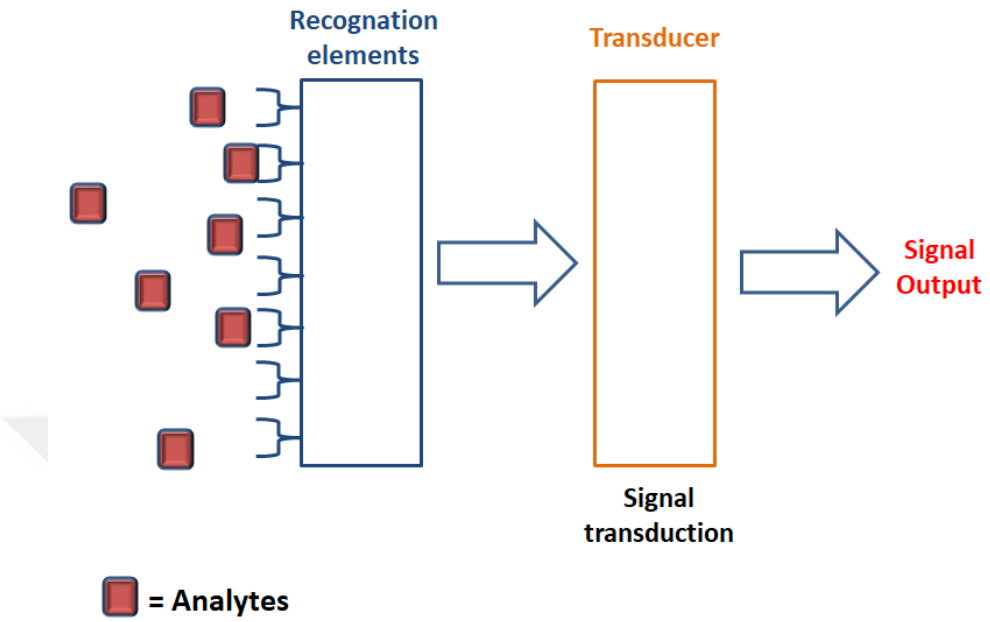

Figure 1.9. Basic elements of a biosensor

1.2.3.5. Medical devices

The intended use of medical devices is medical purposes, and they must be designed for these purposes. A scaffold is one of the most common ones that must imitate the mimic of the extracellular matrix or replace damaged tissues or organs. There are some successful attempts for using smart polymers as medical issues such as heart valves (Fallahiarezoudar et al., 2015), tracheal tissue (Hsieh et al., 2018), brain (Lancaster et al., 2013), retina (Singh et a., 2018) and skin (Ge et al., 2016).

Incorporating smart polymers into designing scaffolds is a crucial improvement for enhancing the activities of medical devices. For instance, Montgomery and coworkers reported that they designed an elastic and microfabricated scaffold by using a biodegradable polymer (poly(octamethylene maleate (anhydride) citrate) that can be participated in functional tissue delivery via injection (Montgomery et al., 2017). Smart materials have tremendous attractive for fabricating customized medical devices.

1.2.3.6. Cell therapy

Regenerative medicine is depending on utilizing stem, primary, or progenitor cells to facilitate the regeneration of damaged tissue or organs. Based on this approach, cell therapy is considered as a promising therapeutic approach in regenerative medicine. Cell-based therapy can be designed for some prominent disorders and diseases such as cardiovascular, neurological. Stem cells can differentiate into specifically functional cell types. This behavior provides enormous opportunities for tissue regeneration and repair in the human body. Stem cells are crucial for therapeutic strategy its inherent self-renewal potential (Peng et al., 2018; Labusca et al., 2018).

Smart polymers can participate in the designing of stem cells. 3D bioprinting method can be supported with smart polymers with encapsulated cells to control cell proliferation or differentiation. Smart polymers can play an important role in the regulation of differentiation of stem cells due to their response abilities to external stimuli. Specific biological environment conditions can be designed by smart polymers with stem cells to develop clinical approaches for the regeneration and repair of damaged tissues (Huang et al., 2019).

2. MATERIAL AND METHOD

2.1. Materials

2.1.1. Laboratory equipment

Laboratory equipment used in this thesis and the suppliers are listed in **Table 2.1**.

Table 2.1 Laboratory equipment and suppliers

Equipment	**Supplier**
Balances	OHAUS Model:PA214C
Centrifuges	DLAB Model:DM0412
	Sigma Model:1-14
Differential Scanning Calorimeter	Tetra DSC7000X
Equipment	Supplier
Magnetic stirrers	Lab Companion JEIO TECH Model:MS-12BB
Mini Vortex Mixer	ISOLAB Model:MI0101001
NanoDrop	Thermo Scientific NanoDrop 2000
Orbital Shaker	ISOLAB - MODEL:618.12.001
	ISOLAB Model:613.11.001
pH meter	HANNA Model: HI2215
Refrigerator	Arçelik Model:570465MB
Scanning Electron Microscope	FEI QUANTA 450 FEG ESEM
Simultaneous Thermogravimetric Analyzer	HITACHI STA7200
Spectrophotometer	Photolab 6600 UV–VIS
Ultrasonic bath	BANDELİN Model:RK100H
UV Lamb	UVGL-58 Handheld UV Lamb
Vacuum oven	VACUCELL
Water purification systems	ANT TEKNİK MODEL: Direct Q-3UV

2.1.2. Chemicals

Chemicals used in this study are listed in **Table 2.2**.

Table 2.2 Chemicals and Suppliers

Chemical	Supplier
4,4'-diphenylmethane diisocyanate (MDI) (95%)	Kimpur Kimteks Polyurethane Corporation
Acetone (≥ 99.8%)	Merck
Acetonitrile (ACN)	Merck
Benzyl-N,N-dimethyl dithiocarbamate (BDC)	Sigma Aldrich
Dimethylformamide (DMF)	Merck
Dimethyl Sulfoxide (DMSO)	Merck
Dimethoxy-2-phenylacetophenone (DMPA) (99%)	Sigma Aldrich
Ethanol (EtOH)	Merck
Ethylene glycol dimethacrylate (EGDMA)	Sigma Aldrich
Methanol (MeOH)	Merck
N,N′-Ethylenebis (acrylamide) (EbAM)	Sigma Aldrich
N,N'-Methylenebis (acrylamide) (MBAM) (99%)	Sigma Aldrich
N-Isopropylacrylamide (NIPAM) (97%)	Sigma Aldrich
Triethylamine (≥99.0%)	Merck
Quercetin	Merck

2.1.3. Buffers and solutions

Buffers and solutions used in this study and their compositions are listed in **Table 2.3**.

Table 2.3 Buffers used in the study

Buffer	Composition
pH 4.0 buffer	10.21 g potassium hydrogen phthalate and 1 ml of 0.10 M HCl mixed in 1L distilled water.
pH 7.4 buffer	8 g of NaCl, 200 mg of KCl, 1.44 g of Na_2HPO_4, and 240 mg of KH_2PO_4 added to 800 mL of distilled water. Then added distilled water until volume is 1 L.
pH 9.0 buffer	4.77 g sodium tetraborate and 46 ml of 0.10 M HCl mixed in 1L distilled water.

2.1.4. Natural materials

The natural materials used in this thesis are listed in Table 2.4.

Table 2.4. Natural materials and suppliers

Natural Materials	Supplier
Bacterial Cellulose	
Castor Oil	Zag Kimya
Plant oil acrylate methyl ricinoleate (AMR)	It was kindly provided by Dr. Gökhan Cayli

2.2. Methods

2.2.1. Preparation of quercetin solution

2.2.1.1. The stability of quercetin

In this study, the effects of pH changes and various solvents on the stability of quercetin were investigated. Quercetin, ethanol (EtOH), methanol (MeOH), dimethylformamide (DMF), dimethyl sulfoxide (DMSO), and acetonitrile (ACN) were supplied from MERCK.

Quercetin was dissolved in EtOH, MeOH, DMF, DMSO, and ACN to obtain final

concentrations of 500 μM. Spectrophotometric measurements were performed periodically.

2.2.1.2. The solubility of quercetin

In this study, the effects of pH changes and various solvents on the solubility of quercetin were investigated. Quercetin, ethanol (EtOH), methanol (MeOH), dimethylformamide (DMF), dimethyl sulfoxide (DMSO), and acetonitrile (ACN) were supplied from MERCK. Quercetin was dissolved in EtOH, MeOH, DMF, DMSO, and ACN and diluted by organic solvents (final concentrations were 500 μM). Besides, different solvents were prepared with buffer and organic solvents in different ratios.

In the calibration process, 3 mg of quercetin was dissolved in 10 ml MeOH, and this solution was diluted to 500 μM and 250 μM by MeOH. So 1.0 mM, 500 μM and 250 μM quercetin concentrations were obtained, then 200 μL were taken from all of the solutions and added to 1800 μL of buffer (pH:7.4). Finally, 25, 50, and 100 μM of quercetin concentrations were obtained. All of the measurements concerning quercetin were performed using a UV/Vis spectrophotometer at 371 nm.

2.2.1.3. Loading capacities

The optimum quercetin concentration for an efficient loading was determined by analyzing different quercetin concentrations (200 μM, 100 μM, 50 μM, 25 μM, and 10 μM). The loading concentration was defined as 100 μM. 3 mg quercetin was dissolved in 10 ml MeOH. 1 ml of solution from the stock solution was taken and added 9 ml of buffer (pH: 7.4). The dialysis membrane, including the hydrogel (**Figure 2.1**), was transferred into the quercetin solution and kept 18 hours at RT for loading. After 18 hours, quercetin loading was tested via UV/vis spectrophotometric measurements. The absorbance of quercetin in loading solution (1:9 MeOH:buffer) decreases due to the decrease of quercetin concentration during loading. A_{w0} is the initial absorbance of quercetin in MeOH/buffer solution, A_{ch} is the quercetin absorbance in the solution, A_l is the percentage of absorbed quercetin.

Loaded quercetin percentage in the hydrogel can be defined as equation 1:

$$(A_l) = [(A_{w0} - A_{ch}) / A_{w0}] * 100 \quad (1)$$

Figure 2.1 The appearances of the solutions before and after loading

2.2.1.4. Release behaviors

The release process was performed at different temperatures, room temperature (25°C, RT) and body temperature (37°C). Especially 37°C is quite crucial for release studies because this temperature is close to the body temperature. Therefore, that temperature is essential for CDRS. Besides, 37°C is above LCST for thermoresponsive polymers based on NIPAM.

Quercetin was loaded into hydrogels when the temperature was at room temperature through the swelling behavior of thermoresponsive hydrogel at under body temperature. When the temperature reached close to body temperature (above LCST), the hydrogel shrank, and quercetin was released to the aqueous solution at body temperature.

A_{h0} is the initial absorbance of quercetin in the hydrogel. A_w is the quercetin absorbance in MeOH/buffer solution, and A_r is the percentage of released quercetin.

Released quercetin percentage in the hydrogel can be defined as equation 2:

$$(A_r) = [(A_{h0} - A_w) / A_{h0}]*100 \quad (2)$$

2.2.2. Synthesis of the hydrogels

2.2.2.1. Synthesis of the hydrogels using BDC as a photoinitiator

This part of the present thesis includes the synthesis of BDC based thermoresponsive hydrogels. **Table 2.5** shows the reagents of the BDC based hydrogels. In the synthesis, EbAM, NIPAM, BDC, and MeOH were used as a crosslinker, monomer, photoinitiator, and solvent, respectively. All of the materials in **Table 2.5** were dissolved in MeOH. Then photopolymerization was realized under UV irradiation (365 nm) at room temperature overnight. Then the hydrogels were transferred to the dialysis membrane and put them to 1L MeOH and H_2O. After that, drying process of the hydrogels was realized with vacuum at 40 °C for two days.

Table 2.5 Reagents used in the synthesis of BDC based hydrogels

Reagent	Molar amount (mmol)	Mass (mg)	Volume (ml)
EbAM	1.07	179.96	-
NIPAM	3.2	362.11	-
BDC	0.96	202.90	-
MeOH	-	-	16

2.2.2.2. Synthesis of the hydrogels with varied molar ratios of NIPAM

The molar ratio of NIPAM was varied to synthesize thermoresponsive hydrogels. **Table 2.6** shows the reagents used for the synthesis of these hydrogels. In the synthesis, EbAM, NIPAM, BDC, and MeOH were used as a crosslinker, monomer, photoinitiator, and solvent, respectively. The main aim of this study is to examine the effects of the molar ratio of monomer on the release behaviors of hydrogels.

All of the reagents in **Table 2.6** were dissolved in MeOH. Then photopolymerization was realized under UV irradiation (365 nm) overnight. The hydrogels were transferred to the dialysis membrane and then washed in 1L MeOH, followed by washing in H_2O. After that, drying process of the hydrogels was realized with vacuum at 40 °C for two days.

Table 2.6. Reagents used for the synthesis of the hydrogels with varied molar ratios of NIPAM

	Reagent	Molar amount (mmol)	Mass (mg)	Volume (ml)	Equivalency	[M] %
H-N1	EbAM	0.36	60.55	-	1	5
	NIPAM	0.36	40.74	-	1	
	BDC	0.0054	1.14	-	-	
	MeOH	-	-	2.4	-	-
H-N3	EbAM	1.07	179.96	-	1	5
	NIPAM	3.2	362.11	-	3	
	BDC	0.96	202.90	-	-	-
	MeOH	-		16	-	-
H-N10	EbAM	0.036	6.05	-	1	5
	NIPAM	0.36	40.74	-	10	
	BDC	0.07776	16.43	-	-	-
	MeOH	-		1.1	-	-

2.2.2.3. Synthesis and comparison of EbAM and EGDMA based hydrogels

EGDMA and EbAM based hydrogels were synthesized to investigate the effects of different crosslinkers and molar ratios on the release and swelling performances of the hydrogels. For the synthesis of hydrogels in **Table 2.7**, firstly, NIPAM was dissolved in MeOH, and then other ingredients were added into NIPAM solutions. Photopolymerization was realized by UV irradiation (365 nm) during 1h. After that, hydrogels were transferred to falcons from vials, and 2 ml distilled water was added. They were centrifuged with 4500 g and for 10 min. The supernatant removed and precipitated part was dried under vacuum at 40 °C for two days.

2.2.2.4. Synthesis of plant oil based hydrogels using acrylate methyl ricinoleate (AMR)

The synthesis of hydrogels using a plant oil based monomer instead of conventional monomers was carried out. The reagents of AMR based hydrogels can be seen in **Table**

2.8. In addition, their performances were compared with EGDMA based hydrogels whose reagents are listed in **Table 2.8** below.

Table 2.7 Synthesis of EGDMA and EbAM based hydrogels in H_2O

	Reagent	Molar amount (mmol)	Mass (mg)	Volume (µl)	Equivalency	[M], %
1%EbAM	EbAM	0.01	1.68	1.60	1.00	20
	NIPAM	1.00	113.16	-	100.00	
	DMPA	0.01	1.31	-	-	-
	H_20	-		500	-	-
10%EbAM	EbAM	0.10	16.82	16.00	1.00	20
	NIPAM	1.00	113.16	-	10.00	
	DMPA	0.01	1.54	-	-	-
	H_20	-		600	-	-
25%EbAM	EbAM	0.25	42.05	40.01	1.00	20
	NIPAM	1.00	113.16	-	4.00	
	DMPA	0.01	1.92	-	-	-
	H_20	-		700	-	-
1%EGDMA	EGDMA	0.01	1.98	1.89	1.00	20
	NIPAM	1.00	113.16	-	100.00	
	DMPA	0.01	1.31	-	-	-
	H_20	-		500	-	-
10%EGDMA	EGDMA	0.10	19.82	18.86	1.00	20
	NIPAM	1.00	113.16	-	10.00	
	DMPA	0.01	1.54	-	-	-
	H_20	-		600	-	-
25%EGDMA	EGDMA	0.25	49.56	47.15	1.00	20
	NIPAM	1.00	113.16	-	4.00	
	DMPA	0.01	1.92	-	-	-
	H_20	-		700	-	-

Table 2.8. Synthesis of AMR based and EGDMA based hydrogels

	Reagent	Molar amount (mmol)	Mass (mg)	Volume (µl)	Equivalency	[M], %
AMR0.01	AMR	0.02	7.36		1.00	20
	NIPAM	2.00	226.32	-	100.00	
	DMPA	0.01	2.56	-	-	-
	H_20	-	-	1000	-	-
AMR0.04	AMR	0.08	29.44		1.00	20
	NIPAM	2.00	226.32	-	25.00	
	DMPA	0.01	2.56	-	-	-
	H_20	-	-	1000	-	-
AMR0.10	AMR	0.20	73.60		1.00	20
	NIPAM	2.00	226.32	-	10.00	
	DMPA	0.01	2.56	-	-	-
	H_20	-	-	1000	-	-
AMR0.25	AMR	0.50	184.00		1.00	20
	NIPAM	2.00	226.32	-	4.00	
	DMPA	0.01	2.56	-	-	-
	H_20	-	-	1000	-	-
1%EGDMA	EGDMA	0.02	3.96	3.77	1.00	20
	NIPAM	2.00	226.32	-	100.00	
	DMPA	0.01	2.56	-	-	-
	H_20	-	-	1000	-	-
4%EGDMA	EGDMA	0.08	15.86	15.09	1.00	20
	NIPAM	2.00	226.32	-	25.00	
	DMPA	0.01	2.56	-	-	-
	H_20	-	-	1000	-	-
10%EGDMA	EGDMA	0.20	39.64	37.72	1.00	20
	NIPAM	2.00	226.32	-	10.00	
	DMPA	0.01	2.56	-	0.05	-
	H_20	-	-	1000	-	-
25%EGDMA	EGDMA	0.50	99.11	94.30	1.00	20
	NIPAM	2.00	226.32	-	4.00	
	DMPA	0.01	2.56	-	-	-
	H_20	-	-	1000	-	-

For the synthesis of the hydrogels in **Table 2.8**, firstly, NIPAM was dissolved in MeOH, and then other ingredients were added to NIPAM solutions. Photopolymerization was carried out under UV irradiation (365 nm) for 1 h. After that, hydrogels were transferred to falcons from vials, and 2 ml distilled water was added. They were centrifuged at 4500 g and for 10 min. After removing the supernatant, the drying process for the precipitated was realized under vacuum at 40˚C for two days.

2.2.2.5. Synthesis of CO and BC based hydrogels

In this study, BC based hydrogels (**Table 2.9**) were synthesized with and without CO. There are two steps of the polymerization; the first one is to have MDI modified BC with and without CO. The second step aims to gain thermoresponsive properties to MDI modified polymers.

The polymerization processes were realized with the procedure reported by Wang's study (Wang et al., 2018). The molar ratio between CO, the glucose unit of BC, and MDI was set as 1:1:1. 15.0 mg of BC was cut into as small pieces as possible. Then, BC pieces were mixed with MDI and CO (H-WCO in Table 2.9), whereas for H-NCO (in Table 2.9), only MDI was integrated to BC. Then, both of the hydrogels had similar synthesis approaches shown in Table 2.9. Triethylamine (TEA) (0.76 μL) was added to the mixtures and then 400 μL of dehydrated acetone was mixed. All of them were incubated at 40 °C for 48 h. So BC organogels were obtained as MDI modified form. These new structures were washed with acetone for three times.

For second step of polymerization, the purpose is to introduce the thermoresponsive properties to MDI-modified hydrogels by introducing NIPAM. Firstly 50.0 mg of NIPAM and 0.5 mg of MBAM were weigthed and dissolved in 370 μL of distilled water, after that the BC-based hydrogels were mixed with this solution. After keeping all of them at RT for 12 h, distilled water (1.0 mL) was added. All mixtures were mixed by shaker for 15 min. After that, DMPA was used as a photoinitiator and added to initiate the polymerization reaction with the ratio of 1.0% mol of NIPAM. Photopolymerization was realized by UV irradiation for 1 h. After that, H-WCOT and H-NCOT were obtained and then the distilled water was used for washing of the

hydrogels three times and the drying process was realized with vacuum at 40˚C for two days.

Table 2.9. Reagents used for CO based hydrogels

	Reagent	Molar amount (mmol)	Mass (mg)	Volume (µl)	Equivalency
H-WCOT	BC		15		
	MDI	0.08	20.00	16.26	1
	CO	0.08	74.80	77.84	1
	NIPAM	0.4419	50.01	-	5 1/2
	DMPA	0.004419	1.13	-	0.01
	MBAM		0.50		
	H_20	-	-	370	-
H-NCOT	BC		15		
	MDI	0.08	20.00	16.26	1
	NIPAM	0.4419	50.01	-	5 1/2
	DMPA	0.004419	1.13	-	0.01
	MBAM		0.50		
	H_20	-	-	370	-

2.2.2.6. Synthesis of hydrogels with varied molar ratios of BC

The purpose of this part of the present study is to investigate the effects of the molar ratio of BC on the characteristics of hydrogels. Accordingly, with this purpose, BC ratio was changed, and detailed information was given in **Table 2.10**.

In this section, there are three groups of CO and BC based hydrogels, whose syntheses procedures were clearly defined by Wang and coworkers (Wang et al., 2018). The molar ratio between MDI, the glucose units of BC, and CO were set as 1:0.5:1, 1:1:1, and 1:2:1 for H-BC1, H-BC2, and H-BC3, which are in Table 2.10, respectively.

Firstly, BC (dried BC, as seen in **Figure 2.2**) was weighed as 15 mg, 30 mg, and 60 mg and then they were cut into as small pieces as possible. After that, BC pieces were added to MDI and CO and 2 ml dehydrated acetone was integrated to all of the mixtures after the addition of TEA (0.76 µL, 1.52 µL, 3.04 µL), all of them were incubated at

40˚C for 48 h, so BC organogels were obtained as MDI modified form. After this process, MDI modified BC materials were washed with acetone three times and the drying process was realized with vacuum at 40˚C for two days.

Table 2.10. Reagents used in the synthesis of BC based hydrogels

	Reagent	Molar amount (mmol)	Mass (mg)	Volume (µl)	Equivalency
	BC	0.08	15.31		0.50
	MDI	0.17	42.49	34.55	1.00
	CO	0.17	158.92	165.37	1.00
H-BC1	NIPAM	0.45	51.03	-	2.65
	DMPA	0.00	1.16	-	0.01
	MBAM		0.51		
	H_20	-	-	377.00	-
	BC	0.17	30.00		1.00
	MDI	0.17	42.50	34.55	1.00
	CO	0.17	158.95	165.40	1.00
H-BC2	NIPAM	0.88	100.00	-	5.20
	DMPA	0.01	2.26	-	0.01
	MBAM		1.00		
	H_20	-	-	740.00	-
	BC	0.34	61.25		2.00
	MDI	0.17	42.50	34.55	1.00
	CO	0.17	158.94	165.39	1.00
H-BC3	NIPAM	1.80	204.17	-	10.61
	DMPA	0.02	4.62	-	0.01
	MBAM		2.04		
	H_20	-	-	1510.00	-

The second step of the polymerization aims for MDI modified BC materials to gain thermoresponsive characters. For this purpose, NIPAM and MBAM were weighed and dissolved in distilled water and added to hydrogels at the ratio described in Table 2.10.

All of the them were kept at RT for 12 h, and then the radical polymerization reaction was initiated by adding DMPA. After the photopolymerization processes, the distilled water was used for washing of BC/NIPAM hydrogels three times, and the drying process was realized under vacuum at 40˚C for two days.

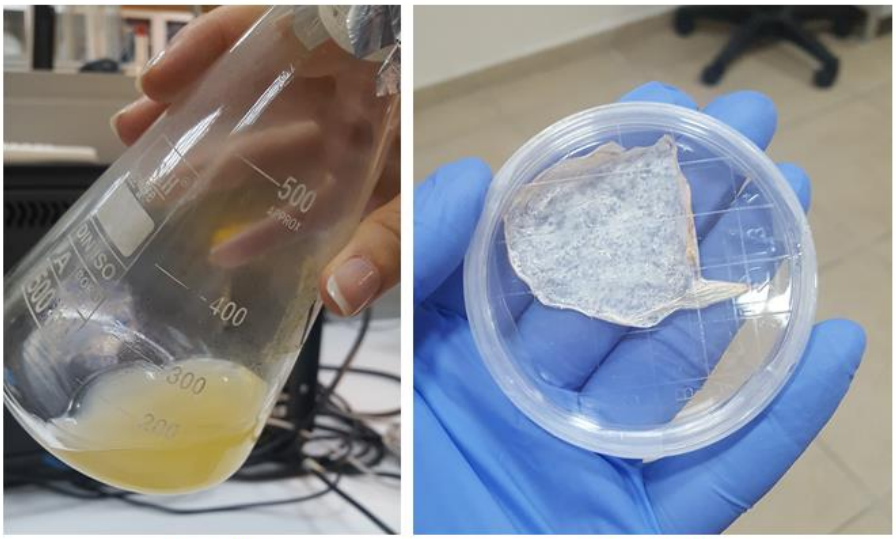

Figure 2.2. Wet and dry BC

Investigation of crosslinker effects on the structure and properties of hydrogels was aimed at this part of the thesis. There are two different hydrogels in this study, given in **Table 2.11**. The synthesis procedure was the same as the synthesis of H-BC1.

Table 2.11. Hydrogels with/without MBAM

Hydrogel/*Components*	*BC*	*CO*	*MDI*	*NIPAM*	*MBAM*	*DMPA*
H-NC	0.5	1	1	1	-	1
H-WC	0.5	1	1	1	1	1

2.2.3. Swelling and deswelling studies

This part aims to understand the swelling ratio of the hydrogels. So these results can be used as a piece of prior knowledge about the loading of quercetin.

1 ml distilled H_2O, and approximately 10 mg polymer was used for swelling tests. The polymer was taken from the distilled water and weighed periodically, and measurements

were evaluated for having a curve related to time versus water amount in the polymer. Also, the same amount of polymer was weighed but without water as control groups.

The swelling degree of thermoresponsive hydrogels is calculated as described below:

Degree of swelling = [(Ww – Wd) / Wd] x100 (3)

Ww and Wd are expressed below:

Ww: the weight of the swollen hydrogel,

Wd: the weight of the dry hydrogel

The deswelling behaviors of the hydrogels were examined at 40°C that is above the LCST. Hydrogels were removed from the water at regular time intervals and firstly the excess water was removed then the hydrogels were weighed. Water retention (WR) is calculated as follows:

% Water retention = [(Wr – Wd)/(Ws – Wd)] x 100 (4)

Wr defines the weight of the hydrogel at a determined time at 40°C whereas Ws expresses the weight of the hydrogel at equilibrated swelling at RT.

2.2.4. Characterization of hydrogels

The characterization of the hydrogels was realized after the synthesis processes. According to this purpose, the evaluation of structures of hydrogels can be analyzed by FTIR spectroscopy. Furthermore, TGA and DSC experiments were used to investigate the thermal behaviors of hydrogels. SEM analyzes also were obtained to understand the surface properties of hydrogels.

2.2.5. Cytotoxicity analyzes

Cytotoxicity of BC hydrogels was analyzed by MTT (3-(4,5-Dimethylthiazol-2-yl)-2,5-diphenyltetrazolium bromide) assay in COS-7 cells (African green monkey kidney fibroblast-like cell line) (Mosmann, 1983). COS-7 cells (14×10^4 cells/well) were seeded in 24-well cell culture plates with a complete medium including Dulbecco's Modified Eagle Medium (DMEM), high glucose with %10 L-glutamine (Gibco) and supplemented with 10% fetal bovine serum (FBS, Lonza®) and incubated at 37°C in

5% CO_2. Different amounts of BC hydrogels ranging from 1 mg/ml to 20 mg/ml were added to the cells after the 24-h growth period. All experiments were carried out in duplicates, and the cells which were not exposed to hydrogels were used as a control group. Cytotoxicity was measured after a further 24 h of incubation. 100 μL of sterilized MTT (5 mg/mL) reagent was added to each well, and plates were incubated for 4h. Then, the medium was removed, and 500 μL of DMSO was added to each well to dissolve formazan products. After incubation in the dark for 15 min. on an orbital shaker, 100 μL of the dissolved formazan was transferred into 96-well plate to measure the absorbance at 570 nm using AMR-100 Eliza Plate Reader. The quantity of formazan is directly proportional to the number of viable cells, and cell viability was calculated according to the following formula:

Cell Viability (%)=(Absorbance of the test sample)/(Absorbance of the control group)x100 (5)

3. RESULTS AND DISCUSSION

3.1. Synthesis of Thermoresponsive Hydrogels by Using Conventional Monomers

In this thesis, quercetin was used as a model drug molecule. Quercetin is a member of phenolic flavonoids and has special properties on human health. Also, it is one of the most powerful antioxidants (Behnaz et al., 2012). Besides that property, it also has several properties such as anticancer (Behnaz et al., 2012; Materska, 2008) antiviral (Behnaz et al., 2012; Materska, 2008), anti-inflammatory (Materska, 2008), anticarcinogenic (Behnaz et al., 2012; Materska, 2008) and antibacterial (Materska, 2008) activities. Most of vegetables and fruits contain quercetin; some of the most common ones are green apple (Behnaz et al., 2012), tea, onions (Behnaz et al., 2012; Prior, 2003) cabbage, lemon, green tea (Behnaz et al., 2012).

There are some limits to using quercetin in biomedical applications, especially for the pharmaceutical area due to its low water solubility (Curcio et al., 2012). It is believed that some novel drug carrier systems based on hydrogels can be employed to increase water solubility and water stability of the quercetin molecule. This section of the thesis aims to investigate the solubility and the stability of the quercetin molecule in aqueous solutions and to optimize the medium for further studies.

3.1.1. The stability of quercetin

Different organic solvents were investigated to analyze the stability and the solubility of quercetin. It is aimed to examine the effects of various chemical solutions and pH value on the solubility and the stability of quercetin. The UV-Vis spectra of quercetin were recorded by Nanodrop Spectrophotometer. Scans were obtained with a wavelength range of 190 to 490 nm at time t=0, 10, 30, 60, 120, 180, 240, 300 minutes, and 24 hours. Firstly, stability experiments were performed for quercetin. 1.0 mM of quercetin was dissolved in MeOH, EtOH, DMF, DMSO, and ACN (**Figure 3.1**) individually and diluted each solution to 500 μM. Then spectrophotometric measurements were carried out by Nanodrop Spectrophotometer.

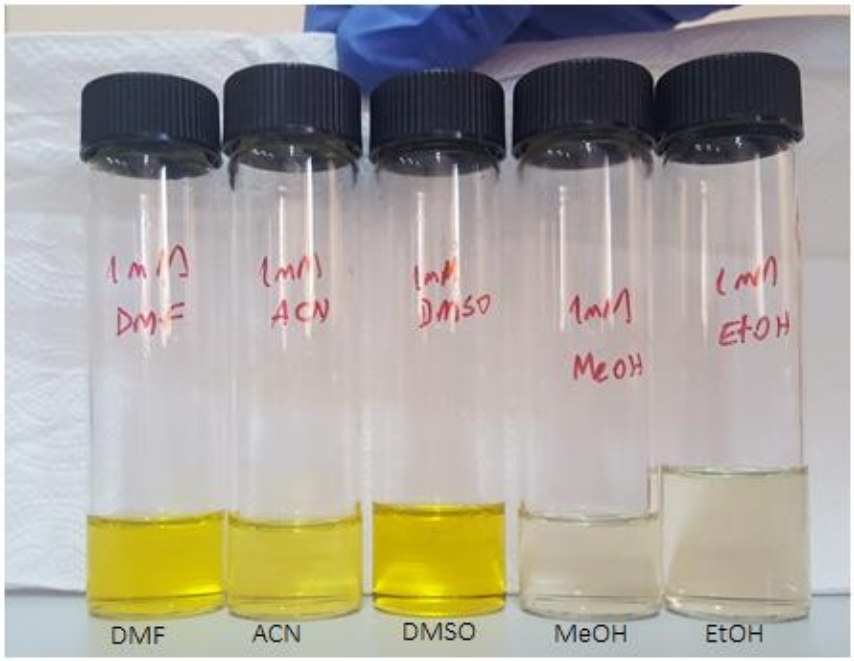

Figure 3.1 1.0 mM of quercetin solutions in different solvents

Figure 3.2 shows the data concerning the stability of quercetin. 500 µM of quercetin was prepared in MeOH, EtOH, DMF, DMSO, and ACN. The changes in the maximum absorbance were analyzed periodically. It can be seen clearly that quercetin in MeOH and DMSO had a more stable character. The quercetin absorbance in other solvents had changes in their bands around 371 nm with time. Quercetin in MeOH initially had absorbances at 256 and 371 nm and after 24h there was no additional peaks. Quercetin in EtOH had peaks at wavelengths of 257 and 377 nm at initial, and no more different peaks were observed, only the absorbance values of these peaks decreased over time. Quercetin in DMSO had also peaks at 260 nm and 378 nm. No shift was observed at these wavelengths, but the absorbance values decreased after 24 h. Quercetin in DMF had a peaks at 261 and 377 nm at initial, absorbance values of these peaks changed over time. ACN had also peaks at 256 and 372 nm at initial and their absorbance values increased over time. According to all of the results presented in **Figure 3.2**, quercetin was found to be more stable in MeOH compared to other solvents.

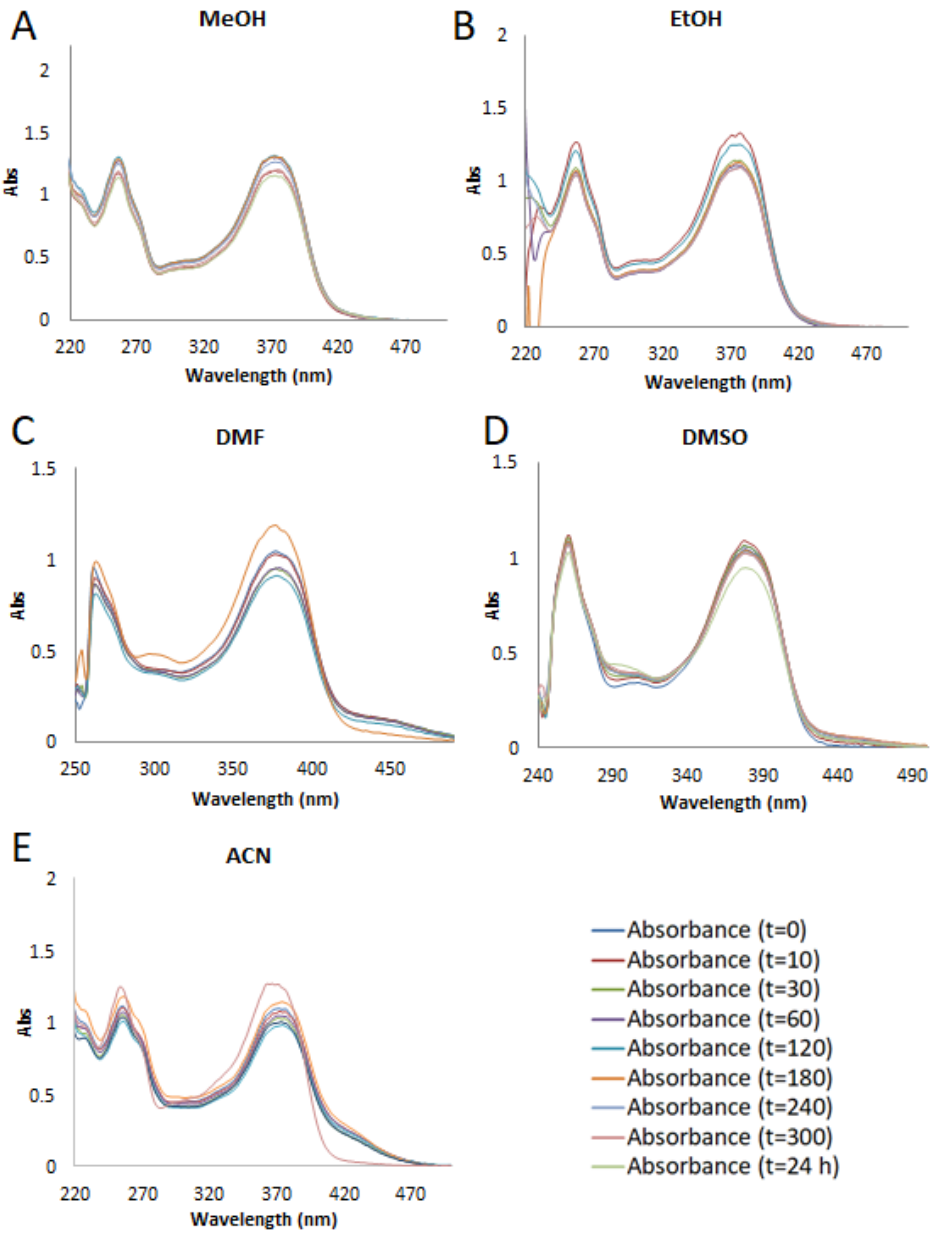

Figure 3.2. The solubility of quercetin in different solvents respect to time (A. Quercetin in MeOH; B. Quercetin in EtOH; C. Quercetin in DMF; D. Quercetin in DMSO; E. Quercetin in ACN)

3.1.2. The solubility of quercetin

The main aim of the present thesis is to design a smart polymeric system that can be used in drug delivery applications. Therefore the system must be working in body conditions. So, the solubility and the stability of quercetin in aqueous solutions were investigated.

For this purpose, different solvent compositions were prepared by mixing MeOH, EtOH, DMF, DMSO, ACN with the different ratio of the buffer, pH 7.4.

Figure 3.3 shows the spectrophotometric measurements concerning the solubility and the stability of quercetin in different solvents such as MeOH, EtOH, DMF, DMSO, and ACN with a buffer (pH7.4) ratio of 50%. It can be seen from Figure 3.3-A that the solution including MeOH:buffer (50:50, v:v) had peaks 272, 323 and 381 nm at the beginning of incubation period. There was not any difference in the spectrum until 24 h. According to the data of 24 h, the absorbance values at wavelengths of 272 nm and 381 nm decreased, whereas the absorbance value at 323 nm increased. Figure 3.3-B demonstrates the UV spectrum of quercetin in EtOH:buffer. It had peaks at 257, 324 and 378 nm at initial conditions. Absorbance values of the peaks at 257 and 378 nm decreased over time, while absorbance value of 324 increased after 24 h. The UV spectra of quercetin in DMF:buffer, (50:50) is shown in Figure 3.3-C. Significant changes in the maximum absorbances over time were detected. DMF:buffer solution had peaks at around 257, 324 and 392 nm at initial conditions, but the characteristics of these peaks changed over time. The absorbance value of 257 nm decreased over time, but the absorbance value of 324 nm increased over time. After 24 h, the peaks at 324 and 392 nm disappeared; a new peak at 338 nm occurred. When quercetin was incubated in DMSO:buffer, (50:50, v:v), absorbance values were changed significantly over time (Figure 3.3-D). It had peaks at 277, 324 and 401 nm at initial. When the changes of the peaks over time were examined, it was observed that the absorbance value of 277 nm decreased dramatically and the peak disappeared after 24 h. Moreover, the peak at 324 nm disappeared over time and a new peak at 334 nm showed up after 24 h. Furthermore, the peak at 401 nm disappeared over time. For ACN:buffer, (50:50, v:v), significant peaks were observed at around 259, 270, 324 and 380 nm at initial conditions (Figure 3.3-E). Absorbance values of 259 and 270 nm decreased over time and they disappeared after 24 h. Moreover, the peak at 324 nm disappeared over time and a new peak arised at 337 nm after 24 h. Furthermore, the absorbance value of 380 nm decreased over time and disappeared after 24 h. With this study, it was concluded that quercetin exhibits different behaviors in different solvents. Quercetin was affected least in MeOH and EtOH by adding of buffer solution. If all the data were evaluated together with the results of **Figure 3.2**, it was concluded that MeOH is the proper

solvent to have quercetin solutions. Studies in the biomedical field require environments compatible with human physiology. Therefore providing the best solubility of quercetin in aqueous media is very important for biomedical applications. For this purpose, the studies with the results in **Figures 3.2** and **3.3** are very important for the continuation of this thesis.

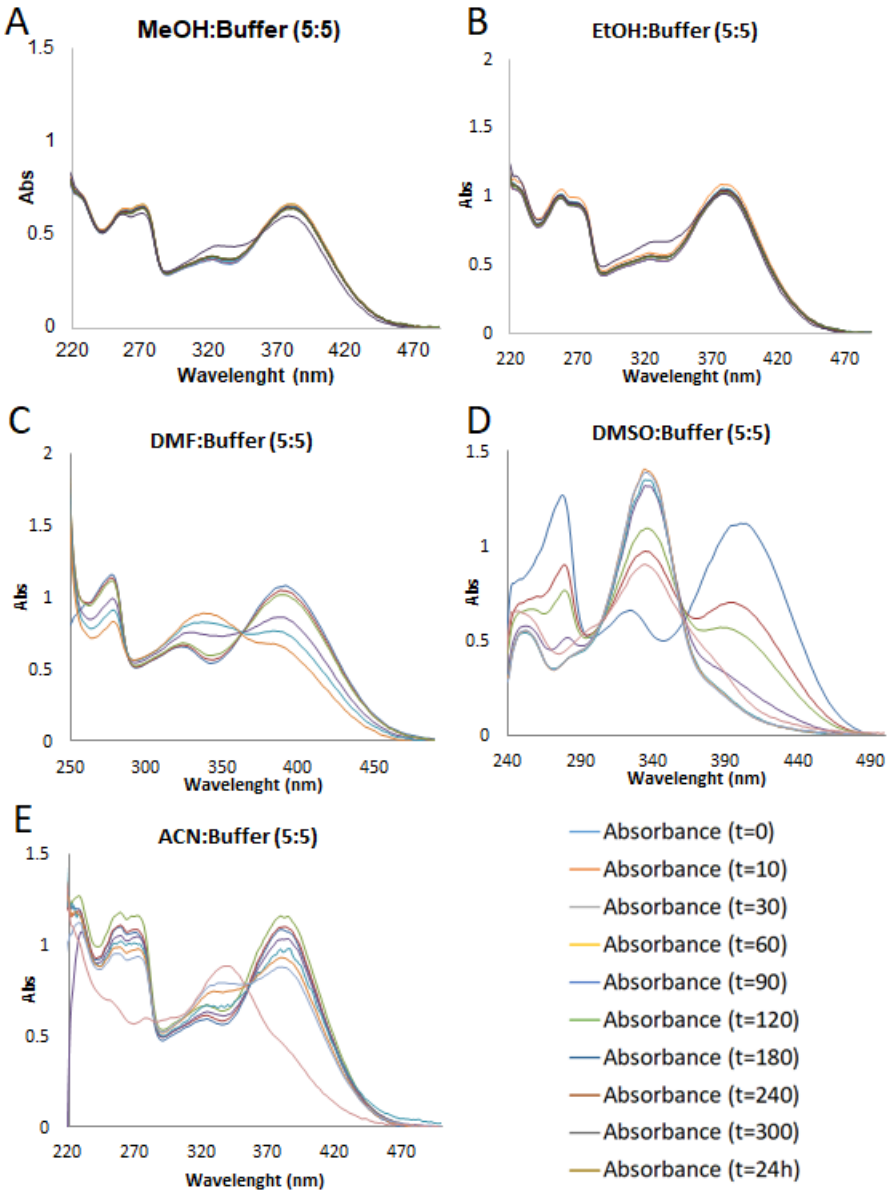

Figure 3.3. The stability of quercetin in various organic solvent: buffer (50:50) (A. MeOH:Buffer; B. EtOH:Buffer; C. DMF:Buffer; D. DMSO:Buffer; E. ACN: Buffer)

Besides solvent types and ratio of the buffer, pH plays a crucial role in the stability and solubility of quercetin. Therefore, the pH values of the aqueous solutions were monitored, and the observational results were presented in **Table 3.1**. The term turbid identifies the observation of the appearances of quercetin solutions. + defines the clear quercetin solution as visually. The results were obtained at RT.

Table 3.1 The pH values of quercetin in various aqueous solvents.

Ratio of solvents		**MeOH**		**EtOH**		**DMF**		**DMSO**		**ACN**	
No.	**buffer pH:7.4**	**pH**	**result**	**pH**	**result**	**pH**	**results**	**pH**	**result**	**pH**	**result**
1	9	7,67	+	7,64	+	7,87	+	7,54	turbid	7,68	turbid
2	8	7,8	+	7,78	+	8,04	+	8,05	+	7,86	turbid
3	7	8,16	+	8,1	+	8,45	+	8,41	+	8,07	+
4	6	8,37	+	8,27	+	8,78	+	8,99	+	8,21	+
5	5	8,65	+	8,53	+	9,22	+	9,7	+	8,24	+
6	4	8,96	+	8,76	+	9,6	turbid	10,18	turbid	8,56	+
7	3	9,19	+	8,96	turbid	9,67	turbid	10,75	turbid	8,48	turbid
8	2	9,65	+	9,35	turbid	9,9	+	10,26	turbid	8,43	turbid
9	1	10,12	+	9,5	turbid	10,04	+	10,61	+	8,18	turbid
+ Refers to clear solutions											

Figure 3.4 should be examined to support the results in **Table 3.1**. The solubility of quercetin in EtOH is given as an example in **Figure 3.4**, below. When the ratio of EtOH increased, the solution of quercetin seemed turbid.

When the results of **Table 3.1** are analyzed in detail, all of the solvents, except MeOH, had turbid solutions. Moreover, when the pH value increased, the solutions seemed turbid.

According to the results of **Figure 3.2, 3.3**, and **Table 3.1**, MeOH was chosen as the proper solvent for quercetin. Besides, it will be used for the loading and release studies in the present thesis. Furthermore, since pH 7.67 is close to the physiological pH 7.4, MeOH(1):Buffer(9) was defined as the optimum condition for the studies performed during the thesis. The studies carried out in the biomedical field should be compatible with body conditions. So the experiments should be conducted in aqueous solutions

with a pH 7.4. MeOH(1):Buffer(9) provided a proper aqueous medium for the dissolution of quercetin.

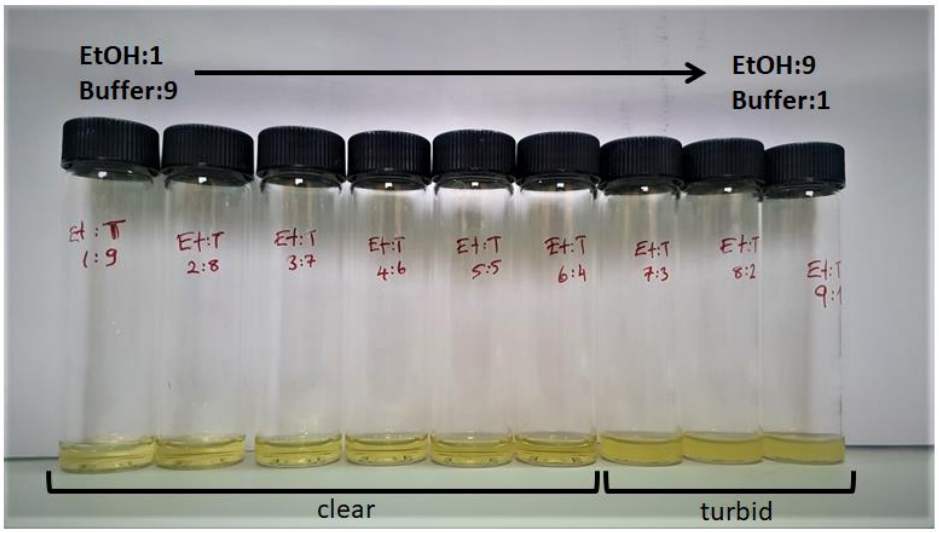

Figure 3.4 The solubility of quercetin in various EtOH:Buffer solutions

After the determination of proper solvent composition for quercetin, the calibration curve of quercetin was obtained. UV/Vis spectrum of quercetin was obtained, and the maximum absorbance value was determined at 371 nm. According to absorbance values at 371 nm, the calibration curve was obtained as below.

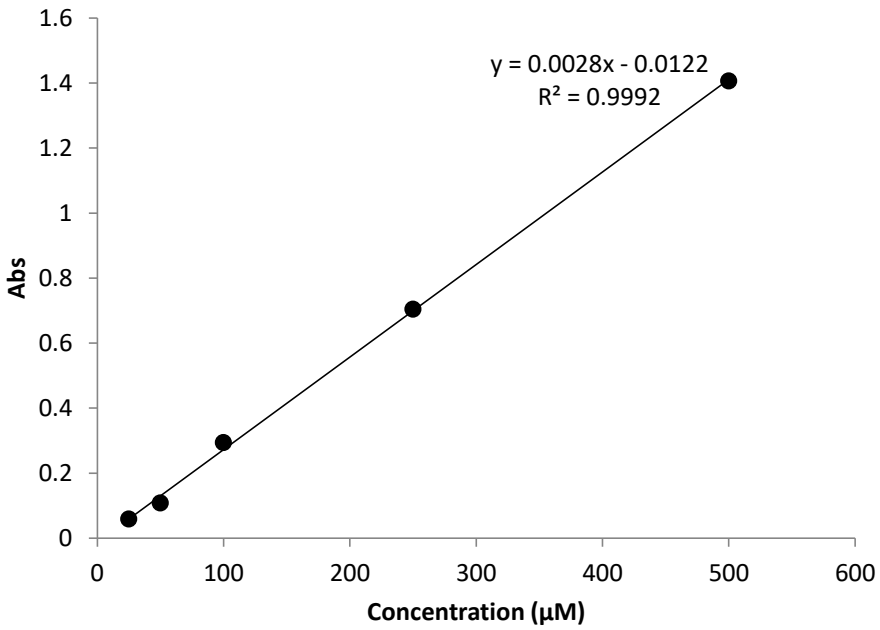

Figure 3.5. The calibration curve of quercetin

Figure 3.5 shows the linear calibration curve of quercetin with an R^2=0.9992. This curve was obtained with a quercetin solution prepared in MeOH:Buffer. Firstly 1 mM quercetin solution was prepared with MeOH, and then it was diluted by MeOH to obtain the calibration concentrations present in **Figure 3.5**. Similar to the results of **Figure 3.2** and **3.3**, and **Table 3.1**, Bancirova (2015) studied the solubility of quercetin in different solvents as EtOH, MeOH, and DMSO. The maximum absorbance values were recorded for quercetin in these solvents by spectrophotometric measurements were 385 nm, 390 nm and 330 nm for EtOH, MeOH and DMSO, respectively. In the mentioned study, quercetin was dissolved in EtOH, MeOH, and DMSO and diluted to a final concentration of 10 μM. The changes in the absorption spectra during the quercetin autooxidation respect to time were investigated by Bancirova, also, a new peak at 330 nm for quercetin dissolved in all solvents was observed (Bancirova, 2015). Bancirova reported that the absorption spectra of flavonoids consist of two distinctive bands in a broad range of 240–400 nm. The range of 240–280 nm and 300–380 nm were demonstrated the B-ring and the A–C benzoyl system, respectively by Bancirova (2015). Furthermore, a weak peak at around 300 nm was attributed to the C-ring only. Their results were similar to the results in **Figure 3.2** and **Figure 3.3**. We also had new peaks at around 334, 337 and 338 nm for DMSO, ACN and DMF with respect to time (**Figure 3.3**).

Similar to the results of **Figure 3.4** and **Table 3.1**, quercetin solubility in various ratios of water:EtOH was evaluated in Abraham's study (2014). They used a model for predicting the solubility of quercetin in water-ethanol mixtures. They reported the solubility of quercetin in water-ethanol mixtures is similar to the ethanol rich mixtures (Abraham et al., 2014). The obtained results can be supported by the results of Brett's study (2003). They claimed that quercetin was affected by pH changes as an acidic or alkaline medium (Brett et al., 2003). Duan (2014) also studied the effects of strong acid and alkaline solution on structures of quercetin and observed the changes by the UV/Vis spectrum. Different pH values of quercetin in aqueous ethanol solution were analyzed with UV-Vis measurements. Two characteristic adsorption bands at 374 nm and 256 nm were detected, while quercetin was in 50% (v/v) aqueous ethanol solution. When the pH was set at 14.0 with sodium hydroxide, it was reported as the band at 374 nm shifted to about 400 nm, and the band at 256 nm disappeared, a new band at 314 nm appeared. They measured the absorbance of quercetin correlated with different pH values. Firstly

they dissolved the quercetin in 50 % (v/v) aqueous ethanol solution and the properties of the solution were straw yellow with a pH of 6.8, and it seemed as transparent solution. After pH was set 14.0 with sodium hydroxide, the color of the quercetin solution turned to brown yellow. Then they set pH value to 7.0 and had a brown transparent solution. Besides, the precipitate appeared when the solution was concentrated with removing most of the ethanol. Moreover, they washed the precipitate with water to neutral pH and dissolved in 50 % (v/v) aqueous ethanol solution. When the pH was set to 1.0, transparent solution obtained with straw yellow. The straw yellow, the transparent filtrate was obtained by concentrating the acid solution. The aim of this action is to remove most of the ethanol. Finally, 50 % (v/v) aqueous ethanol solution and water were used for washing the residue. However, pH was 7.0; there were two different measurements, such as UV/Vis spectrum of precipitate and UV-Vis spectrum of the filtrate. So it was found out that UV/Vis spectrum of precipitate was the same with UV/Vis spectrum of quercetin. A slight shift of UV-Vis spectrum was obtained for 50% (v/v) aqueous ethanol solution while pH was 1.0. It was concluded that UV/Vis spectrum of quercetin was the same with the precipitation whereas it was different from the UV/Vis spectrum of the filtrate. Degradation of quercetin can be realized with strong acid and alkaline as reported by Duan et al., 2014. (Duan, 2014). These results are proofs for ours given in **Figure 3.3** correlated with pH effects on solubility. Similar to results presented in **Table 3.1**, the solubility of quercetin is affected by pH changes, so these results are also proved by Duan (2014). The effect of pH on the solubility and stability of quercetin were also proved by Wang et. al. (2016). According to their results, it can be reported that quercetin is unstable at alkaline pH (Wang et al., 2016). Additionally, Pakade and coworkers (2017) reported that pH conditions of the environment were effective factors on structural characteristics of quercetin because quercetin has acidic hydrogens on the hydroxyl groups. Quercetin tended to get deprotonated while basic conditions, but it remained protonated when pH was acidic conditions (Pakade et al., 2017). Another study includes the quercetin solubility in various water:EtOH and water:MeOH solutions. Their results demonstrated that the solubility of quercetin increased with increasing temperature. However, when the temperature was constant, the solubility of quercetin could increase with increasing mole fractions of alcohol (Razmara et al., 2010). Slightly different from these studies, Amorati et al. (2017) studied the

antioxidant activity of quercetin in water solution and reported that the reactivity of quercetin in pH 7.4 was 40 fold more than activity in pH 2.1 according to oxygen-uptake kinetic measurements (Amorati et al., 2017). Effect of pH on the intensity of fluorescence of aluminum (III)–quercetin complex was evaluated by Pavun and coworkers (2014). They reported that the optimum pH value was pH 3.3. Their studies were maintained at pH 3.3 and in the presence of 70% (v/v) methanol/acetate buffers (Pavun et al., 2014). The quercetin release from polymeric nanoparticles was investigated by Pool's team. According to their results, it could be reported that release behavior was dependent on pH (Pool et al., 2012).

3.1.3. Synthesis of thermoresponsive hydrogels

In this section of the thesis, different hydrogels were synthesized by using conventional monomers. The thermoresponsive characteristics of the hydrogels were evaluated by investigating loading and release profiles and swelling performances. The factors which affect release performances of the hydrogels were examined.

Firstly, one simple thermoresponsive hydrogel (Hydrogel_01) was synthesized by using EbAM and NIPAM. The procedure of the synthesis was given in section 2.2.2.1 in detail. In this study, NIPAM, EbAM, and BDC were used as the monomer, crosslinker, and photoinitiator, respectively and equivalencies of reagents were set as 1:3:0.9 for NIPAM, EbAM, and BDC. Polymerization was realized at RT overnight. Experiments on determining loading capacities, the effects of temperature and pH changes on release behaviors were realized with Hydrogel_01. In the previous section, MeOH was determined as a suitable solvent to dissolve quercetin. Moreover, it was mixed with buffer, pH 7.4, in different ratios and MeOH (1):Buffer (9) was selected as the medium for the experiments in the thesis.

Loading studies of the Hydrogel_01 were performed and then release behavior was investigated at RT and 37°C. The effects of pH on the release characteristics of Hydrogel_01 were investigated with buffer solutions at pH 4.0 and pH 9.0. Furthermore, the release profiles of pH 4.0 were compared with the release profiles of physiological buffer (pH 7.4) at RT and 37°C. Temperature and pH changes can be defined as environmental factors. The molar ratio of NIPAM and the type of crosslinker were evaluated as factors on the structures of the hydrogels correlated with release and

swelling performances. Therefore the molar ratio of NIPAM of Hydrogel_01 was varied, and the effects of the molar ratio on release behavior were examined.

Additionally, the effects of molar ratio and the type of crosslinkers on release and swelling behaviors were investigated. The differences in the structures of the hydrogels caused by crosslinkers were identified by FTIR spectra.

3.1.3.1. Loading capacities

The quercetin loading process was described in section 2.2.1.3. The hydrogels were put inside the dialysis membranes separately, and then they were transferred into the quercetin solutions with different concentrations. In **Figure 2.1**, on the left dialysis membrane containing hydrogel in quercetin solution and on the right, only the quercetin solution before the loading can be seen.

Figure 3.6 shows the loading ratio of quercetin into the hydrogels vs time for the first 5 hours. Although George et al. (2019) reported that the quercetin loading time was 24 h, our spectrophotometric measurements of quercetin showed that quercetin was degraded after 18 h. When Figure 3.6 was evaluated, it can be seen that only 50% of 200 µM quercetin was loaded into the hydrogel. This significant difference may be caused by the low aqueous solubility of quercetin. The loading ratios for quercetin solutions of 10-100 µM were around 70%. Therefore, 100 µM was chosen as the loading concentration.

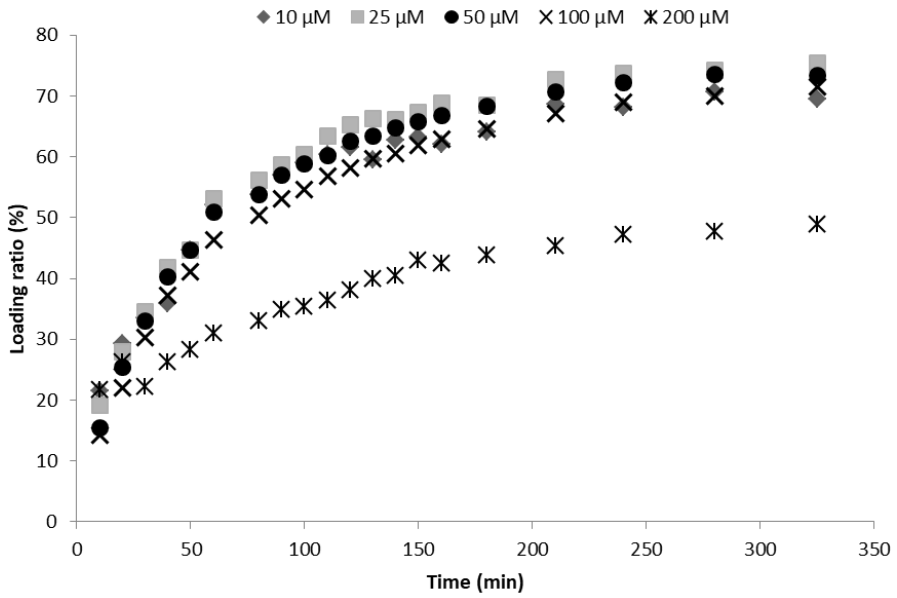

Figure 3.6 Quercetin loading ratio (%) with various concentrations

3.1.3.2. Factors affecting release performances

Several factors affect the release behaviors of hydrogels. Some of these factors like pH, light, ionic strength, and temperature, can be classified as environmental factors, whereas others like monomer composition, can be effective in the structures of the hydrogels. In this section, temperature and pH were defined as environmental factors. At the same time, the molar ratio of NIPAM and crosslinkers and also the types of crosslinkers were classified as factors related to the hydrogel structures. The experiments concerning the effects of the temperature and pH were performed with Hydrogel_01. Then, the molar ratio of NIPAM was varied, and release behaviors were examined. Moreover, the types and the molar ratio of crosslinkers were changed, and the effects were investigated. The release procedure was given in detail in section 2.2.1.4.

Temperature effects on release profiles

In this study, the investigation of the effects of temperature changes was aimed. For this purpose, the experiments were performed at two different temperature values as 25°C and 37°C. The Hydrogel_01 was synthesis with NIPAM, so that the hydrogel was expected to exhibit perfect thermoresponsive properties.

Release studies were realized with the dialysis membrane as the loading process. **Figure 3.7** shows the differences in the appearances of the solutions inside the dialysis membranes at different temperatures. When the temperature was 37 °C, the hydrogel was shrunk. However, at room temperature, the hydrogel didn't shrink rather solvated, so the solution was transparent.

Figure 3.8 shows the release profiles of the Hydrogel_01 quantitatively. The release curves show the release performances at two different temperatures and prove the thermoresponsive properties of the Hydrogel_01. The release performances were evaluated for the first 60 min (**Figure 3.8**). There were no significant differences for the first 10 min, but then high temperature affected the release behavior. A significant difference could be seen in 20 min, and then the difference between the release ratios increased. The reason for the same release concentrations at RT and 37°C in the first 10 minutes may be the burst effect.

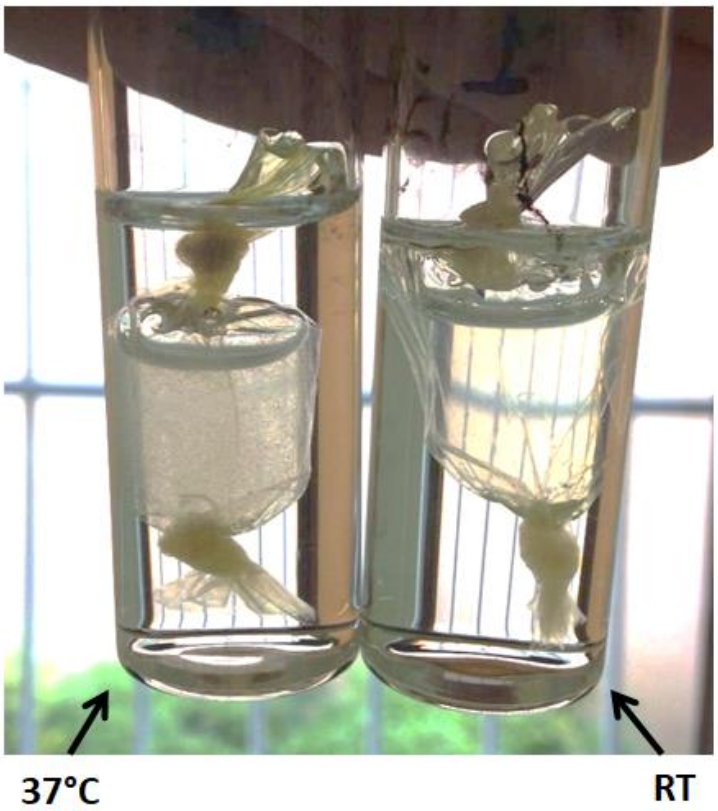

Figure 3.7. Quercetin release behavior of Hydrogel_01 at RT and 37°C

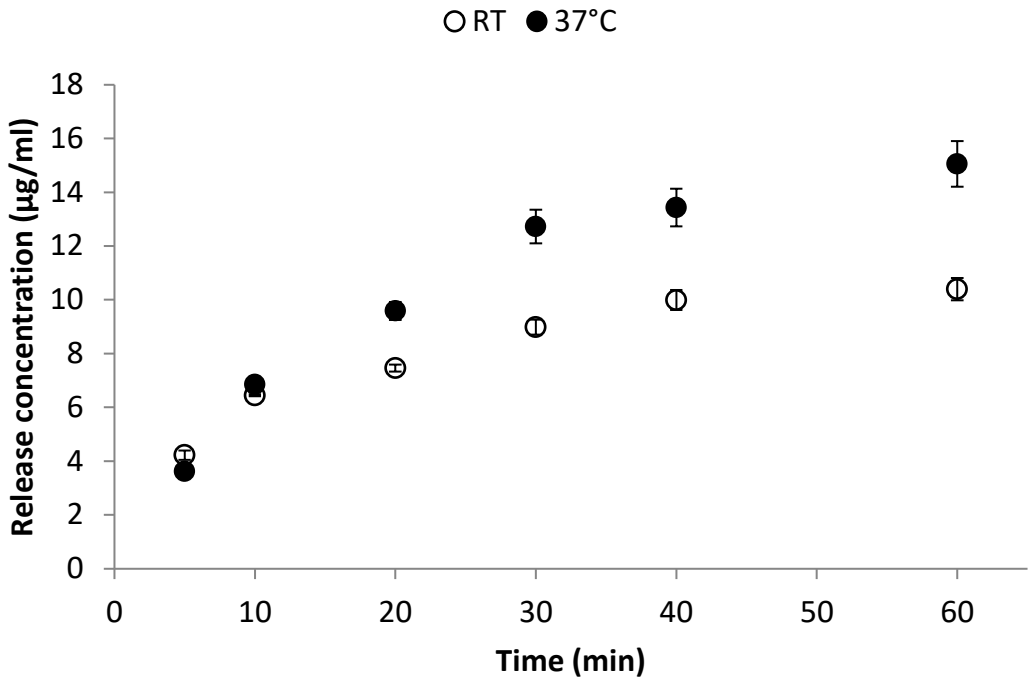

Figure 3.8 Quercetin release profiles of Hydrogel_01 at RT and 37°C

In this study, the hydrogels based on NIPAM were synthesized to have thermoresponsive properties. The detailed analyzes on the thermoresponsive hydrogel were realized by release studies at three different temperatures that prove the LCST value of NIPAM.

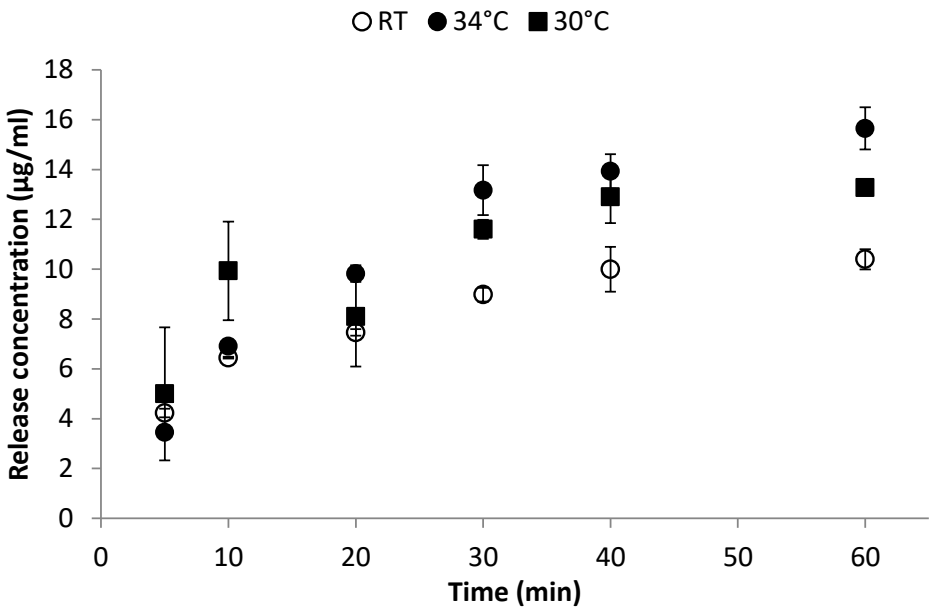

Figure 3.9. Quercetin release profiles of Hydrogel_01 at various temperatures

When **Figure 3.9** was investigated, it can be seen that the Hydrogel_01 gained thermoresponsive properties. Its release behavior was consistent with the characteristics of NIPAM. Above the LCST value of NIPAM (32°C), 15 µg/ml of the release concentration was achieved at 34°C, and 13 µg/ml was obtained at 30°C in 60 min. In contrast, the lowest release concentration (10 µg/ml) was achieved at RT. There was a negligible difference in the first 5 min, and then there was a small increase at 30°C. After 20 min, the differences between the temperatures became significant. The maximum release concentration was obtained at 34°C as expected. A significant difference between the release temperatures was observed in the first 60 min.

Chouhan's study (2009) can be examined in detail to support the results of **Figure 3.8** and **Figure 3.9**.

pH effects on release behaviors

Since pH changes can affect the release behavior and quercetin stability, the release behavior of Hydrogel_01 was tested at different pHs to clarify this situation. Therefore,

pH of aqueous media was set up at pH 4.0 and pH 9.0, respectively (**Figure 3.10**).

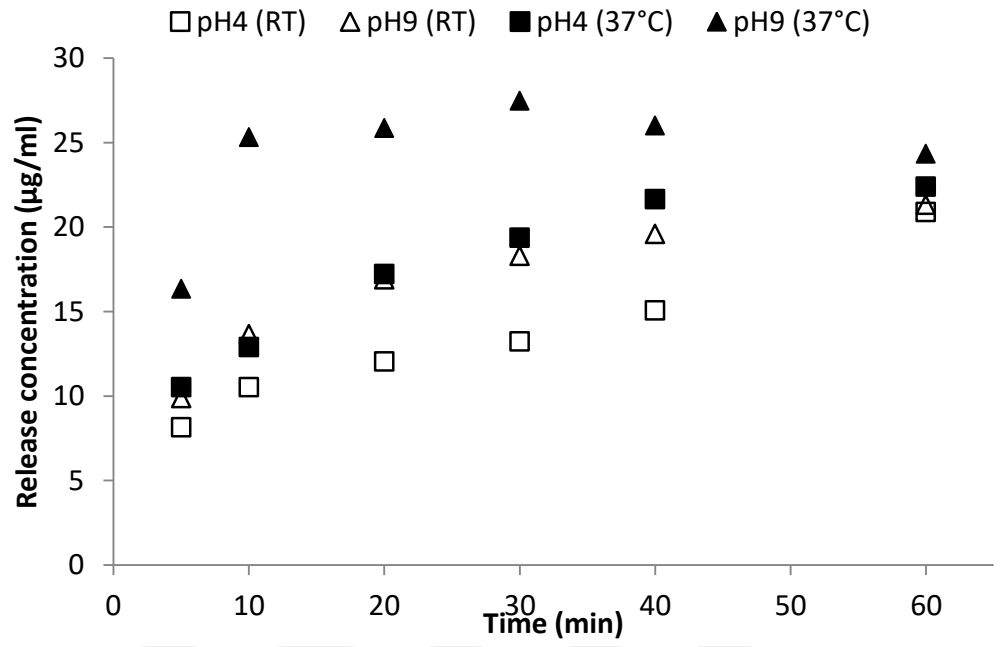

Figure 3.10 Quercetin release profiles of Hydrogel_01 at pH 4 and pH 9

When **Figure 3.10** was analyzed, for the first 5 min, there was a significant difference for the release concentration at pH 9.0 and 37°C. This difference increased even more after 10 min. The release concentration at pH 4.0 at RT was the lowest compared to other conditions. Release concentrations at 37°C were always higher than at RT for all conditions. In 40 min, it was seen that the release concentrations began to approach each other. At pH 9.0, an immediate release was achieved in 10 min at 37 °C. Besides, while the experiments were going on, it was visually observed that the quercetin solution became turbid at pH 9.0, especially at 37°C after 50 min, so pH 4 had better results for CDRS for this study.

It was thought that the results of the study mentioned above should be compared with a physiological pH (pH 7.4). **Figure 3.11** demonstrates the comparison of the release ratios at pH 4.0 and pH 7.4. Through the first 5 min, release concentration was slightly higher at pH 7.4 and 37°C. Besides, the difference between the release concentrations at 37°C and RT was more significant at pH 7.4. This difference proved that the thermoresponsive property of the Hydrogel_01 at pH7.4 was more clearly observed. So, it was decided that pH 7.4 is more useful for release studied in this thesis.

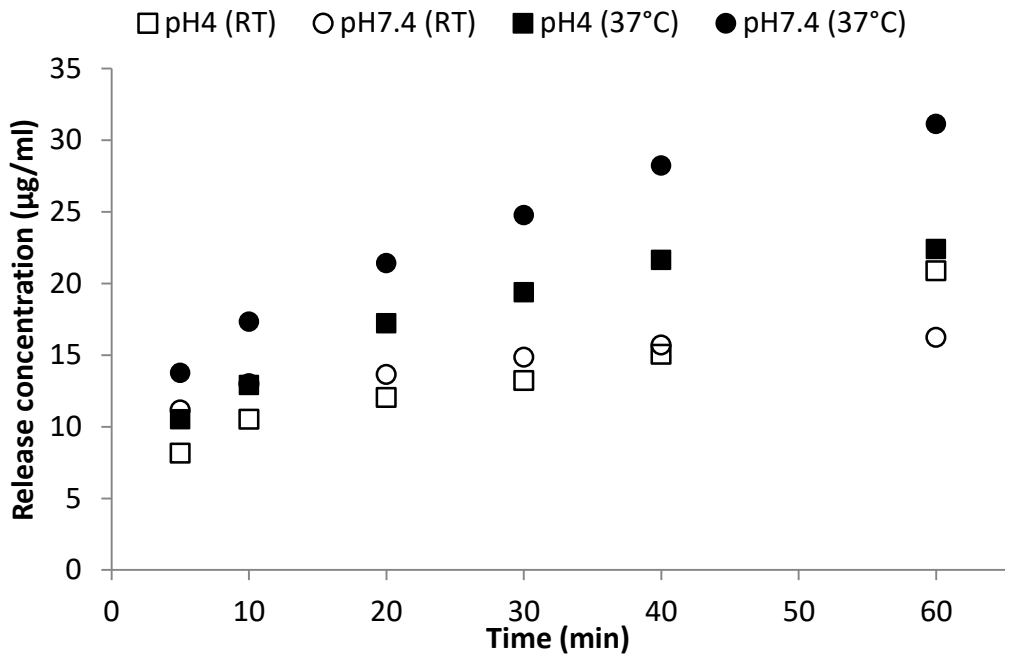

Figure 3.11 Quercetin release profiles of Hydrogel_01 at pH 4 and pH 7.4

The effects of NIPAM ratio on release performances

This part of the present thesis includes the results of release values associated with the molar ratio of NIPAM in hydrogels. Three different hydrogels, given in **Table 3.2**, that have different molar ratios of NIPAM in their structures, were investigated in terms of release behaviors. In the synthesis, other compounds and the molar ratios were kept constants for Hydrogel_01. Only the molar ratio of NIPAM of Hydrogel_01 was changed.

The yields of hydrogels were calculated as 7 %, 20 %, and 28.5%, respectively. When the molar ratio of NIPAM increased, the polymerization yield was also increased. So, monomer concentration affected the polymerization positively in this experiment.

Table 3.2 Three different hydrogels with the varied molar ratio of NIPAM

HYDROGELS	**Molar equivalencies**	
	NIPAM	**EbAM**
H-N1	1	1
H-N3	3	1
H-N10	10	1

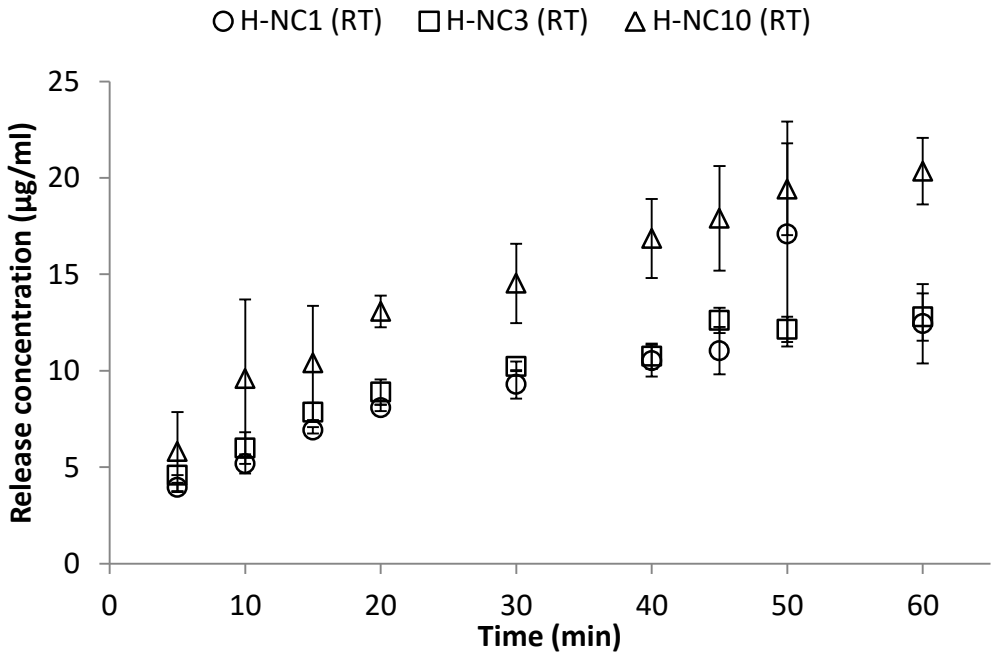

Figure 3.12 Quercetin release profiles of H-N1, H-N3, and H-N10 at RT

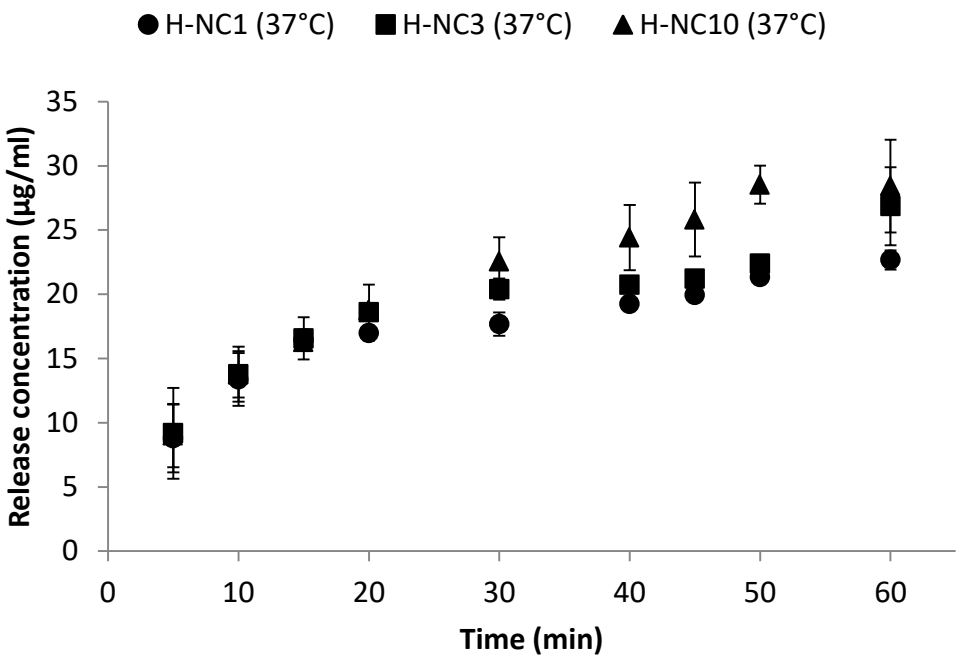

Figure 3.13 Quercetin release profiles of H-N1, H-N3, and H-N10 at 37°C

When **Figures 3.12** and **3.13** are examined, it can be seen that there is a correct proportion between the release ratio and the molar ratio of NIPAM in hydrogels. The minimum release values for both of the temperatures were obtained for H-N1

containing a minimum molar ratio of NIPAM (**Table 3.2**). When the release concentrations at RT were examined, it was observed that after the fifth minute, the difference began to occur for H-N10. Until 40 min, the release concentrations were nearly the same for H-N1 and H-N3. If the release concentrations of the hydrogels at 37°C were evaluated, no significant differences were observed between release concentrations of all of the hydrogels for the first 20 min. After 20 min, H-N10 had higher release concentrations. Release concentrations were higher at 37°C than RT, at 25°C, for all of the hydrogels. Hydrogels clearly demonstrated their thermoresponsive properties by differences between release concentrations at RT and 37°C.

The effects of different crosslinker types on release behaviors

Crosslinker types and the molar ratios were also investigated in this study. For this purpose, six different hydrogels were synthesized. The procedures of the synthesis processes were given in section 2.2.2.3 section. Detailed information releated to the hydrogels was given in **Table 2.7**. Two different types of crosslinkers were used, one is a hydrophobic crosslinker (EGDMA), and the other one is a hydrophilic crosslinker (EBAM). Both of them have different molar ratios, changing from 1 % to 25 % (**Table 2.7**). The molar ratios of other compounds such as NIPAM and DMPA were kept constant for each hydrogel. The effects of crosslinkers on yields of polymerization, and release and swelling behaviors of the hydrogels were examined.

The yields of hydrogels were calculated as 74.71%, 62.67%, 56.18%, 85.84%, 81.21%, and 93.24%, respectively, according to the hydrogels given in Table 2.7. The yields of EGDMA based hydrogels decreased when the molar ratio of EGDMA increased. The reason for this may be the hydrophobic character of the EGDMA. The yields of EbAM based hydrogels didn't decrease by increasing of EbAM and 25%EbAM had maximum yield; the reason may be the hydrophobic property of EbAM. Quercetin loading procedure was described with details in section 2.2.1.3. Following the result about quercetin solubility, 3 mg of quercetin was dissolved in 10 ml MeOH and diluted 10 times with buffer of pH 7.4 to obtain 100 μM of final quercetin concentration. Then drug loading procedure, as shown in **Figure 2.1**, was performed. Release processes were realized according to the procedure in section 2.2.1.4.

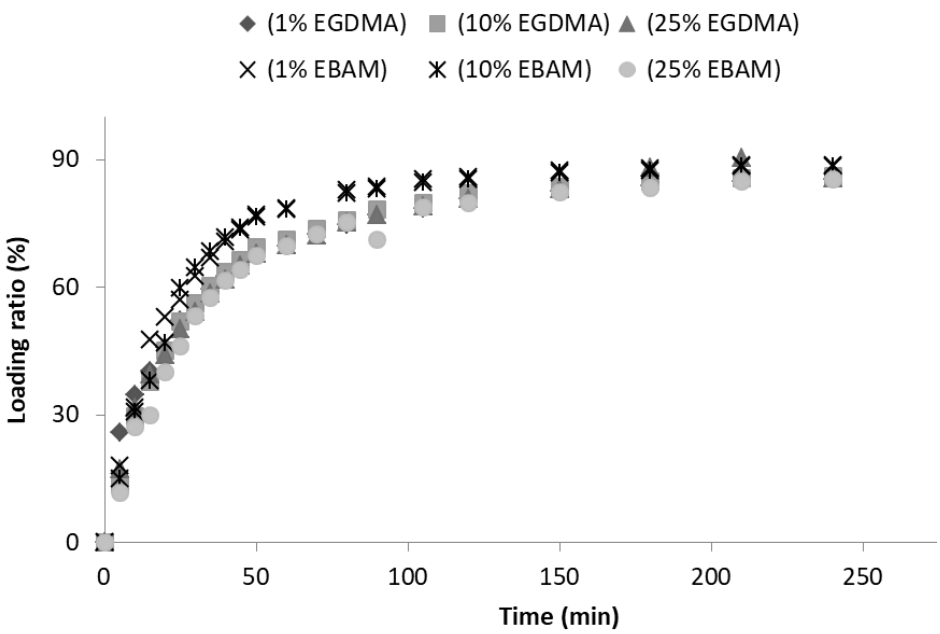

Figure 3.14 Quercetin loading ratio (%) of EbAM and EGDMA based hydrogels

Loading performances can be examined with the results presented in **Figure 3.14**. According to the loading curves, there was no significant difference between the loading performances of hydrogels.

Figure 3.15 expresses the release behaviors of the EGDMA and EbAM based thermoresponsive hydrogels. The release concentrations of EGDMA based hydrogels were detected at 20 µg/ml. There were significant differences between release concentrations at RT and 37°C for EGDMA based hydrogels.

When the release concentrations in the first 5 and 10 min were examined in detail, it was reported that the release concentrations decreased as the crosslinker concentration increased. The reason for this may be that the increase in the crosslinker concentration causes a more compact structure in the hydrogel. Therefore, the release behavior of the hydrogel may be negatively affected.

Figure 3.15 also shows the data of EbAM based hydrogels. The maximum release concentrations of EbAM based hydrogels belong to 1% EbAM as nearly 20 µg/ml. When the concentration of EbAM increased, the release concentration of EbAM based hydrogels decreased. Besides, there were significant differences between release concentrations at RT and 37°C for EbAM based hydrogels; release concentrations were higher at 37°C.

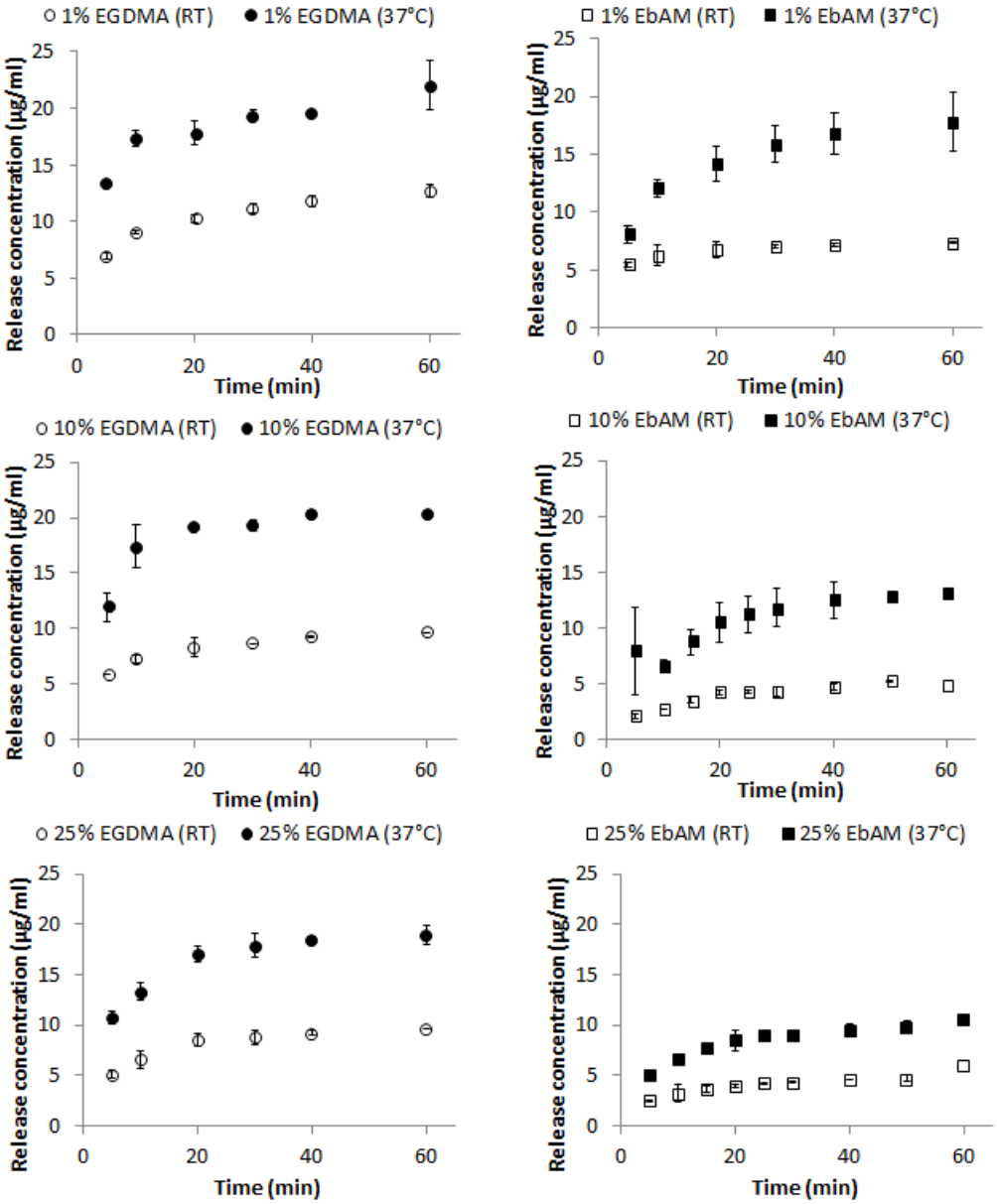

Figure 3.15 Quercetin release profiles of EGDMA and EbAM based hydrogels

When the release concentrations of EGDMA and EbAM based hydrogels were compared, in general, values of EGDMA based hydrogels were higher than EbAM based hydrogels. The reason for these release concentrations could be associated with the hydrophobic character of EGDMA and the hydrophilic character of EbAM. The release was realized at pH 7.4, so EGDMA based hydrogels shrank immediately in pH 7.4 due to its hydrophobic character. The release ratio was higher in the first 10 min for EGDMA based hydrogels at 37°C compared to RT. This can be explained by Bucatariu and coworkers (2014). They studied on loading/release performances of propranol from N-

hydroxyethylacrylamide and NIPAM based thermoresponsive hydrogels. They explained that hydrophobic interactions were favored at 37°C. Therefore they reported that a large amount of propranol was expulsed in the first 5 min mechanically due to the sudden collapse of the swollen hydrogels; then, the release rate was reduced because of steric and hydrophobic interactions. They reported that a high amount of propranol was released at the beginning of due to the "pumping effect" at 42°C (Bucatariu et al., 2014). Similar to their results, it is found in the present work that release behaviors of EGDMA based hydrogels were higher and faster at 37°C than RT by hydrophobic interactions due to EGDMA (**Figure 3.15**). On the contrary, lower release value was observed in EbAM based hydrogels due to its hydrophilic character. When EbAM concentrations increased, the affinity of the hydrogel to physiological buffer increased. Therefore hydrogels couldn't shrink easily to release quercetin. These properties could be observed for both of the temperatures, as RT and 37°C. These behaviors can be accepted as evidence for the thermoresponsive properties of hydrogels. Thermoresponsive properties were provided clearly for all of the hydrogels.

Xu and coworkers (2018) studied a quercetin-loaded thermosensitive injectable hydrogel system (Qu-M–hydrogel composites) and quercetin release from this system. The release profiles were observed approximately 9 days. 20% release value could be reached after 4 days in their study (Xuet al., 2018). Quercetin release from pure chitosan cellulose hydrogels at pH 7.4 was examined by George and coworkers (George et al., 2019). They obtained release data during 12 h, and release value was reported as approximately 15 % after 1 h (George et al., 2019).

3.1.3.3. Swelling behaviors

The swelling properties of all hydrogels were investigated according to the procedures explained in section 2.2.3. Equation 3 was used to calculate the swelling ratio. It is well known that EGDMA is a hydrophobic crosslinker while EbAM is a hydrophilic crosslinker. For that reason, the effects of these crosslinkers on swelling performances were demonstrated in **Figure 3.16**. Hydrogels, given in Table 2.7, were investigated in terms of release behaviors.

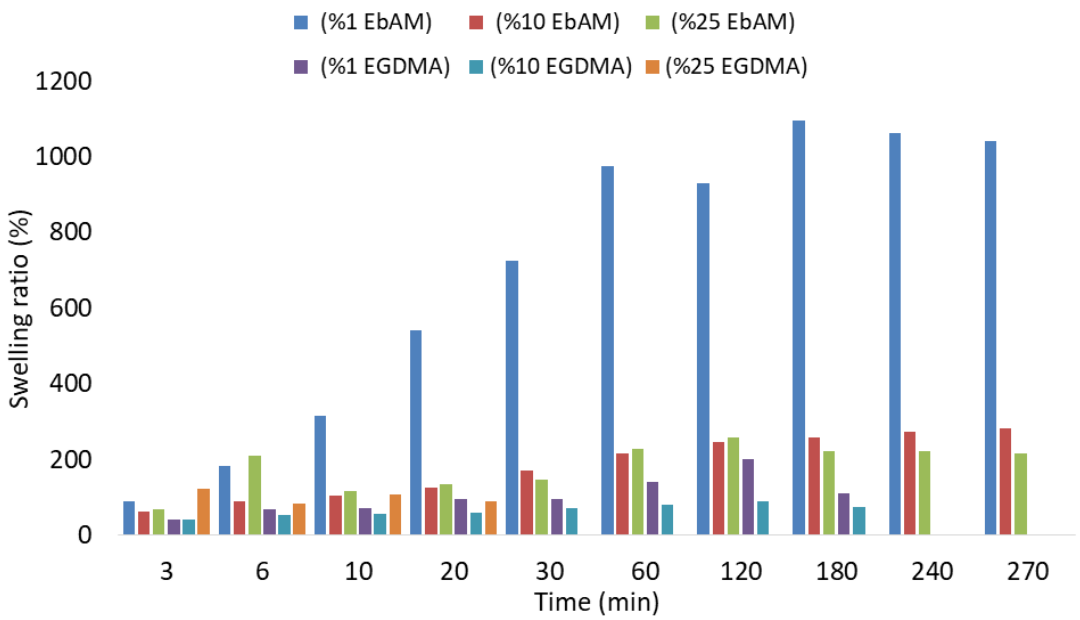

Figure 3.16. Swelling performances of EGDMA and EbAM based hydrogels

For the first 10 min, there are no significant differences between swelling properties of hydrogels except 1% EbAM. After 20 min, 25% EGDMA based hydrogel was degraded into small pieces, so that data of that hydrogel could not be obtained after 20 minutes. Similarly to this situation, swelling ratios of 1% EGDMA and 10% EGDMA based hydrogels couldn't be achieved after 180 min. Consequently, the swelling degree of EGDMA based hydrogels was lower than the others. If the results of EGDMA based hydrogels are evaluated within themselves, there was no significant difference for the first 20 min, after that 1%EGDMA had a slightly higher swelling ratio compared to 10% EGDMA. It was expected that when the ratio of crosslinker was increased, the hydrophobic interactions would increase. Thus, the 25% EGDMA had the lowest swelling behaviors.

When the EbAM based hydrogels are evaluated, it can be reported that their swelling profiles are higher than the EGDMA based hydrogels. Moreover, these hydrogels were not degraded into pieces. It has been observed that the EbAM based hydrogels have higher stability than EGDMA based hydrogels. The maximum swelling characters belong to 1% EbAM based hydrogels, and it can be reported that the ratio of EbAM increased, the swelling performance of the hydrogel decreased. As a result, it can be reported that when the crosslinker ratio increases, swelling performances decreases (**Figure 3.16**). It was supported by El-Ghazawy (2014) that the inverse proportion

between crosslinker density and swelling degree were determined (El-Ghazawy et al., 2014). Similarly, less of a swelling behavior was mentioned for the highly crosslinked hydrogel (Komatsu et al., 2019). As support these results, Zarrintaj and coworkers (2018) underlined the swelling ratio decreased with increasing the integrity of materials. Its swelling procedure was similar to that used in the present study (Zarrintaj et al., 2018). They evaluated swelling properties of gelatin-aniline dimer samples; it was observed that ratio decreased with increased aniline dimer due to its hydrophobic nature (Zarrintaj et al., 2018). Similarly, the EGDMA ratio increased while swelling behaviors decreased because of the hydrophobic properties of EGDMA. Moreover, they had a maximum swelling ratio of 600% for pure gelatin, whereas minimum swelling ratio, 300%, belonged to 40% aniline dimer material (Zarrintaj et al., 2018). However, in the present study, maximum swelling ratio related EGDMA based hydrogels was observed as approximately 300%. Nada and coworkers (2018) noted that hydrogels that included the highest cross-linking concentration showed the lowest degree of swelling. Besides, they underlined that higher cross-linking density could lead or reducing the capability of water absorption of the hydrogel (Nada et al., 2018). As supporting these results, Tang and coworkers (2017) also expressed that a high crosslinker ratio causes a low swelling ratio. Moreover, they demonstrated that the temperature-dependent swelling ratios in deionized water were measured as a function of hydrogel composition.

3.1.3.4. Characterization of hydrogels

In this study, the comparison of hydrogels was performed to see if there is a difference in the structures of EGDMA and EbAM based hydrogels. The detailed information about hydrogels is given 2.2.2.3 and Table 2.7. Additionally, their loading/release behaviors and swelling characteristics were evaluated. In this section, the structures of the hydrogels were examined by FTIR analyses. **Table 3.3** gives information about the functional groups of the hydrogels.

Figure 3.17 shows the FTIR spectra of hydrogels. EGDMA and EbAM based hydrogels have characteristic bands at 1170 cm^{-1} and 1230 cm^{-1} that refer C-O stretching and secondary Amide. 1530 cm^{-1} and 1630 cm^{-1} expressed Amide II (C-O) and Amide I (C=O) whereas 1720 cm^{-1} showed C=O (ester acrylate). The band at around 1230 cm^{-1} of EGDMA based hydrogels is weak because it comes from NIPAM only. A strong peak at

1720 cm^{-1} appeared due to the presence of acrylate ester moieties correlated with EGDMA. Therefore only EGDMA based hydrogels had this peak. CH_2 stretching vibrations are observed at 2970 cm^{-1} and bands at about 3200 cm^{-1} caused by NH_2 stretching. The bands at 2971 cm^{-1}, and 2927 cm^{-1} represent vibrations of -CH3 of the side chains of PNIPAM, -CH2 of the main chains, respectively. So these bands can be seen for all of the hydrogels.

Table 3.3 FTIR spectra of the EbAM and EGDMA based hydrogels

	wavenumbers (cm^{-1})					
Functional groups	**EBAM 1%**	**EBAM 10%**	**EBAM 25%**	**EGDMA 1%**	**EGDMA 10%**	**EGDMA 25%**
C-O secondary Amide	1130;1170 1230	1065;1170 1230	1129;1170 1239	1130;1170 1248	1129;1169 1227	1130;1169 1241
Amide II (C-O)	1530	1529	1528	1531	1535	1535
Amide I (C=O)	1633	1629	1628	1633	1639	1639
C=O (ester acrylate)				1720	1725	1721
CH_2	2927-2970	2901;2971	2933;2971	2929;2970	2922;2970	2932;2970
NH_2	3284	3279	3276;3284	3288	3284	3281

FTIR spectra of hydrogels can be seen in **Figure 3.18**. Both of EGDMA and EBAM based hydrogels have characteristic bands with their structural properties. There are some differences between the FTIR spectra of EGDMA and EbAM based hydrogels. Following the examination of FTIR spectra, the most significant differences are seen at 1720 cm^{-1} for EGDMA-based hydrogels and around 1230 cm^{-1} for EBAM-derived hydrogels. The band at 1720 cm^{-1} is directly proportional to crosslinker concentration. The intensity of the band at 1720 cm^{-1} is higher for 25% EGDMA based hydrogels than the band for 1% EGDMA based hydrogel. Therefore, it confirms that there is a correlation between the intensity of the band and the concentration of the crosslinker. Furthermore, EbAM based hydrogels have no band at the same wavenumber. Besides, Amide I and II are due to the

presence of NIPAM and EBAM in hydrogels. Therefore the intensity of these bands is seen more clearly.

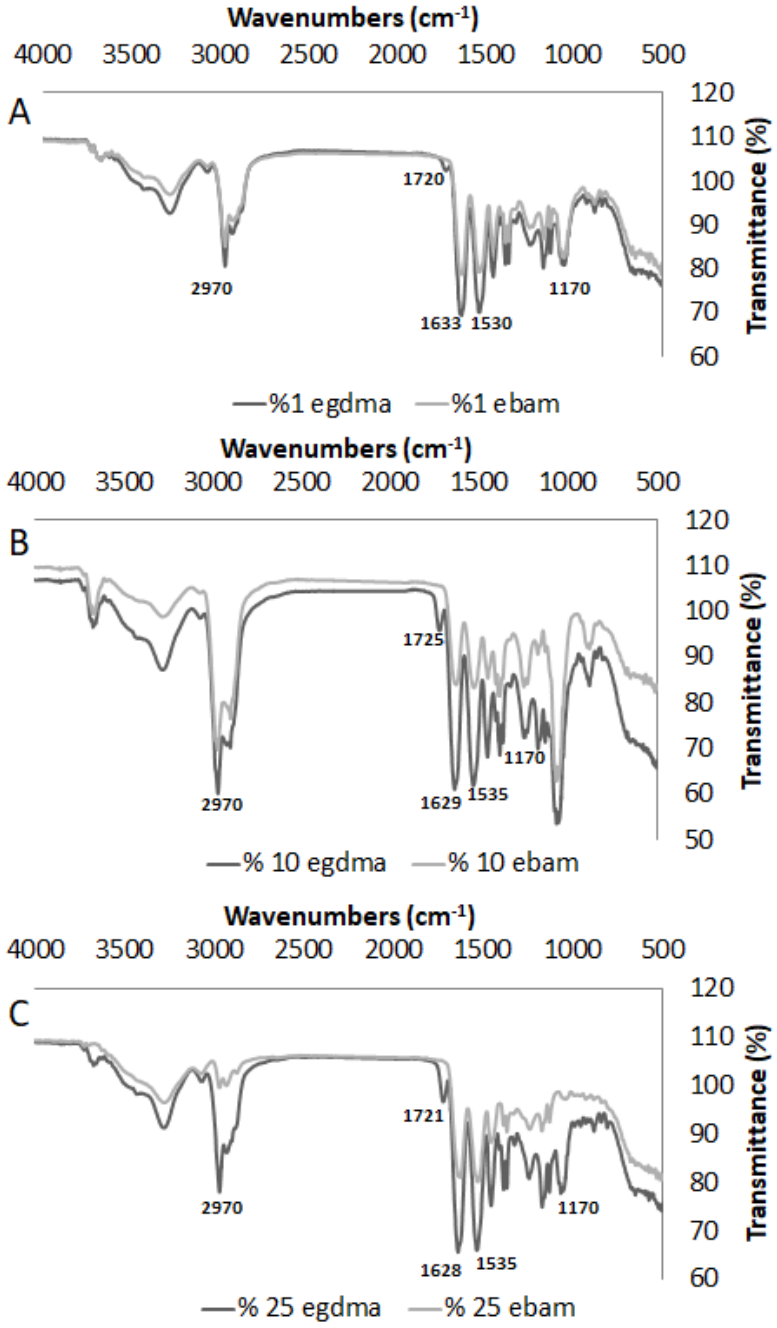

Figure 3.17 FTIR bands of EbAM and EGDMA based hydrogels (A. 1% EbAM and EGDMA; 10% EbAM and EGDMA; 25% EbAM and EGDMA)

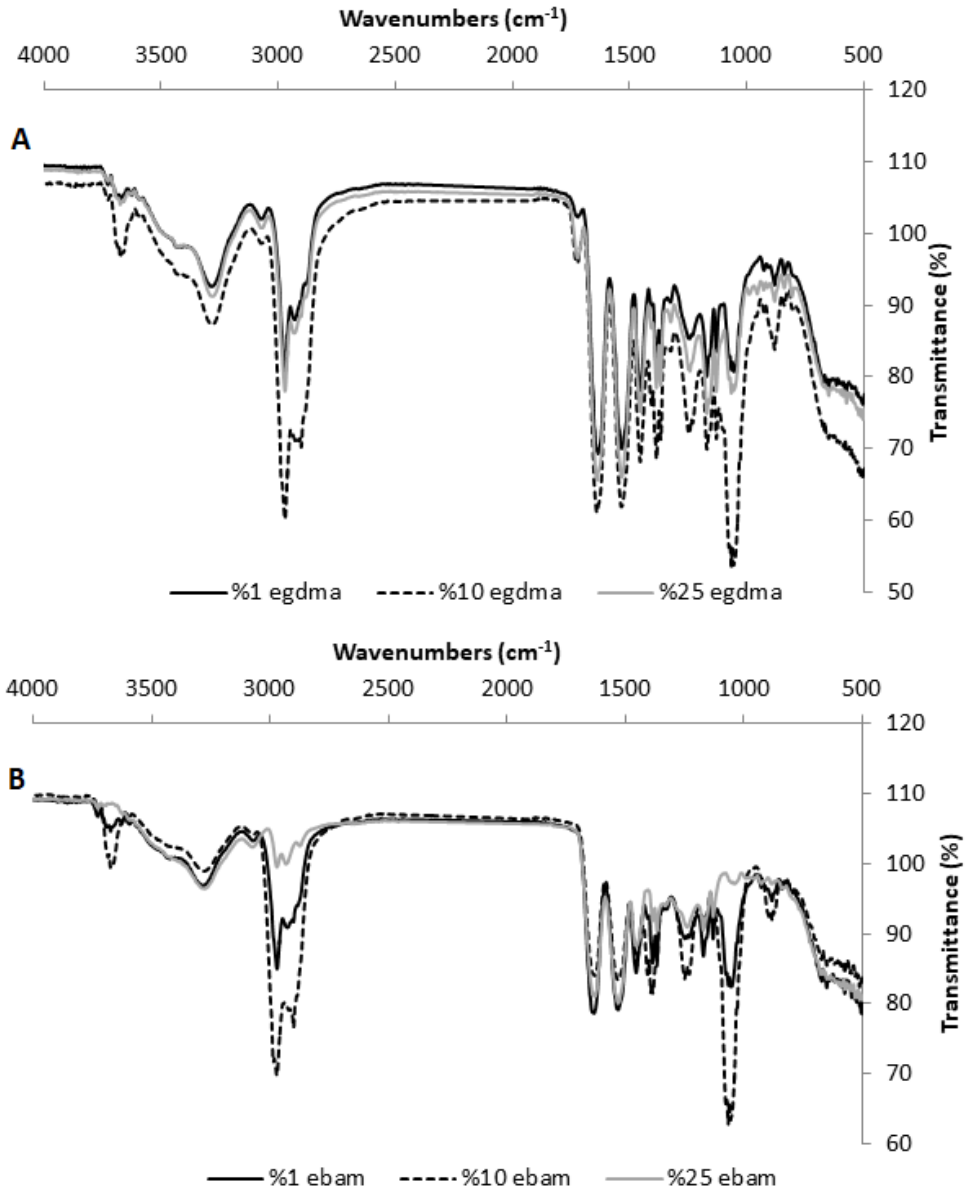

Figure 3.18 FTIR bands of hydrogels based on two different crosslinker groups (A. EGDMA based hydrogels; B. EbAM based hydrogels)

To determine whether the polymerization was successfully realized, FTIR spectra should be investigated. Following a detailed examination of **Figure 3.17** and **3.1**8, it can be concluded that there is no peak at around 1600 cm^{-1} originated from the vinyl group of monomer. So it can be understood that there is no unreacted monomer left, the polymerization occurred.

3.2. Synthesis of Thermoresponsive Hydrogels by Using Renewable Monomers

3.2.1. Characterization of renewable monomers

FTIR spectroscopy was used for the structural characterization of hydrogels and starting materials. FTIR analyses were performed around 500-4500 cm^{-1}. 32 times of scanning were realized for all samples. 4 cm^{-1} resolution was used to obtain FTIR spectra To identify the chemical bonds of the hydrogels. FTIR spectra of starting materials were matched by FTIR spectra of the hydrogels (**Table 3.4** and Figure **3.19**).

Table 3.4 FTIR spectra of the starting materials used for the synthesis

Functional groups	**Wavenumber (cm^{-1})**			
	CO	**BC**	**NIPAM**	**MDI**
C-N stretching		-	-	1103
R-OH	-	1052-1106	-	-
alkyl ethers -CH2-O-CH2	-	1159	-	-
hydrogen bending vibrations	1459	-	-	-
amide II			1544	1517
amide I			1617	-
ester carbonyl groups	1741	-	-	-
–N=C=O groups			-	2240
CH vibration	2854-2923	2800-2970	2933;2967	-
OH absorption band	3500	3000-3700	-	-
NH stretching	-	-	3280	-

Characteristic of FTIR bands for CO are seen in **Figure 3.19-A** and **Table 3.4**; the bands at 1459 cm^{-1}, 1741 cm^{-1}, 2854 $cm^{-1,}$ and 2923 cm^{-1} are specific for CO. 1459 cm^{-1} indicates the hydrogen bending vibrations while asymmetrical CH_3 deformations refer the band at 1450 cm^{-1}. Ester carbonyl groups can be observed as a strong band at 1741 cm^{-1} (Bellamy, 1975). 2900 cm^{-1} refers CH vibration, 3500 cm^{-1} expresses the OH absorption. Similarly to these results (**Table 3.4**) regarding CO, the characteristic bands for CO were detected at 1745 cm^{-1} and 3500 cm^{-1} that expressed terminated hydroxyl groups and a carbonyl (C=O) of aliphatic ester as reported by Kunduru et al., 2015.

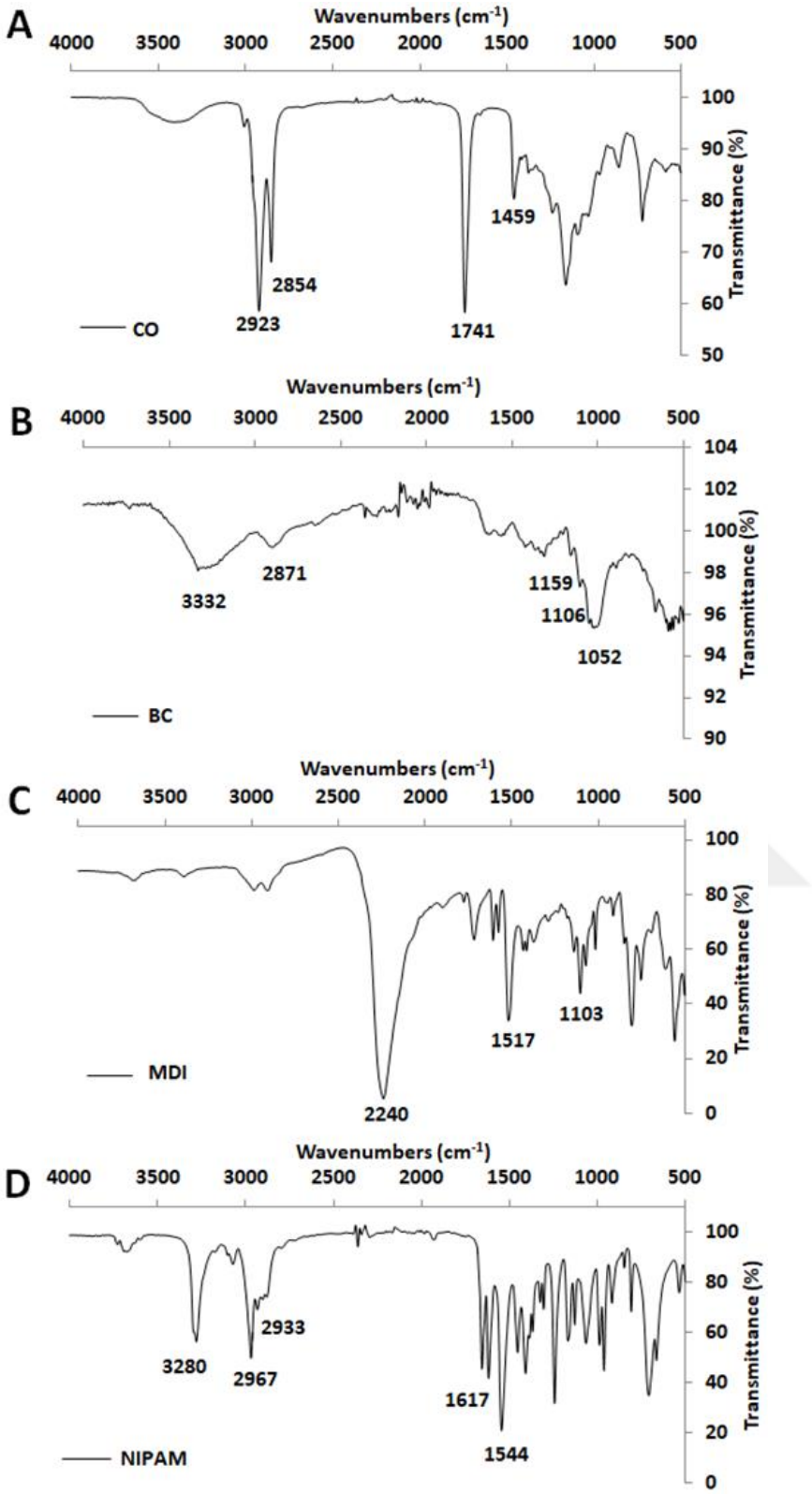

Figure 3.19. FTIR spectra of starting materials; CO (A), BC (B), MDI (C), and NIPAM (D).

BC has characteristic bands at 1052 cm^{-1}, 1106 cm^{-1}, 1159 cm^{-1}, 2871 cm^{-1} and 3332 cm^{-1} (**Figure 3.19-B**). R-OH was indicated by the bands around 1052 cm^{-1}, 1106 cm^{-1} (Gao et al., 2011). The band at 1159 cm^{-1} presents alkyl ethers -CH2-O-CH2-. 2800 cm^{-1} and 2970 cm^{-1} refer –CH stretching, whereas –OH stretching is seen as a broad band at 3000-3700 cm^{-1}. FTIR spectra of BC were evaluated by Auta and coworkers (Auta et al., 2017). The band at 1153 cm^{-1} caused by asymmetrical C-O-C stretching whereas the band at 2950 cm^{-1} occurred due to C-H stretching, reported by Auta et al., 2019 (Auta et al., 2017).

The characteristic bands of MDI were observed near 1103 cm^{-1}, 1517 cm^{-1}, and 2240 cm^{-1} (**Figure 3.19-C**). A strong band was indicated near 1100 cm^{-1} corresponding C-N stretching of -C-N=O compounds. Furthermore, C-N stretching of MDI can be seen as a band at 1103 cm^{-1}. The band at 1517 cm^{-1} is due to amide II that has lower frequencies in the solution. 2240 cm^{-1} refers –N=C=O groups as expresed by Wong et al. (2012). The results of the last part of Figure 3.19-D are fixed to NIPAM; CH_3 stretching can be seen at 2933 cm^{-1} and 2967 cm^{-1}, while the band at 3280 cm^{-1} is due to NH stretching (Bellamy, 1975).

3.2.2. Synthesis and characterization of AMR based thermoresponsive hydrogels

The purpose of this study is to employ a renewable material based crosslinker, AMR, instead of chemical ones. Four different hydrogels were synthesized with AMR as a crosslinker according to the procedure described in the 2.2.2.4 and **Table 2.8**. The synthesis of hydrogels was performed with varied molar ratios of AMR (**Table 3.5**). NIPAM was used as a thermoresponsive monomer, and DMPA was used as a photoinitiator. The yields of AMR based hydrogels, AMR0.01, AMR0.04, AMR0.10, AMR0.25, were 45%, 12%, 22%, and 10%, respectively.

When the yields were examined, it could be reported roughly that the yields decreased as the ratio of AMR increased. The reason for this situation may be the oil-based structure of the AMR. Furthermore, the use of an aqueous medium as the polymerization solvent may have caused some solubility problems for AMR. As the concentration of AMR increased, the number of intermolecular hydrophobic interactions of AMR increased as well. Due to the presence of water in the medium, all AMR molecules could not take place in the reaction, and this process may have caused a decrease in the yield.

Table 3.5. AMR based thermoresponsive hydrogels

Hydrogels	Equivalencies of Monomers in Hydrogels	
	AMR	NIPAM
AMR0.01	0.01	1
AMR0.04	0.04	1
AMR0.10	0.10	1
AMR0.25	0.25	1

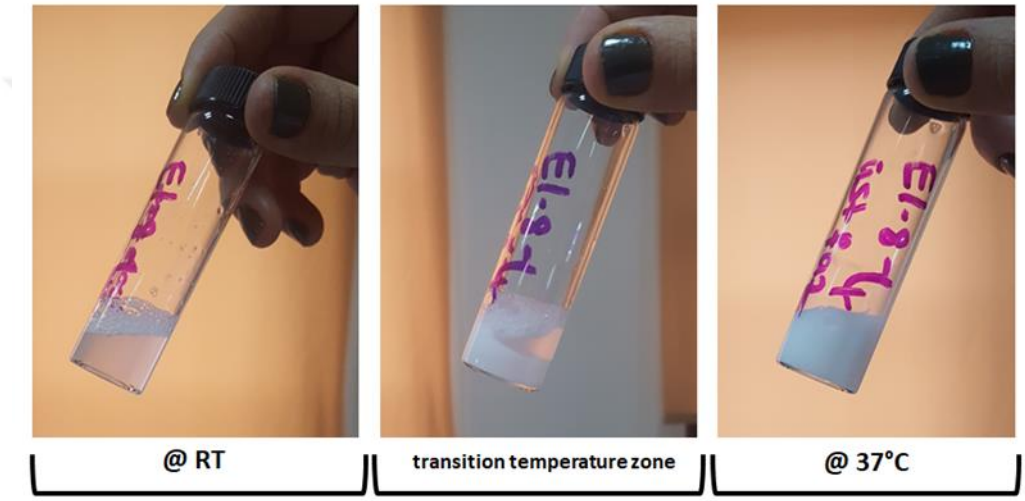

Figure 3.20 Thermoresponsive behavior of AMR0.01

3.2.2.1. Characterization of the hydrogels

In this section, four different hydrogels were investigated according to their FTIR spectra. The detailed information about hydrogels was given in **Table 2.8**, and **Table 3.5** and **Figure 3.21**. Additionally, the synthesis procedure was explained in 2.2.1.5.

The FTIR bands related to AMR based hydrogels are given in **Table 3.6**.

In **Figure 3.21**, amide-I, amide-II were demonstrated at 1639 cm^{-1} (1643 cm^{-1} for AMR0.10 and 1658 cm^{-1} for AMR0.25), 1536 cm^{-1} (1535 cm^{-1} for AMR0.04 and AMR0.10) and 1533 cm^{-1} (for AMR0.25), respectively.

It was observed that all of the hydrogels have characteristic bands: 1170 cm^{-1} (1168 cm^{-1} for AMR0.10 and 1166 cm^{-1} for AMR0.25) was detected for C-O stretching, 1243 cm^{-1} (1245 cm^{-1} for AMR0.04 and AMR0.25) refered secondary amide, 1536 cm^{-1} (1535 cm^{-}

^{1} for AMR0.04 and AMR0.10) and 1533 cm^{-1} (for AMR0.25) expressed amide II (C-O) and 1639 cm^{-1} (for AMR0.01 and AMR0.04) demonstrated amide I (C=O) (Bellamy, 1975). In addition, CH_2 stretching vibrations are expressed at 2970 cm^{-1} and bands at around 3200 cm^{-1} indicated by NH_2 stretching. Similarly to these results, Auta et al. (2017) reported that -C-O-C- was seen at 1220 cm^{-1}, -C=C and -C-N were detected at 1525 cm^{-1} and 1600 cm^{-1} whereas -C=O was referred at 1700 cm^{-1} and –NH was expressed at 3290 cm^{-1}.

Table 3.6 FTIR spectra of the AMR based hydrogels

	wavenumbers (cm^{-1})			
Functional groups	**AMR0.01**	**AMR0.04**	**AMR0.10**	**AMR0.25**
$CH=CH_2$	985	985	985	985
C-O	1130;1170	1065;1170	1130;1168	1132;1166
secondary Amide	1243	1245	1243	1245
hydrogen bending vibrations	1457	1455	1455	1455
Amide II (C-O)	1536	1535	1535	1533
Amide I (C=O)	1639	1639	1643	1658
C=O (ester acrylate)	1725	1724	1725	1725
CH_2	2917;2969	2931;2971	2927;2967	2925
NH_2	3278	3280	3276	3297

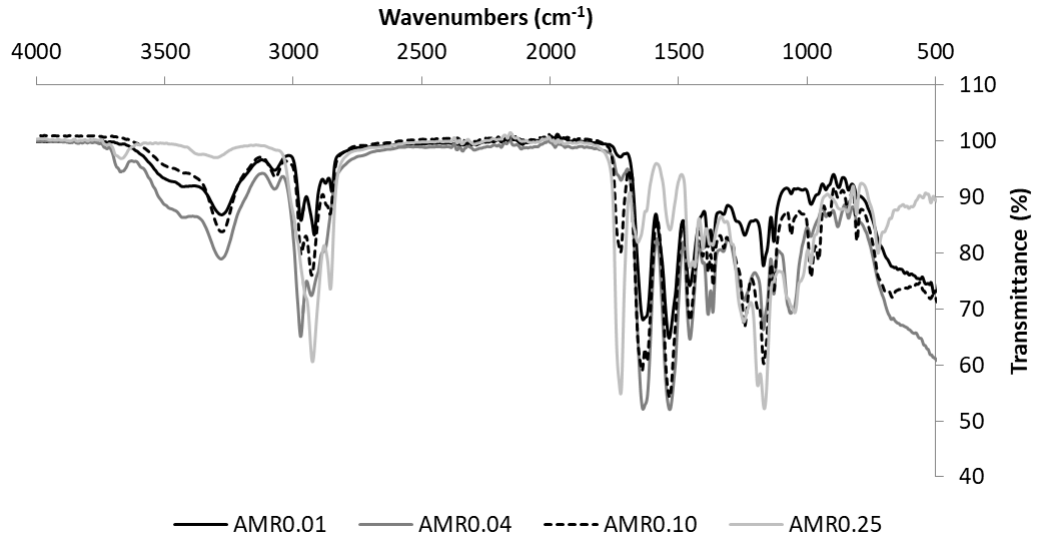

Figure 3.21 FTIR bands of AMR based hydrogels based

The bands specified for AMR, were demonstrated by Cakir Hatir et al. (2019). They reported that characteristic bands of AMR were observed at 1739, 1722, 1404, 1269, 1192, 1045, 985, and 810 cm^{-1} (Hatir et al., 2019). Most of these bands couldn't be observed in **Table 3.6**. Furthermore, in **Table 3.6**, a strong peak at 1725 cm^{-1} (1724 cm^{-1} for AMR0.04) was observed for hydrogels instead of two separate ester carbonyl bands at 1739 and 1722 cm^{-1}. Therefore, the two ester groups shifted to 1725 cm^{-1}, and one ester carbonyl was detected instead of two peaks because saturated ester moieties were generated by the polymerization of the acrylate groups. This is the evidence of the synthesis of AMR based hydrogels successfully.

3.2.2.2. Release behaviors

Loading procedure was explained in section 2.2.1.3, 100 µM was used as the initial quercetin concentration. The release procedure was described in section 2.2.1.4. The 60 min. release profiles of hydrogels at RT and 37°C are given in **Figure 3.22** and **3.23**.

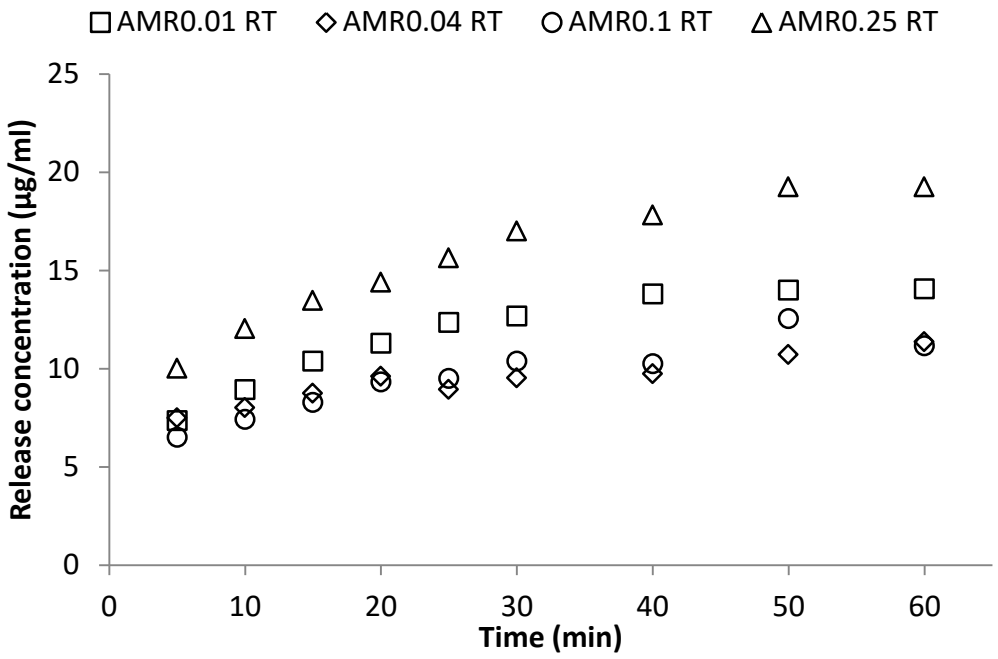

Figure 3.22 Release profiles of AMR based hydrogels at RT

Figure 3.22 shows the release profiles of AMR based hydrogels at RT. For the first 5 min, AMR0.25 had higher release concentration. After the first 10 min, the release concentration of AMR0.01 also increased due to its lower compact structures. Any

significant differences were not detected for other AMR based hydrogels. The effects of the molar ratio of AMR on release concentrations of the hydrogels were detected significantly for only AMR0.25.

The release concentrations of AMR based hydrogels at 37 °C were examined in **Figure 3.23**. For the first 5 min, significant differences were obtained between release concentrations of the hydrogels. AMR0.25 had higher release concentration due to its higher AMR ratio. Hydrophobicity of AMR0.25 increased due to the oil-based nature of AMR in the physiological buffer during release performances. The behavior of AMR0.25 based on hydrophobicity was supported by the data in **Figure 3.26**, including swelling experiments. After 25 min, the difference between release concentrations of AMR0.04 and AMR0.1 decreased. However, the differences between the release profiles of AMR0.01 and AMR0.25 were remarkable. After 50 minutes, the release concentrations of the AMR0.04, AMR0.1 and AMR0.25, except AMR0.01, were very close to each other.

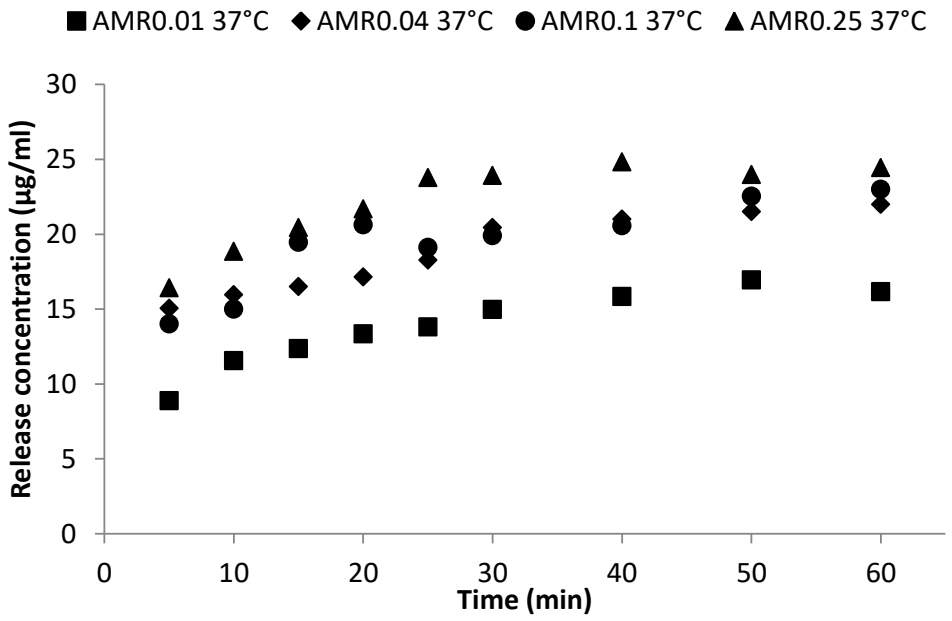

Figure 3.23. Release profiles of AMR based hydrogels at 37 °C

In this experiment, AMR0.25 had maximum release concentrations. This hydrogel was obtained by using AMR, a renewable material. For understanding the success of using AMR as a crosslinker, the release profile of the AMR0.25 hydrogel was compared with

the release performances of 25% EGDMA hydrogel. The release concentrations were given in **Figure 3.24**.

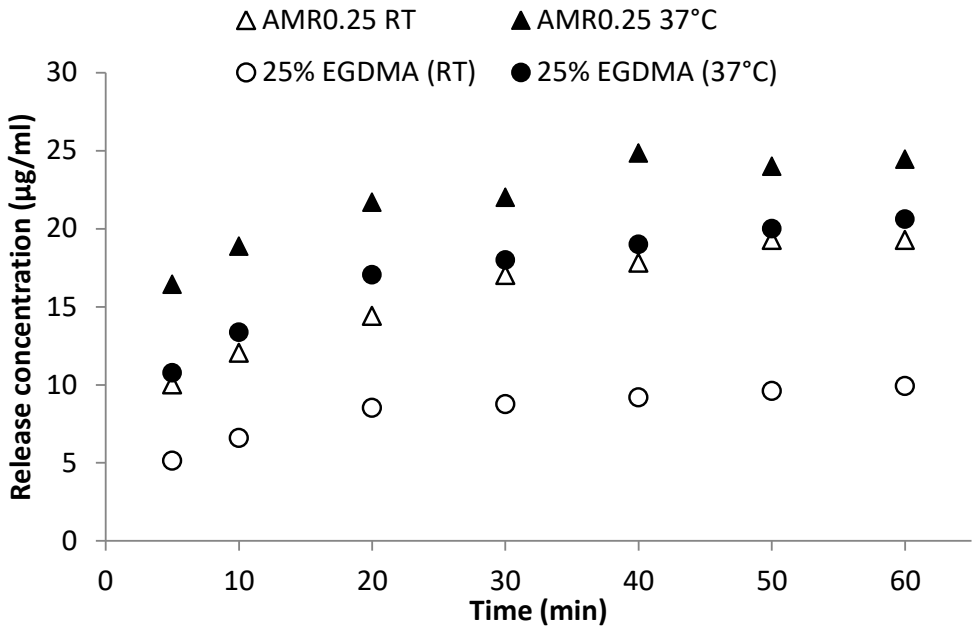

Figure 3.24. Release profiles of AMR0.25 and 25% EGDMA

When **Figure 3.24** was evaluated, AMR0.25 had higher release concentrations than the values of 25% EGDMA for both of the RT and 37°C. As the differences between release concentrations at RT increased over time, release concentrations at 37°C were getting closer to each other over time. **Figure 3.24** is the evidence for thermoresponsive characters of the AMR based hydrogels.

3.2.2.3. Swelling performances

The swelling procedure of AMR based hydrogels was expressed in detail in section 2.2.2.4, Table 2.8, and Table 3.5. The hydrogels were named as AMR0.01, AMR0.04, AMR0.10, and AMR0.25. The swelling properties of the hydrogels were investigated according to the procedures explained in section 2.2.3. Equation 3 was used to calculate the swelling ratio.

Figure 3.25 shows the swelling behaviors of the hydrogels. The initial dry form of hydrogels is seen in **Figure 3.25-A**. Depending on the swelling behavior of the hydrogel, size of the hydrogel changed over time. After 10 minutes of incubation, there was a noticeable difference in the size of the hydrogel (**Figure 3.25-B**). **Figure 3.26**

supported this situation with numerical data. The swelling ratio of AMR0.01 was reported as 200% in the first 10 minutes of incubation.

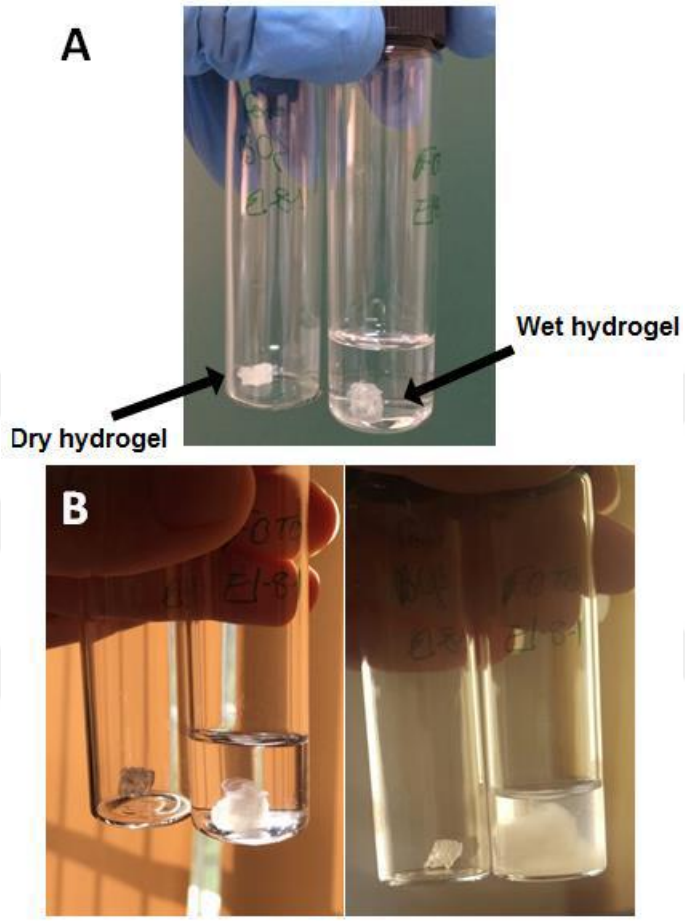

Figure 3.25-A The swelling procedure, swelling behavior of the AMR0.01 in water (t=0), **B**. Swelling behavior of the hydrogel in the water at t=10 min (left) and t=24 hours (right)

Figure 3.26 also shows the swelling data of AMR based hydrogels. For the first 3 min, AMR0.25 had the least swelling ratio, whereas AMR0.10 and AMR0.04 had maximum values. After 3 min, AMR0.25 had the lowest swelling ratio, whereas AMR0.01 showed a good swelling profile. In 6th min, AMR0.01 and AMR0.04 had a higher release ratio than AMR0.10 and AMR0.25. If the swelling ratios in the 10th min were examined, it was seen that the AMR0.25 still has the lowest ratio, while the biggest increase was observed with AMR0.01. After 60 min, AMR0.25 was broken up into pieces. AMR0.25 had the highest AMR ratio in its structure, and its swelling ratios were lower than the

other hydrogels due to the oil-based nature of AMR. According to these results, it can be said that increase in hydrophobicity causes a decrease in swelling ratio.

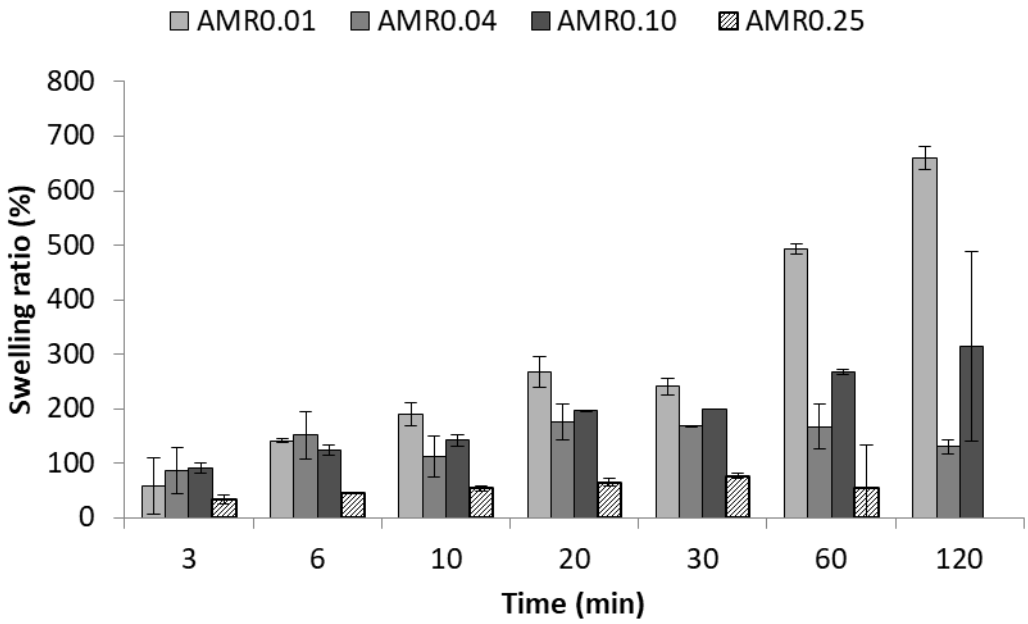

Figure 3.26. The swelling data of AMR based hydrogels

Furthermore, AMR0.01 had the highest swelling ratio after the first 10 min. The reason for this may be the low molar ratio of AMR, in other word hydrophobic character.

Komatsu et al. (2019) reported that when the crosslinking degree is high in a hydrogel, it shows less swelling behavior compared to the hydrogel having a low crosslinking degree. Besides, it was proved that if the crosslinker density increases, the swelling ratio would decrease (El-Ghazawy et al., 2014). As seen in Figure 3.23, this result is associated with AMR based hydrogels. Moreover, Luo also indicated that the crosslinker ratio plays an important role in swelling performances (Luo et al., 2018).

3.2.3. CO based thermoresponsive hydrogels

CO based hydrogels were synthesized according to the procedure in section 2.2.2.5, and detailed information was given in **Table 2.9**. There were four groups of hydrogels in this part; their codes and properties were provided in **Table 3.7**. Two of them have BC and MDI, and the molar ratio of CO, the glucose unit of BC and MDI was set as 1:1:1 for both of the hydrogels. Besides that, both of them have NIPAM and MBAM to gain thermoresponsive characters. The yields of H-WCOT and H-NCOT in Table 2.11, were

16.3% and 34.2%, respectively. Distilled water was used as the solvent for polymerization of the H-WCOT and H-NCOT. The oil-based structure of CO caused some difficulties in the water. Therefore the yield of H-WCOT was lower than the yield of H-NCOT.

Table 3.7 The code of CO based hydrogels

Codes of the hydrogels	Properties of the hydrogels
H-WCO	The hydrogel with CO and without thermoresponsive properties
H-NCO	The hydrogel without CO and thermoresponsive properties
H-WCOT	The hydrogel with CO and thermoresponsive properties
H-NCOT	The hydrogel without CO and with thermoresponsive properties

3.2.3.1. Characterization of the hydrogels

In this part, firstly, structural analyzes were performed with FTIR spectra, then thermal characterizations of the hydrogels were investigated. Moreover, the surface properties were evaluated by SEM. The purpose of this section is to understand the effects of CO on the thermal properties and structures of hydrogels.

Structural characterization

FTIR analyzes of H-WCOT and H-NCOT was evaluated in this part of the present thesis. Additionally, hydrogels with and without CO were investigated before and after gaining thermoresponsive properties. FTIR spectra were obtained before and after introducing NIPAM to hydrogels, and the FTIR bands were examined in detail in **Figure 3.27**.

Table 3.8 shows the bands of hydrogels with/without CO after introducing NIPAM.

Figure 3.27 shows that both of the CO based thermoresponsive hydrogels have bands at 2927 cm^{-1} and 2969 cm^{-1} (**Figure 3.27-A and B**), The specific bands for NIPAM can also be observed at 2933 cm^{-1} and 2967 cm^{-1}(**Figure 3.19-D**). Besides that, the band at 3280 cm^{-1} is distinctive for NIPAM (**Figure 3.19-D**). When hydrogels have thermoresponsive properties, H-WCOT and H-NCOT have a band at 3282 cm^{-1} and

3286 cm^{-1}. Furthermore, when the bands are examined, only the hydrogels with thermoresponsive characters have amide-I, and amide-II groups that confirm the presence of NIPAM in the hydrohels. In **Figure 3.27**, amide-I can be evaluated at 1639 cm^{-1} (for H-WCOT and H-NCOT) whereas amide-II is examined at 1533 cm^{-1} (for H-WCOT) and 1531 cm^{-1} (for H-NCOT). Furthermore, these bands cannot be detected for hydrogels without thermoresponsive characters. This situation provides that both of the hydrogels successfully demonstrated thermoresponsive characteristics.

Table 3.8. FTIR spectra of the CO based hydrogels

Functional groups	**Wavenumber (cm^{-1})**	
	H-WCOT	**H-NCOT**
C-O	1170	1168
secondary Amide	1232	1230
Amide II (C-O)	1533	1531
Amide I (C=O)	1639	1639
ester carbonyl groups	1741	-
CH vibration	2927	2927
CH vibration	2969	2969
NH stretching	3282	3286

When the bands of the H-WCOT and H-NCOT were analyzed, it was observed that both of the hydrogels (H-WCOT and H-NCOT) have characteristic bands at 1170 cm^{-1} (1168 cm^{-1} for H-NCOT) and 1232 cm^{-1} (1230 cm^{-1} for H-NCOT) related to C-O stretching and secondary amide whereas 1533 cm^{-1} (1531 cm^{-1} for H-NCOT) and 1639 cm^{-1} refered C-O (amide II) and C=O (amide I). Besides, there is no significant difference between the spectra of hydrogels with thermoresponsive properties. The reason may be that the FTIR spectrum of the urethane group derived from MDI is very similar to the amide group of PNIPAAm. Auta and coworkers indicated that -C-O-C- and -C=C were demonstrated at 1220 cm^{-1}, 1525 cm^{-1} whereas -C-N was detected at 1600 cm^{-1}. Besides, -C=O and –NH were detected, 1700 cm^{-1}, and 3290 cm^{-1} (Auta et al.,2017).

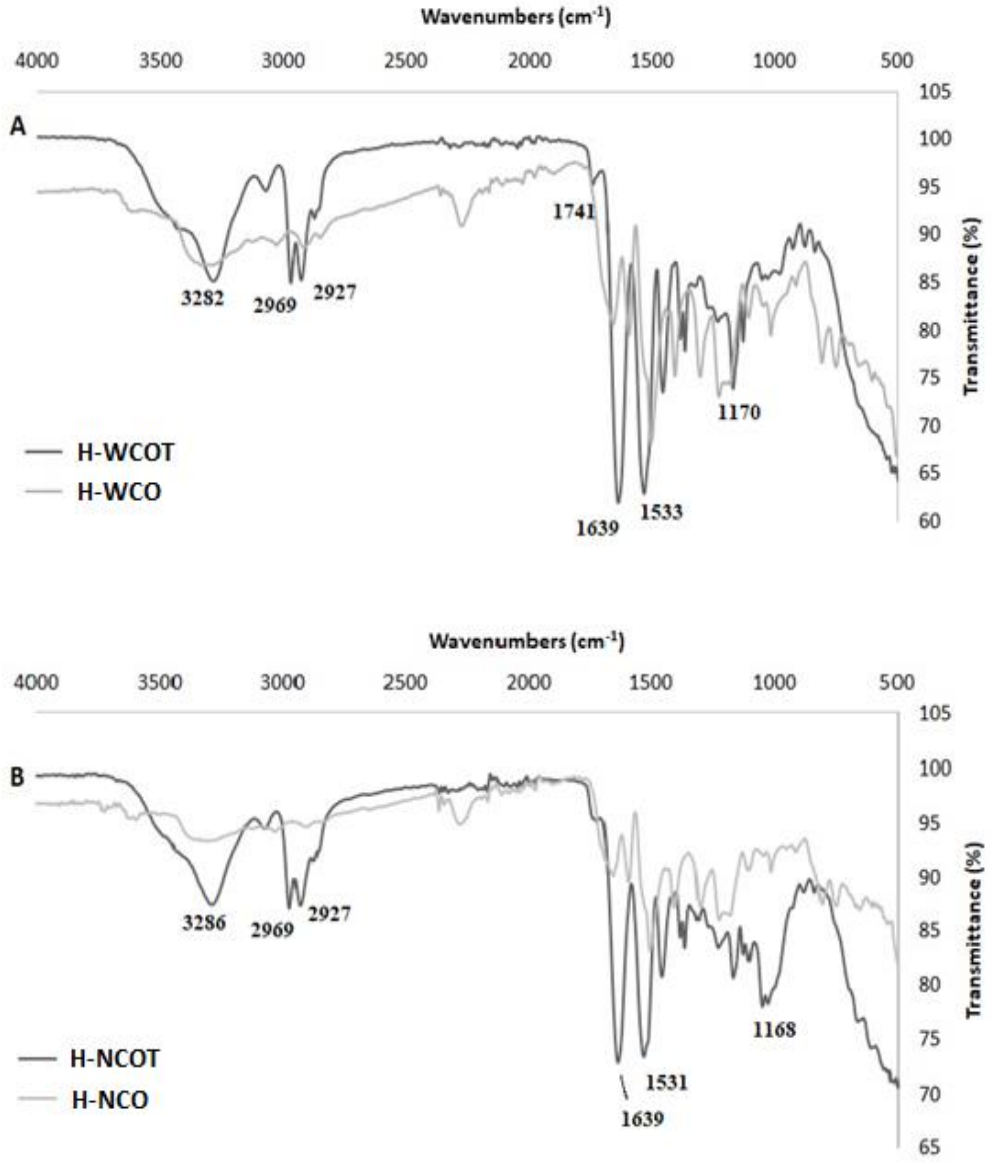

Figure 3.27. FTIR spectra of CO based thermoresponsive hydrogels (A. H-COT and H-WCO; B. H-NCOT and H-NCO)

The critical factor analysed in this study is the presence of CO. Therefore, after confirmation of the thermoresponsive properties of hydrogels, the FTIR bands related to CO were examined. It was seen in **Figure 3.19-A** and **Table 3.4** that CO has a specific band at 1741 cm^{-1}. As expected, only the hydrogel with CO has this band in its spectrum. In contrast, any band at around 1741 cm^{-1} was observed for hydrogel without CO.

In literature, it is reported that the bands at 1730 cm^{-1} and 3350 cm^{-1} are corresponding for ester C=O stretching and O–H functional group, these bands confirmed the esterification reaction of polyol (Salmiah et al., 2015). Additionally, it is stated that C=O bond gives the band at around 1740 cm^{-1}. In another study related to PNIPAAm brushes on the wet BC sheet, obtaning new bands at around 1642 cm^{-1} and 1538 cm^{-1} was reported (Alosmanov et al., 2017).These bands expressed the amide I and amide II stretch vibrations of PNIPAM and the results obtained in this study are consistent with these bands.

Thermal characterization

DSC and TGA were used for the thermal characterization of the CO based hydrogels, H-WCOT and H-NCOT.

DSC thermograms of hydrogels can be seen in **Figure 3.28**.

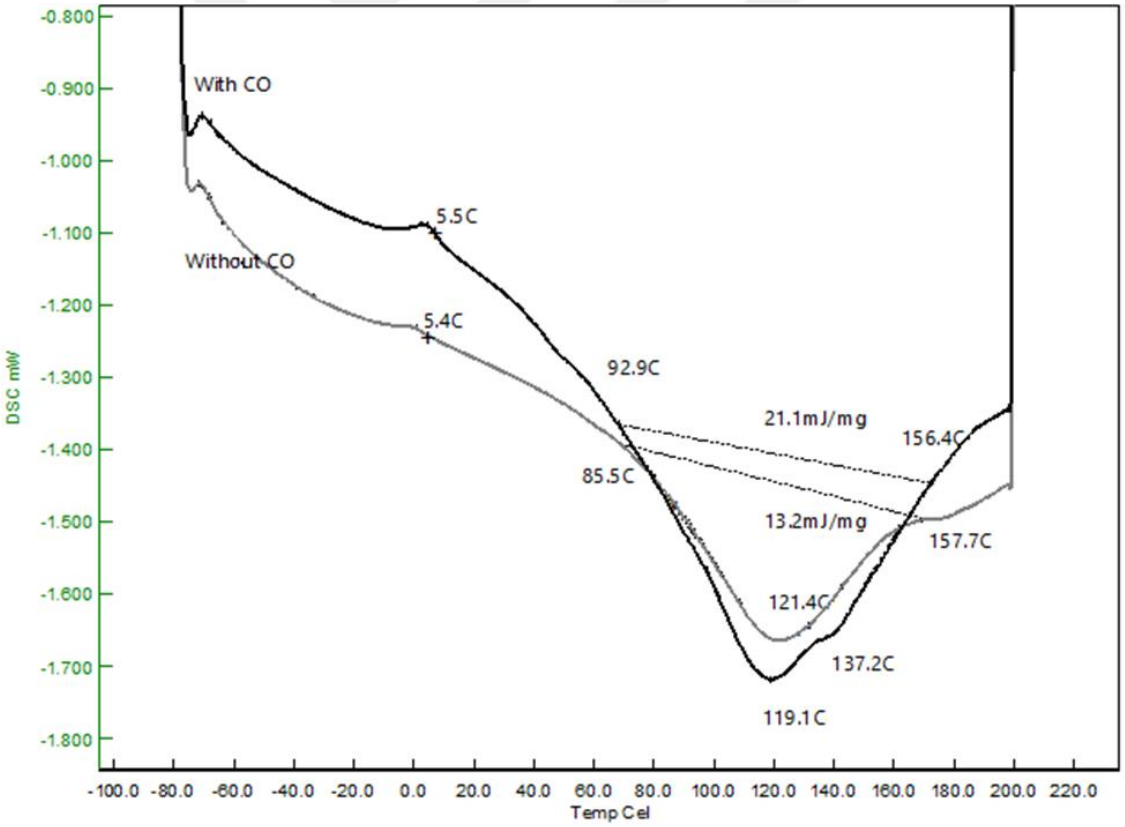

Figure 3.28. DSC curves of H-WCOT and H-NCOT

Both of the hydrogels indicate a Tg at 5°C. Besides, melting behavior was observed from 20 to 180°C (**Table 3.9**).

It can be seen in **Table 3.9** that hydrogel with CO had sharper melting behavior, and 21.1 mJ/mg was measured as absorbed heat. Furthermore, it can be claimed that H-WCOT consumed only 13.2 mJ/mg. H-WCOT had MDI modified BC covered surface; bounded CO segments may be caused for high endotherm, wide melting and sharp peak. TGA results of the CO based hydrogels can be seen in **Figure 3.29**. Experiments were realized under a nitrogen atmosphere and the rate was 200 ml/min, and the rate of heating was 10°C/min.

Table 3.9. Thermal features of H-WCOT and H-NCOT

Polymer	Tg (°C)	Melting Heat (mJ/mg)	Melting Temperature (°C)	5% weight loss temperature (°C)	50% weight loss temperature (°C)
H-WCOT	5.5	21.1	119	110	378
H-NCOT	5.4	13.2	121	139	380

Temperature was changing between 0 and 600°C. According to results, two main segmental losses were obtained for all samples. There are two important parameters to evaluate the thermal behaviors of hydrogels; these are 5% weight lost temperature and 50% weight lost temperature (**Table 3.9 and Figure 3.29**). It was observed that H-WCOT had the highest 5% weight loss temperature at 139°C. H-WCOT demonstrates that the temperature at 110°C. Moreover, both of hydrogels exhibit a 50% weight loss of around 380°C.

Thermal stability of hydrogels can be evaluated with these results. High 5% and 50% temperatures can be defined as the indicators of high thermal resistance. Therefore, these values may be a good indicators for high operating temperatures for hydrogels.

Surface characterization

Surface properties of hydrogels were examined by SEM images of hydrogels (**Figure 3.30**). **Figure 3.30** exhibits SEM images of H-WCOT (A and B) and H-NCOT (C and D), respectively, while both of hydrogels have thermoresponsive features.

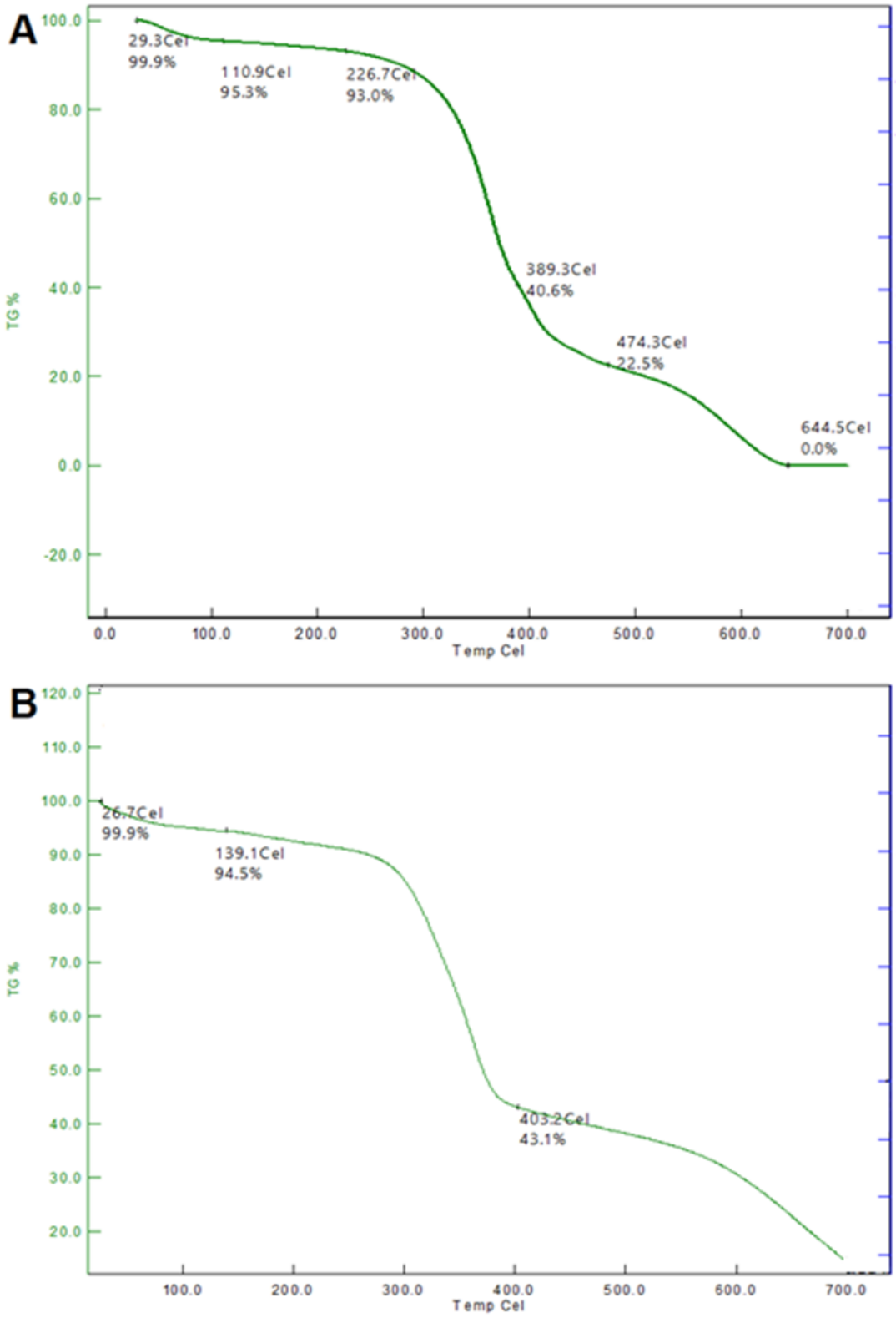

Figure 3.29. TGA curves of CO based hydrogels **A.** H-WCOT; **B.** H-NCOT

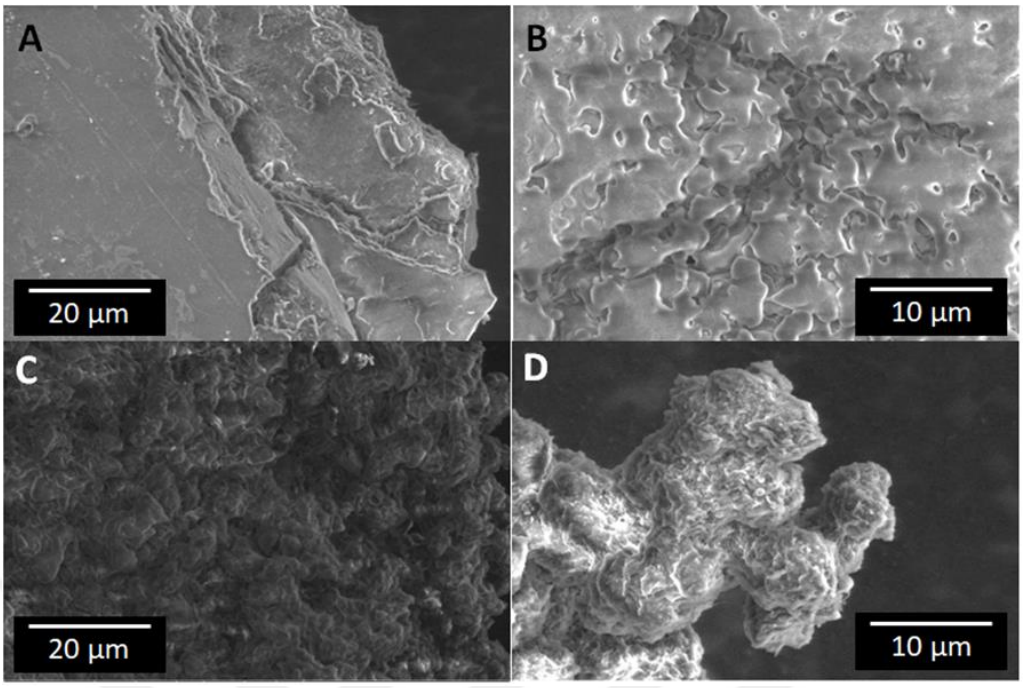

Figure 3.30. SEM images of H-WCOT (A, B) and H-NCOT (C, D).

When the SEM images were analyzed, it was reported that H-WCOT had a layered, homogenous and flat structure and H-NCOT had a spongy structure. Neto et al., 2019 support results obtained in this work. Besides, Wang et al. (2018) reported that the structure of pure BC was in the vertical direction as an excellent layered structure. However, they indicated that the layered structure of BC disappeared due to new BC/PNIPAM composite and porous morphology (Wang et al., 2018). In another study, it was confirmed that the structure of cellulose based composite had capillary effect and more surface area and due to their folds and undulation on their surface (Luo et al., 2018).

In this study, the surface properties of H-NCOT coincided with the informations in the literature as it was reported that cellulose based composites had the spongy structures. One of the reasons for the layered structure of incorporated CO to the BC/NIPAM composite was that pure CO has layered structure (Neto et al., 2019). In this thesis, it was believed that the surface of H-WCOT was modified with CO which covered the surface of MDI modified BC layer by layer. This situation caused the layered architecture for hydrogel with CO. It has also been proven that allyl CO groups may be involved in the radical polymerization reaction (Hatir et al., 2019). In this study,

mentioned allyl groups react with NIPAM and this reaction added cross-linked networks for H-WCOT. So this may be the reason of the layered architecture of this hydrogels.

3.2.3.2. Swelling and deswelling performances

Swelling and deswelling procedures for CO based hydrogels were explained in section 2.2.3, and equations 3 and 4 were used for the calculation. Swelling profiles can be seen in **Figure 3.31**, while deswelling performances are in **Figure 3.32**. **Figure 3.31** also has swelling data for two different temperatures to prove the thermoresponsive behaviors of hydrogels.

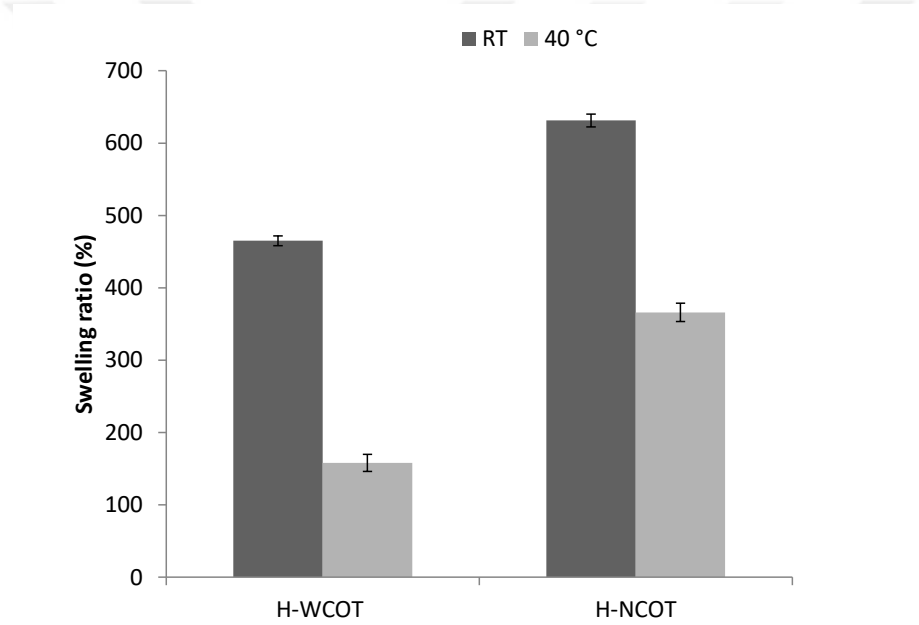

Figure 3.31. The swelling ratio of H-WCOT and H-NCOT

The swelling ratio reached to equilibrium in 180 min at RT. When the results of **Figure 3.31** were evaluated, it was reported that the swelling degree of the hydrogel with CO is lower than the swelling degree of the hydrogel without CO. The reason for this situation is believed to be a hydrophilic network structure of the hydrogel without CO, which does not have hydrophobic CO species. The reason for the differences between swelling ratio of H-WCOT and H-NCOT may be the denser crosslinked network of H-WCOT due to CO. So, H-WCOT had lower swelling ratio than H-NCOT.

If the temperature increased above the LCST, there was a significant decrease in the

swelling ratio of hydrogels. Furthermore, it can be reported that H-WCOT was more sensitive to the temperature changes more than H-NCOT. Besides, the swelling ratio of H-NCOT was higher than H-WCOT for all temperatures.

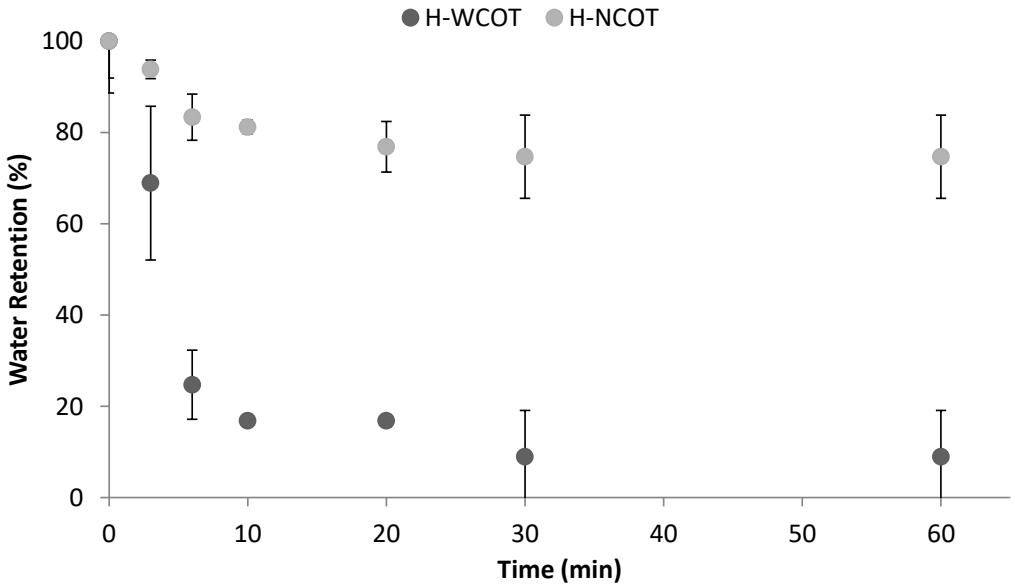

Figure 3.32. Deswelling performances of hydrogels H-WCOT and H-NCOT

Figure 3.32 shows the deswelling behaviors of hydrogels H-WCOT and H-NCOT at 40°C. The responses of H-WCOT and H-NCOT were faster for the first 10 min. H-WCOT and H-NCOT lost 84% and 18% of absorbed water in the first 10 min. In total, H-WCOT and H-NCOT lost absorbed water with a ratio of 91 % and 25 % for the first 60 min, respectively. No significant differences were observed for deswelling ratio after 30 min. Consequently, it can be reported that H-WCOT is more sensitive to temperature change than H-NCOT; but both of the hydrogels showed thermoresponsive behaviors successfully due to NIPAM.

The results can be evaluated with literature. Li and coworkers reported as water affinity of BC was strong. As a result, it may swell with a tendency to fill empty pores (Li et al., 2017). In this study, the compounds of H-NCOT had lower concentration of BC than H-WCOT inside so that it can affect the swelling performances. These results can be supported by Luo's results. They demonstrated that the density of crosslinker is a critical factor on swelling behavior (Luo et al., 2018). Similarly, El-Ghazawy et al. (2014) also presented swelling results and they proved that there was an inverse proportion between crosslinker ratio and swelling performances. Similarly, Komatsu et al. (2019) studied the

relation between swelling properties and monomer concentrations. It was reported that the highly crosslinked hydrogel showed less of a swelling behavior (Komatsu et al., 2019). This information can help to explain why the swelling performance of H-NCOT was higher than the others.

3.2.4. BC and CO based thermoresponsive hydrogels

BC, which is one of the renewable sources, was used as a monomer in this study. There are three different hydrogels whose detailed information was given in **Table 2.10**. The procedure of synthesis also was explained in section 2.2.2.6. The ratio, summary of hydrogels, is given in **Table 3.10** below. NIPAM was used to provide thermoresponsive property to hydrogels. DMPA and MBAM were used as photoinitiator and crosslinker, respectively.

The yields of H-BC1, H-BC2 and H-BC3 were 35 %, 34% and 46 %, respectively. Increasing of BC ratio affected the yields of polymerization positively, especially for H-BC3. As the BC ratio increases, bond formation increases in the polymerization. **Figure 3.33** shows the hydrogels before and after the introduction of NIPAM to hydrogels during polymerization.

Table 3.10. BC ratio of hydrogels

Hydrogel/*Components*	*BC*	*CO*	*MDI*
H-BC1	0.5	1	1
H-BC2	1	1	1
H-BC3	2	1	1

Evaluation of crosslinker effects on structural characteristics of the hydrogels

Investigation of crosslinker effects on the structure and properties of hydrogels was aimed at this part of the thesis. There are two different hydrogels in this study, given in Table 3.11.

Table 3.11. Hydrogels with and without MBAM

Hydrogel/*Components*	*BC*	*CO*	*MDI*	*NIPAM*	*MBAM*	*DMPA*
H-NC	0.5	1	1	1	-	1
H-WC	0.5	1	1	1	1	1

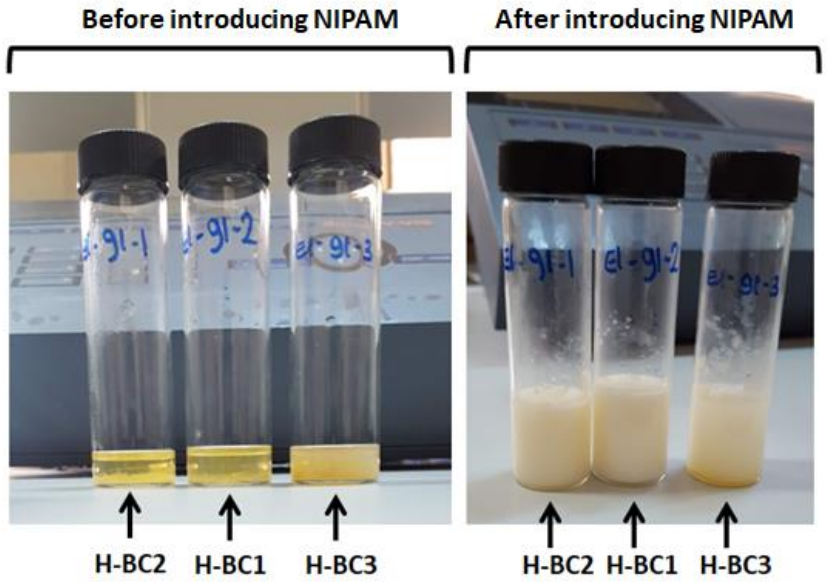

Figure 3.33. Physical appearances of H-BC1, H-BC2, and H-BC3 before and after introducing NIPAM

The procedure of synthesis was similar to the procedure explained in section 2.2.2.6. There are two steps for the polymerization; the first step involves the reactions of BC and CO with MDI. The molar ratio between MDI, the glucose units of BC, and CO were set as 1:0.5:1. In the second step, NIPAM, DMPA were used as monomer and initiator, respectively, for both of the hydrogels given in **Table 3.11**. But H-NC in **Table 3.10** did not have MBAM, as a crosslinker, in its structure. Polymerization was carried out under UV irradiation at 365 nm for 1 hour. The differences between the hydrogels based on the presence or absence of the MBAM were evaluated. The yields of H-NC and H-WC were 7% and 33.4%, respectively. The absence of the crosslinker reduced polymerization yield because the crosslinkers provide a network structure to the hydrogel. Increased crosslinking positively affects bond formation, thereby increasing polymerization yield. **Figure 3.34** shows the physical appearances of the

hydrogels; the H-WC seemed like one piece, whereas the hydrogels without MBAM were broken up into pieces.

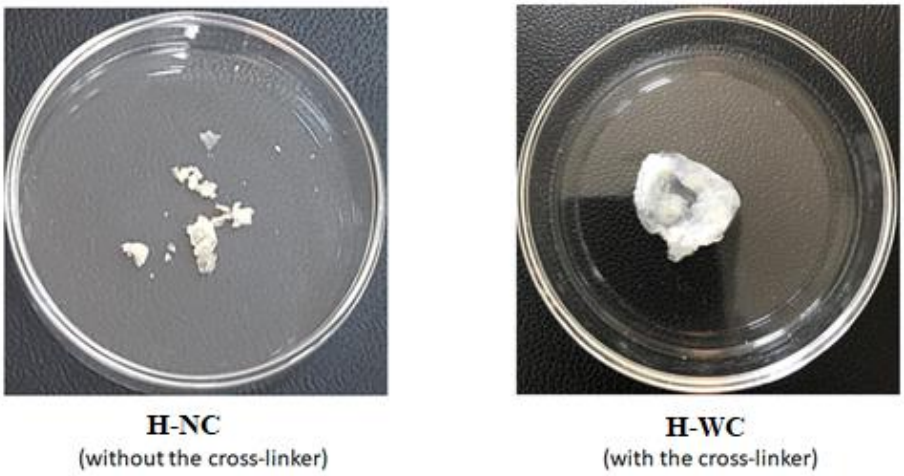

Figure 3.34. Physical appearances of H-NC and H-WC

3.2.4.1. Characterization of the hydrogels

The FTIR analyzes of the three different hydrogels that have different molar ratios of BC reported in **Table 3.9**, were evaluated. The BC effects on structures were examined in **Figure 3.35**, while the hydrogels had thermoresponsive characters. The FTIR data of the hydrogels were examined before and after introducing NIPAM as named H-BC1N, H-BC-2N and H-BC3N, without thermoresponsive property, and H-BC1, H-BC2 and H-BC3, with thermoresponsive property (**Figure 3.35**). Besides, **Table 3.12** shows the FTIR bands of the hydrogels with thermoresponsive properties.

Figure 3.35 shows the presence of thermoresponsive characteristics of hydrogels. In this context, the bands at 2933 cm^{-1} and 2967 cm^{-1}, which indicate the presence of NIPAM, can be seen for H-BC1 and H-BC2 and H-BC3; 2935 cm^{-1} (2931 cm^{-1} for H-BC2, 2929 cm^{-1} for H-BC3) and 2971 cm^{-1} (2971 cm^{-1} for H-BC1, H-BC2 and 2969 cm^{-1} for H-BC3), respectively. Moreover, 3280 cm^{-1} is a specific band for NIPAM (**Figure 3.19-D**), and similarly to this band, the bands at 3278 cm^{-1} and 3282 cm^{-1} were observed for H-BC1, H-BC2, and H-BC3 (Figure 3.35-A, B, C). These bands can prove that the hydrogels have NIPAM in their structures. Besides, the bands depending on the significant differences due to NIPAM are seen in all thermoresponsive hydrogels (Figure 3.35 and 3.37). 1535 cm^{-1} (for H-BC1, H-BC2; 1533 cm^{-1} for H-BC3) and 1629

cm^{-1} (for H-BC2, H-BC3; 1625 cm^{-1} for H-BC1) were detected to identify Amide-II and amide-I groups.

Table 3.12. FTIR bands of BC based hydrogels

Functional groups	Wavenumber (cm^{-1})		
	H-BC1	**H-BC2**	**H-BC3**
C-O	1170	1170	1170
secondary Amide	1241	1228	1230
N= O stretch	1367	1367	1367
hydrogen bending vibrations	1457	1455	1455
Amide II (C-O)	1535	1535	1533
Amide I (C=O)	1625	1629	1629
CH vibration	-	1739	1739
CH vibration	2875	2875	2875
CH vibration	2935	2931	2929
CH vibration	2971	2971	2969
CH vibration	3079	3073	3073
NH stretching	3278	3282	3282

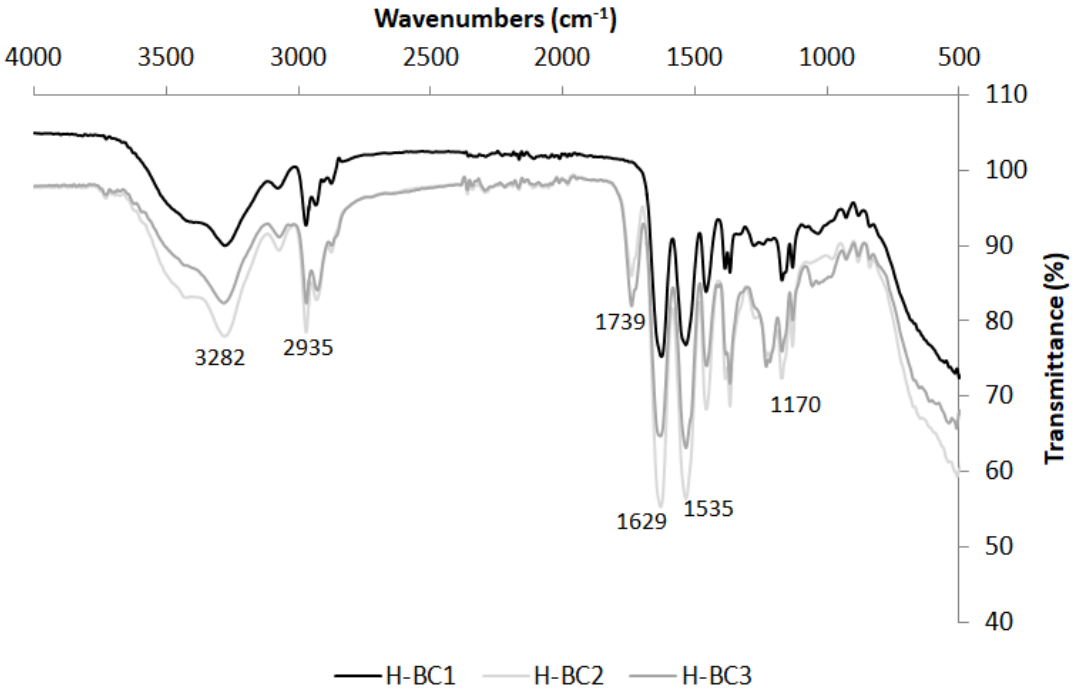

Figure 3.35. FTIR spectra of BC based hydrogels

When the FTIR bands of hydrogels were examined detailed, it can be reported that the bands at 1170 cm^{-1} and 1241 cm^{-1} (1228 cm^{-1} for H-BC2 and 1230 cm^{-1} for H-BC3) referred C-O and secondary Amide. 1367 cm^{-1} and 1455 cm^{-1} (1457 cm^{-1} for H-BC1) exhibited N= O stretch and hydrogen bending vibrations , 1535 cm^{-1} (1533 cm^{-1} for H-BC3), 1629 cm^{-1} (1625 cm^{-1} for H-BC1), between 1739 cm^{-1} and 3073 cm^{-1} (3079 cm^{-1} for H-BC1) and 3282 cm^{-1} (3278 cm^{-1} for H-BC1) corresponding to amide II (C-O) and amide I (C=O), CH vibration and NH stretching (Bellamy, 1975), respectively were detected (**Table 3.11**).

Similar bands were reported by Cakir Hatir et al. (2019) and Alosmanov et al. (2017). In their study, the bands at about 3340 cm^{-1} corresponded to the amide groups in PNIPAM chains. It was indicated that the bands formed by O–H stretching vibrations overlap these bands. Besides, hydrogen bonds formed between the PNIPAM chains and BC surface, and it was believed that the reason for this formation was the substantial broadening of the mentioned band (Alosmanov et al., 2017). Similar states were determined in **Figure 3.35** and **Figure 3.36** in the present study. These can be considered evidence for hydrogels gained thermoresponsive properties by PNIPAM as they are supported by the literature.

Characterization of hydrogels with and without MBAM

In this part, the aim is to evaluated the effects of crosslinker on the structure of the hydrogels.

When **Figure 3.37** is evaluated, the dominant bands were seen at 1170, 1531, 1629, 2846, and 2875 cm^{-1} and they exhibited C-O, amide II (C-O) and amide I (C=O), CH vibration and NH stretching, respectively. These bands are evidence for successful synthesis. Since the crosslinker ratio, MBAM, is quite low, the functional groups that arise from the crosslinker cannot be seen at the FTIR spectra. Thus the effects of the presence of MBA cannot be understood from FTIR spectra.

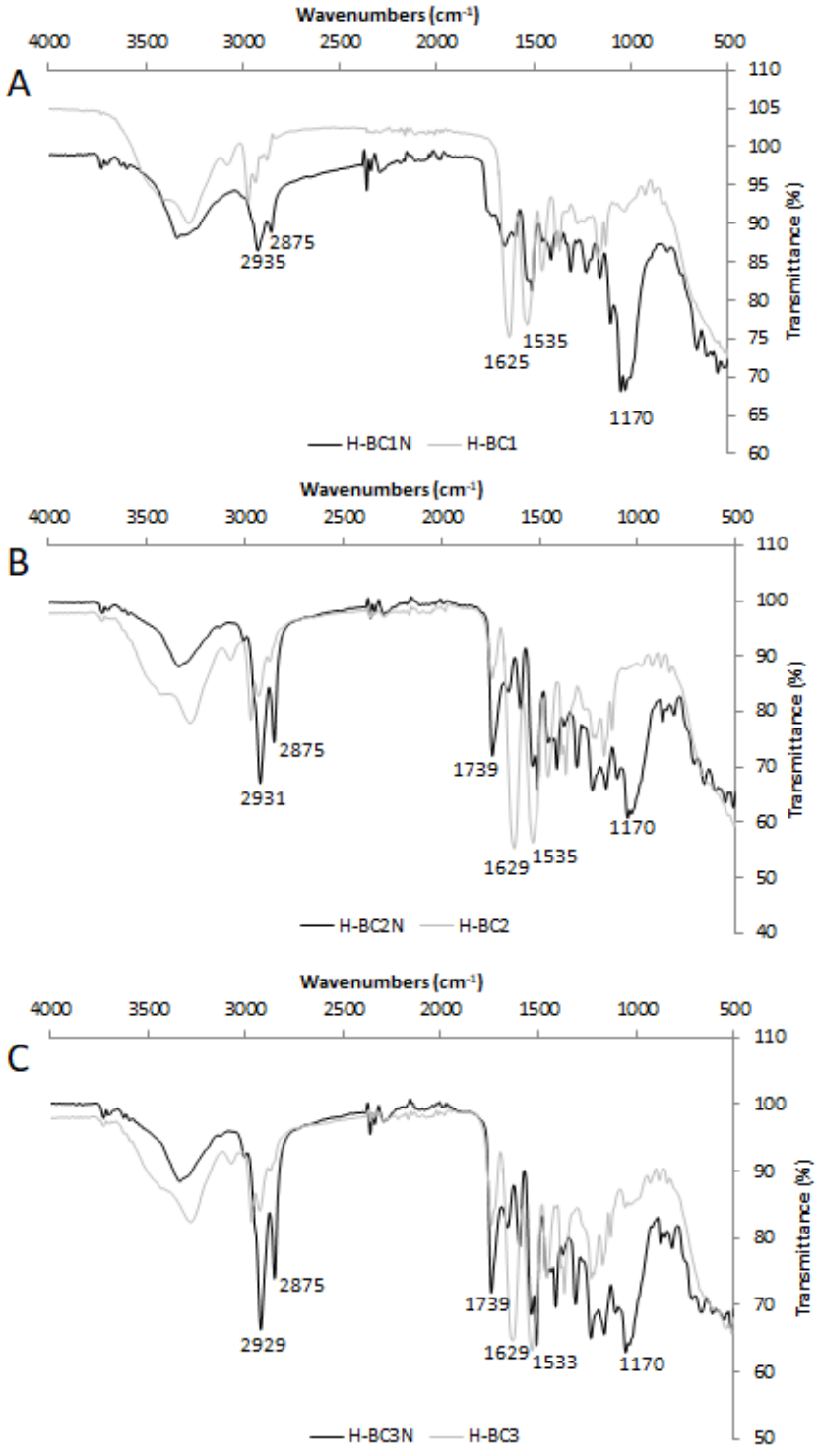

Figure 3.36. FTIR spectra of hydrogels of H-BC1/H-BC1N (A), H-BC2/H-BC2N (B), and H-BC3/H-BC3N (C).

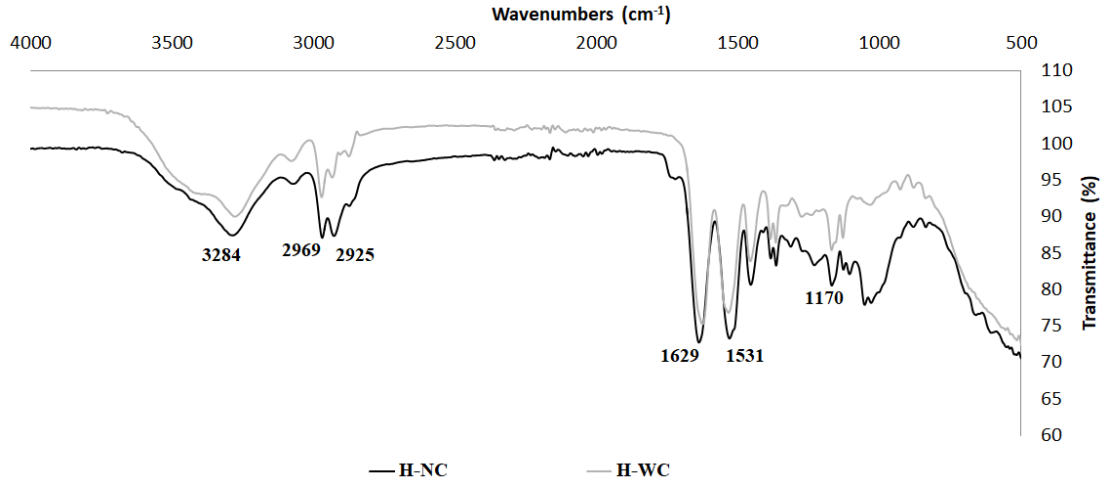

Figure 3.37. FTIR spectra of hydrogels with and without crosslinker

3.2.4.2. Release behaviors

The effects of different ratio of BC on release behaviors of hydrogels were investigated in **Figure 3.38** and **3.39**. The results of release behaviors of hydrogels at RT are presented in **Figure 3.38**. When the release behaviors were examined in detail, H-BC1 had maximum release concentrations for the first 5 min. Its release concentration was higher at 37°C than RT. However, H-BC2 and H-BC3 had the same release concentrations for the first 5 min. The difference between H-BC2 and H-BC3 was observed after 20 min at RT and after 15 minutes at 37°C. Hydrogels reached equilibrium in the first 40 min. H-BC2 has the lowest value, while release concentrations of H-BC1 and H-BC3 were very close to each other after 40 min for both temperatures. It can be concluded that the H-BC1 had maximum release concentrations due to its lower network in its structures. Higher release concentrations of H-BC3 could be correlated with the water absorbance capacity of the BC. Since H-BC3 had maximum BC ratio, it performed higher release behaviors. Furthermore, H-BC3 included a higher molar ratio of NIPAM in its structure, that is why it showed more thermoresponsive properties than H-BC2.

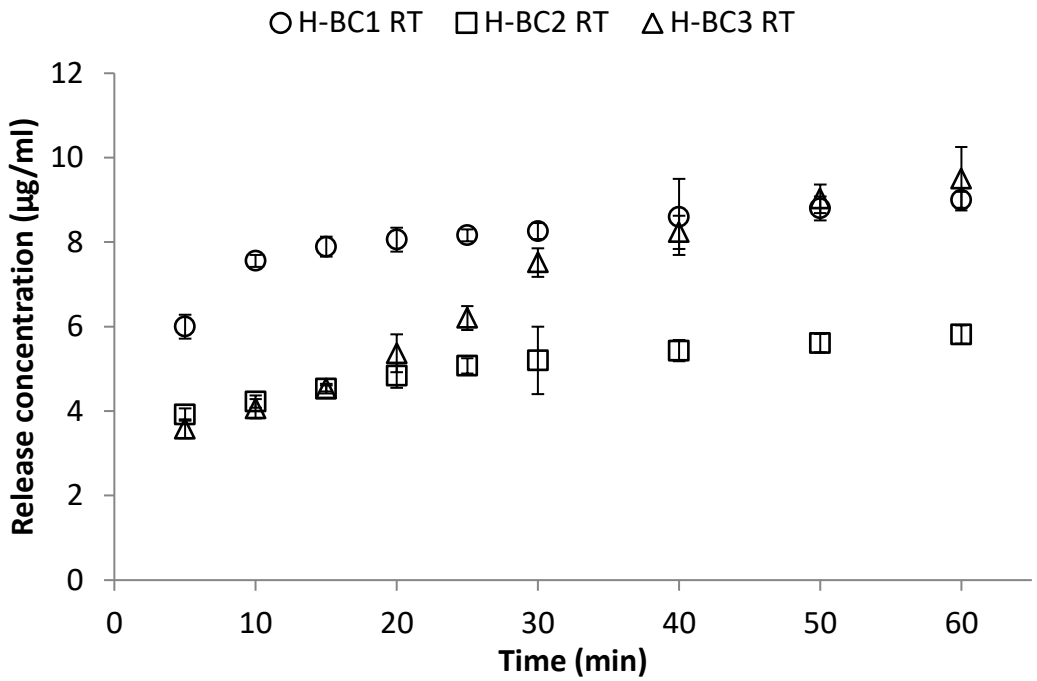

Figure 3.38. Release ratio (%) of BC based hydrogels at RT

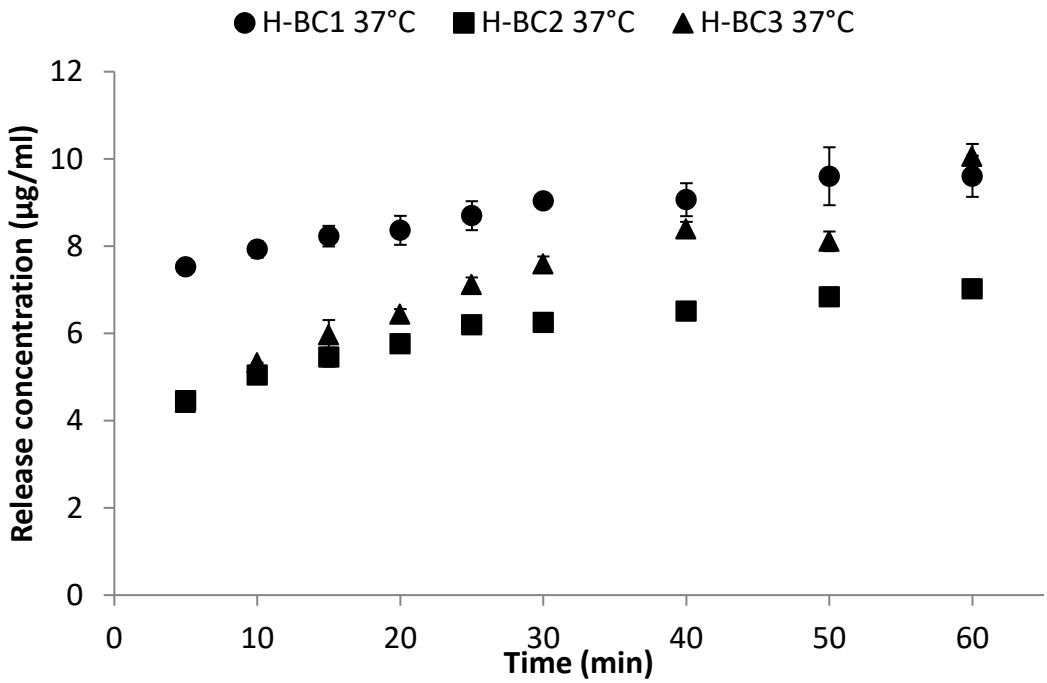

Figure 3.39. Release values (%) of BC based hydrogels at 37°C

3.2.4.3. Swelling and deswelling performances

The swelling and deswelling properties of whole hydrogels were investigated according to the procedures explained in section 2.2.3. Equation 3 and 4 were used to calculate the data. The aim is to investigate the effects of the molar ratio of BC on the swelling properties of hydrogels. Additionally, the deswelling properties of the hydrogels were analyzed.

Figure 3.40 and **3.41** show the physical appearances of the hydrogels. **Figure 3.40** shows the swelling and deswelling performances during temperature changes, whereas **Figure 3.41** is correlated with swelling profiles of hydrogels over time.

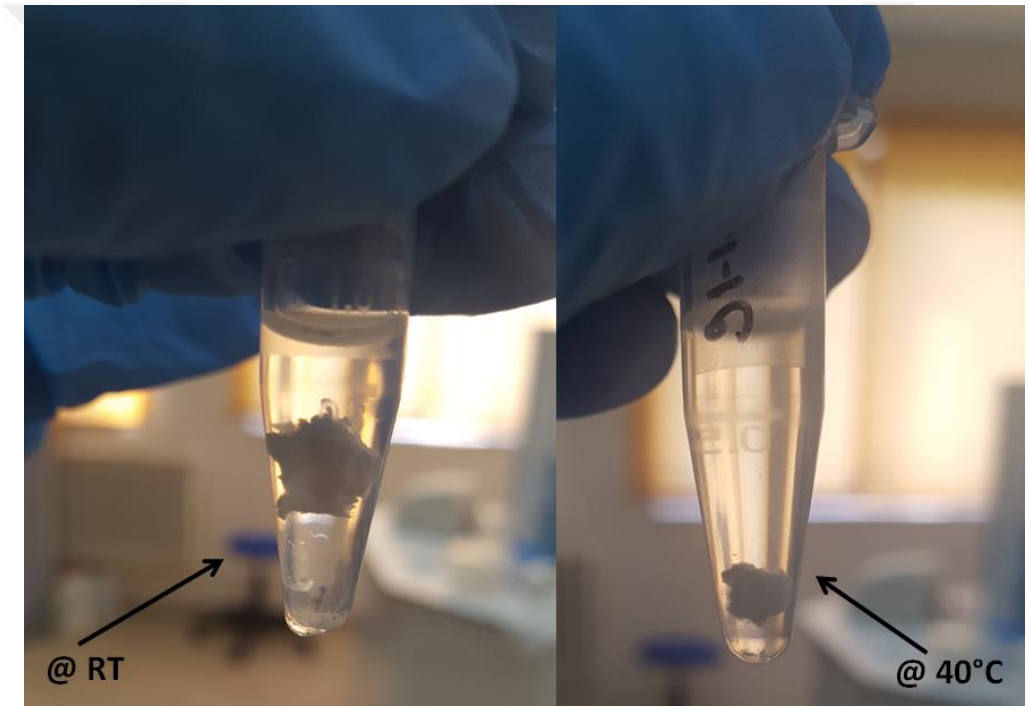

Figure 3.40. Swelling (at RT) and deswelling (at 40°C) performances of BC based hydrogels

When Figure 3.42 is investigated, the performance of H-BC3 is higher than the others. For the first 10 min, there were no significant differences between H-BC2 and H-BC3, except H-BC1. However, after 10 min, the response of H-BC3 is faster than the others. The reason may be the high molar ratio of BC ratio in H-BC3. A similar study was reported by Arikibe et al. (2019). In their research, it was reported that the swelling behavior of hydrogels is related to the BC ratio found in the hydrogel (Arikibe et al.,

2019). Besides that, the strong affinity of BC to water molecules was mentioned by Li's et al. (2017). BC tends to fill the empty pores by swelling performances and its mechanical properties can be affected by increased volumetric dimensions (Li et al., 2017). In another study, a direct proportion between BC and swelling capacity was mentioned (Kucinska-Lipka et al., 2015). On the other hand, it was reported that the samples, including MBAM swell relatively rapidly (Su et al., 2019). These information are important to analyze the results presented in **Figure 3.42**. It can be reported that H-BC3 had the highest MBAM concentration, and its swelling performance was better than the others.

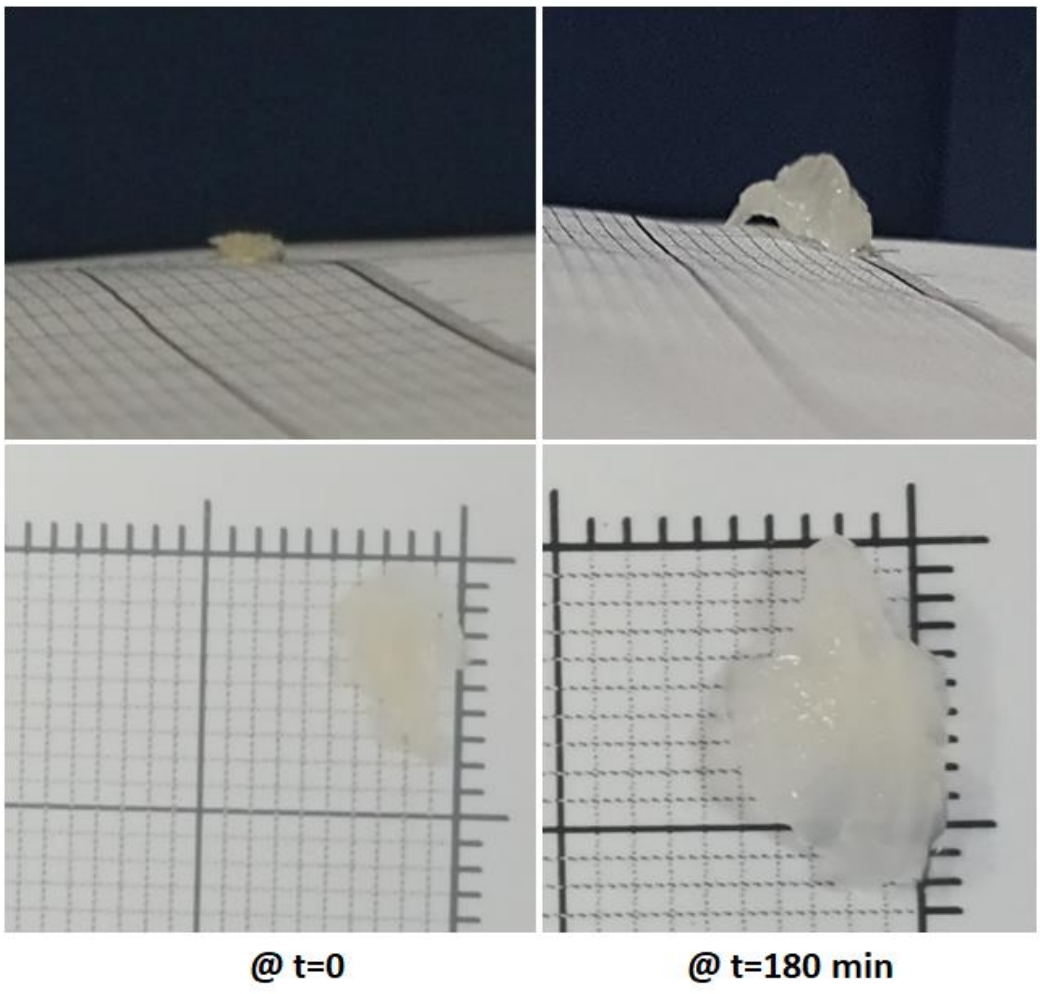

Figure 3.41. Swelling performances of BC based hydrogels over time (at RT)

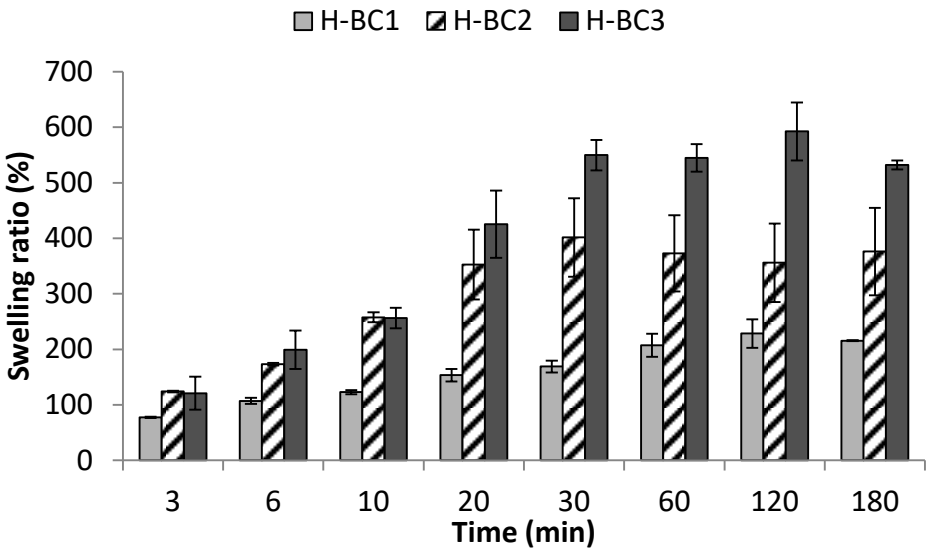

Figure 3.42. Swelling data of BC based hydrogels over time (at RT)

For the evaluation of deswelling characters, the study reported by Krakovský et al. (2019) can be analyzed. They examined the swelling and deswelling properties of various hydrogels based on PNIPAM. They observed that the increase in temperature affected the deswelling profiles. Besides, as reported in their study, hydrogels had the appearance of a slight opaqueness at the temperature above 40 °C (Krakovský et al., 2019). These results are in agreemnt the results showed in **Figure 3.40** and **3.41**. Moreover, they indicated that the deswelling behaviors of hydrogels were continuous and of a smaller extent. Furthermore, conditions for volume phase transition become satisfied for the hydrogels that are crosslinked less (Krakovský et al., 2019). Similar results were demonstrated and proved with deswelling profiles of hydrogels in **Figure 3.43**. The H-BC1, included the lowest molar ratio of BC, had highest deswelling ratio.

According to the results, Tang's study can be analyzed. They indicated that swelling and deswelling behavior were reversible depending on the temperature changes (Tang et al., 2017). It can be seen from **Figure 3.46** that reversible performance is obtain in this study. Wang et al. (2018) also reported that they had three different hydrogels that their ratios of MDI and the glucose unit of BC was set as 0.2 : 1, 1 : 1, and 2 : 1. Their results showed that there were no significant differences between swelling behaviors of the hydrogels; this property was regardless of the MDI ratio difference. However, when the deswelling features were evaluated, it was reported that the hydrogels based on 2:1 (MDI:BC) lost about 40% of water content in the first 10 min and 76% in the 30 min.

The order of water loss rate within 30 min was expressed inversely proportional for the BC ratio in hydrogels (Wang et al., 2018).

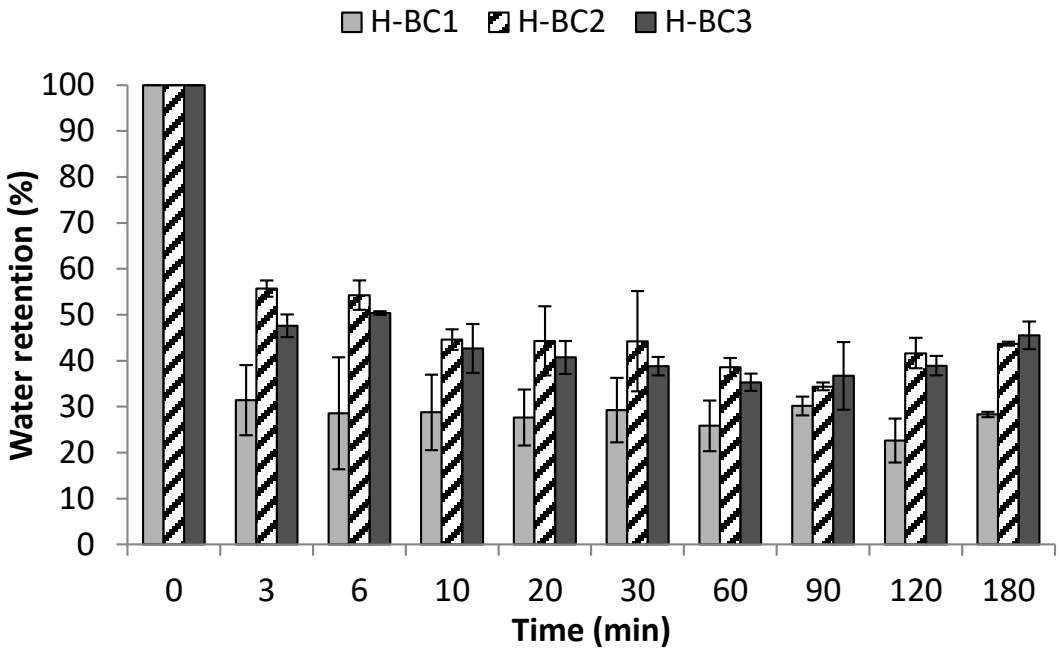

Figure 3.43. Deswelling (at 40°C) ratio of BC based hydrogels vs time

The ratio of swelling of hydrogels decreased significantly by increasing the temperature above LCST. Deswelling characters were obtained at 40°C. All of the hydrogels exhibited fast responses in the first 3 min. H-BC1 lost 68.59 % of absorbed water in 3 min, whereas H-BC2 and H-BC3 lost only 44.26 % and 52.40 % of water content in the same period, respectively. At the end of the 180 min, total water losses were reported as 71.70 %, 56.28 % and 54.20 % for H-BC1, H-BC2 and H-BC3, respectively. Following the deswelling results, it can be indicated that H-BC1 was affected by the temperature differences more than H-BC2 and H-BC3. This behavior of H-BC1 may be related to the BC ratio of the hydrogels. H-BC2 and H-BC3 had more complex structures than H-BC1. So that these structures could limit their deswelling performances.

Swelling behaviors of hydrogels with and without MBAM

Swelling properties of the hydrogels were investigated according to the procedures explained in section 2.2.3. Equation 3 was used to calculate the data.

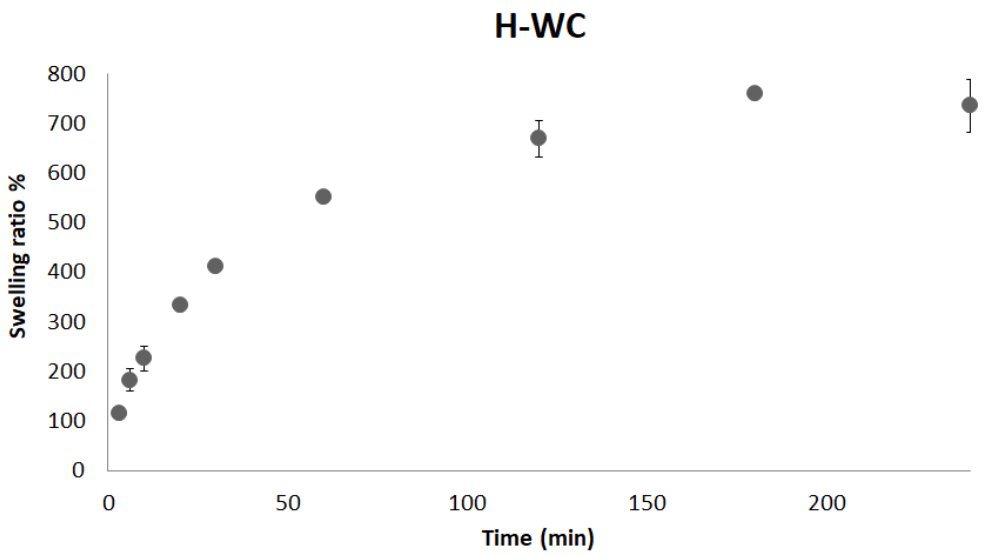

Figure 3.44. Swelling (at 40°C) data of BC based hydrogels over time

The swelling profile of H-WC was seen in **Figure 3.44**. The data of H-NC couldn't be seen in **Figure 3.44**; because this hydrogel had a lot of small pieces and was broken into a lot of pieces during the swelling performance.

3.2.4.4. Cytotoxicity analyzes

The procedure of cytotoxicity analyzes was given in section 2.2.5. This test was applied for BC based hydrogels (H-BC1- H-BC2 and H-BC3). The biocompatibilities of starting materials were also investigated in **Figure 3.45**. These hydrogels were believed to be biocompatible and biodegradable.

Figure 3.45 shows the results of cytotoxicity experiments with the monomers and hydrogels with concentrations ranging from 1 mg/mL to 10 mg/mL for monomers and 1 mg/mL to 20 mg/mL for the hydrogels. Cells showed at least 55% of viability in the presence of 1 mg/mL of each monomer solution (except MBAM) (**Figure 3.45-A**) whereas for the hydrogels with 1 mg/mL concentrations, the viabilities of the cells were at 68% as compared to controls (**Figure 3.45-B**). However, cellular viability reduced with increasing concentration of the monomers, a severe decrease in the cell viability was observed, especially with 5 mg/mL concentrations. There was no decrease in cell viability as the CO concentration increased because CO is a renewable plant-based material and known as biocompatible. So as seen in **Figure 3.45-A**, cell viability was

not affected by increasing concentration of CO. Similarly, BC is known for its biocompatible properties, but cells were affected by the high BC concentrations. MDI was not easily dissolved in PBS, so this may be the reason for its cytotoxicity results because it was expected that the cells would die with an increasing MDI concentration. NIPAM and MBAM had low biocompatibilities as the cell decreased with increasing concentrations. Moreover, Cakir Hatir and coworkers reported cytotoxicity data for EbAM and EGDMA as monomers and EbAM and EGDMA based hydrogels (Cakir Hatir et al., 2019). When the concentration was increased, the cell viability decreased, cells demonstrated at least 70% of viability in the presence of 1 mg/mL of EbAM and EGDMA solution. It was concluded that EbAM affects cell viability. Moreover, they investigated EbAM and EGDMA based hydrogels on cell viability. No significant differences were observed between the cell viability results of EbAM and EGDMA based hydrogels. However, cell viability was affected by increasing concentrations of EbAM and EGDMA based hydrogels. It was reported that cells treated with 20 mg/ml of EbAM based hydrogels, which were synthesized by photopolymerization, showed almost 30% of cell viability (Cakir Hatir et al., 2019).

The results revealed that cells showed at least 69 % viability in the presence of 1 mg/ml of hydrogels, and exposing the cells to higher concentrations of hydrogels or cellulose did not change the cell viability significantly confirming the biocompatibility of the hydrogels. However, the minimum value was 59 % for H-BC1 of 10 mg/ml concentrations. Moreover, it can be reported that there were no significant differences between H-BC1, H-BC3 and H-BC10 and concentrations of each hydrogel. This means BC ratio in hydrogels did not affect the biocompatibilities of the hydrogels. Following the results, it can be reported that the cell viability was independent of the BC concentrations.

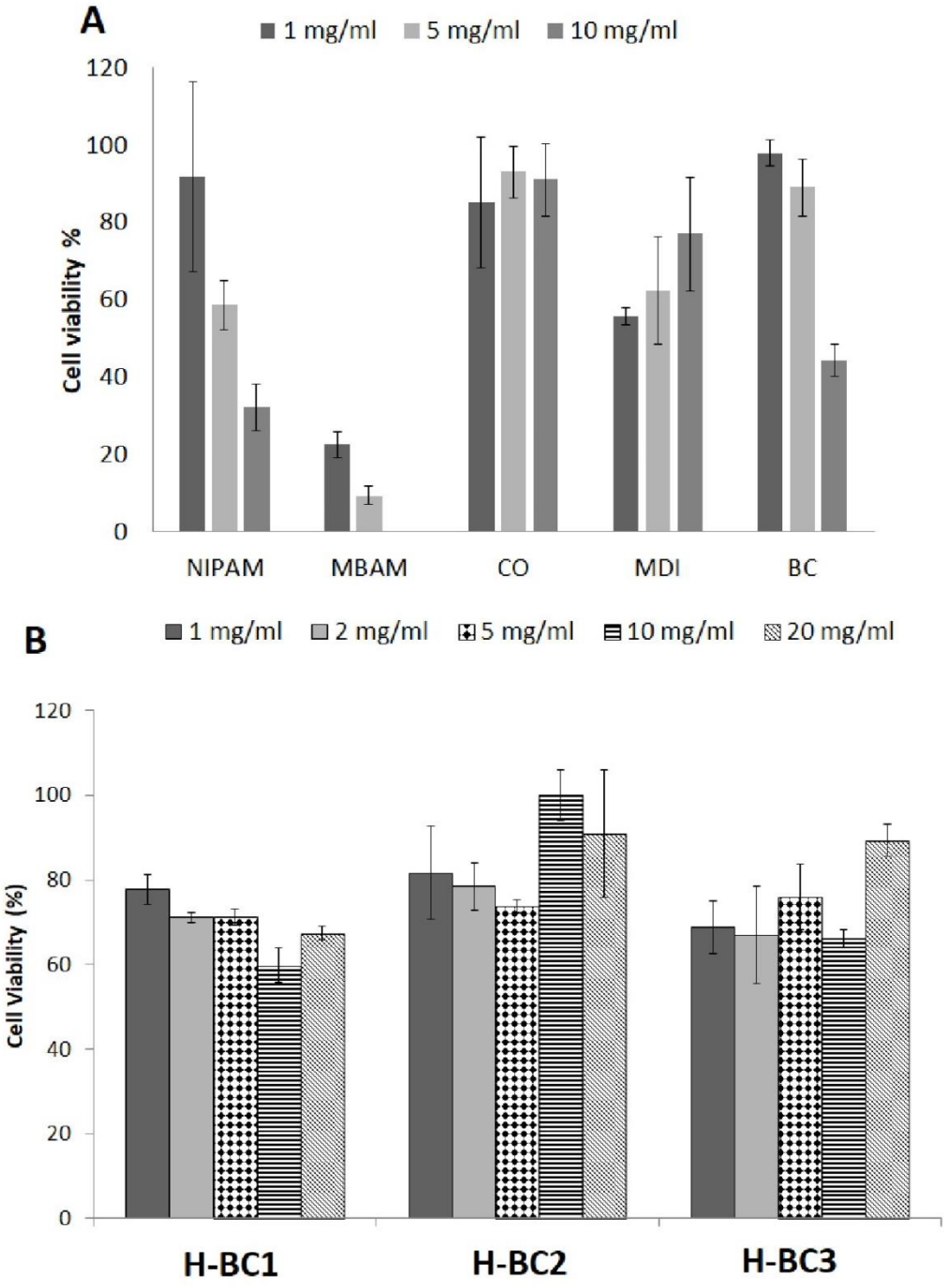

Figure 3.45. Cell viability values of the monomers (A) and thermoresponsive hydrogels (B).

4. CONCLUSION

In the present thesis, the main purpose is to synthesize novel thermoresponsive hydrogels from renewable materials. Analysis of the loading/release and swelling performances of the hydrogels was performed. Moreover, the characterization of all of the hydrogels and cytotoxicity tests were carried out.

Novel thermoresponsive hydrogels were successfully synthesized. Quercetin was used as a model drug molecule in this study to determine the loading/release performances of the hydrogels. The quercetin loading concentration was determined as 100 μM. Then, the factors effecting release performances of the hydrogels were identified, such as temperature, pH, the molar ratio of NIPAM, and the molar ratio and the types of crosslinkers in the hydrogels.

The effects of temperature changes on release behaviors also investigated. The release behaviors were analyzed at RT and 37 °C. The release ratio was higher at 37 °C compared to the release ratio at RT. pH of aqueous media was set up as pH 4.0 and pH 9.0 for testing release performances at various pHs. The maximum release ratio was achieved at pH 9.0 at 37°C, also higher release values were obtained at pH 9.0 for both of the temperature values. Besides, the quercetin was degraded at pH 9.0 after a while, especially at 37°C. Moreover, the release studies were performed at pH7.4 to compare the results obtained at pH 4. The maximum release concentration was achieved at pH7.4 at 37 °C.

After the analysis of the effects of the physical factors on release profiles, the effects of other factors on structures of the hydrogels were examined. In this context, the molar ratio of NIPAM in the hydrogels was changed, and the effects on release behaviors were evaluated. According to the results, there was a correct proportion between the release concentrations and the moar ratio of NIPAM in hydrogels. Besides, monomer and crosslinker concentrations, which are factors that may affect the structures of hydrogels, were changed. The effects of the types of crosslinkers on release and swelling performances of the hydrogels were also evaluated. EbAM, one of the hydrophilic monomers, and EGDMA, one of the hydrophobic ones, were used as different crosslinkers. According to their release and swelling results, it was found that EGDMA based hydrogels had higher release concentrations compared to EbAM based hydrogels. Moreover, the molar ratio of EGDMA did not affect the release concentration

significantly, whereas when the molar ratio ratio of EbAM increased, the release concentration decreased.

Additionally, in the present study, AMR based thermoresponsive hydrogels were synthesized and characterized by FTIR spectroscopy. AMR was used in varied molar ratios, and the release and swelling behaviors of the hydrogels were investigated. Moreover, the obtained results were compared with the results of EGDMA based hydrogels. AMR0.25 had the maximum release concentrations at RT and 37°C for the first 60 min. The molar ratio of AMR didn't affect the release behaviors of hydrogels at RT significantly. It was concluded that AMR could be used in hydrogel synthesis instead of conventional monomers. This study proved that renewable resources could be used in hydrogel synthesis for biomedical applications. Moreover, this study shows that hydrogel based drug release systems can be designed by using renewable resources.

Another study concerning the renewable materials was carried out with BC based hydrogels with and without CO as well. MDI modified BC/PNIPAM hydrogels were successfully synthesized. Thus, how physical and thermal behaviors of hydrogels are affected in the presence of CO was investigated. According to the FTIR spectrum, the hydrogel with CO has a peak at 1741 cm^{-1}, which indicates the presence of CO. Thermal analysis results demonstrated that the hydrogel with CO had a sharper melting behavior. 21.1 mJ/mg was measured as absorbed heat, whereas the H-NCOT absorbed only 13.2 mJ/mg. Following the TGA results, 5% and 50 % of weight loss temperatures were determined. Besides, SEM images showed that the structure of H-WCOT is a layered and flat, and it has homogenous structure; the structure of H-NCOT is a spongy form. Moreover, it was seen from the swelling/deswelling performances that both of the hydrogels gained thermoresponsive properties. The sensitivity of H-WCOT to temperature changes was higher compare to H-NCOT. The swelling value of the hydrogel without CO was higher than the one with CO. To sum up, the hydrogel with CO and the hydrogel without CO lost 91 % and 25 % of water for the first 60 min, respectively.

The last part of the thesis includes the synthesis of the BC based thermoresponsive hydrogels. Three different hydrogels were synthesized with two-step polymerization. The first step involved the reactions between BC, CO, and MDI, while the second step was the introduction of NIPAM to the hydrogels. The molar ratio of BC was changed

from 0.5 to 2, whereas the molar ratios of other components were kept constant. According to the FTIR results, all of the hydrogels gained thermoresponsive properties. Release behaviors of the hydrogels were examined for proving their thermoresponsive behaviors. The maximum release ratio belonged to the hydrogel, including the molar ratio of 1:1:1 for BC:CO:MDI. Following the swelling results, maximum swelling value belonged to the hydrogel that had a maximum BC ratio. Total water loss was reported as 71.7 % for the hydrogel that had a minimum molar ratio of BC. Besides, the cytotoxicity test showed that molar ratio of BC in hydrogels did not affect the biocompatibilities of the hydrogels. In addition to these experiments, the crosslinker effects on the hydrogel were investigated by FTIR and swelling experiments. There were two different hydrogels with and without MBAM. According to the results, there were not any differences between their FTIR results, however, the hydrogel with MBAM had better swelling profiles.

In conclusion, the present thesis provides novel approaches to the synthesis of renewable resources based thermoresponsive hydrogels. Novel renewable resources-based hydrogels developed in this thesis are new alternative materials for biomedical applications. According to the results, a significant increase in the use of BC or CO as renewable resources for the synthesis of thermoresponsive hydrogels is expected. This study is a pioneering study that highlights the importance of renewable materials for biomedical applications.

REFERENCES

Abraham, M. H., Acree Jr., W. E. (2014) On the solubility of quercetin. Journal of Molecular Liquids, 197, 157-159.

Akoğlu, A., Karahan, A. G., Çakmakçı, M. L., Çakır, İ. (2010) Bakteriyel selülozun özellikleri ve gida sanayisinde kullanimi. Gıda, 35(2), 127.

Alaa., M. A., Yusoh, K., Hasany, S. F. (2015) Pure polyurethane and castor oil based polyurethane: synthesis and characterization. Journal of Mechanical Engineering and Sciences (JMES), 8, 1507-1515

Almeida, H., Amaral, M. H., Lobão, P. (2012) Temperature and pH stimuli-responsive polymers and their applications in controlled and self-regulated drug delivery. Journal of Applied Pharmaceutical Science, 02 (06); 01-10.

Alosmanov, R., Wolski, K., Zapotoczny, S. (2017) Grafting of thermosensitive poly(N-isopropylacrylamide) from wet bacterial cellulose sheets to improve its swelling drying ability. Cellulose, 24, 285.

Alquichire, S. A., Ramır´ez, C., Andrade, L., Uscategui, Y., Diaz, L. E., Go´mez-Tejedor, J. A., Vall´es-Lluch, A., Valero, M. F. (2018) Polyurethanes from modified castor oil and chitosan: Synthesis, characterization, in vitro degradation, and cytotoxicity. J. Elastom. Plast., 50(5), 419.

Amorati, R., Baschieri, A., Cowden, A., Valgimigli, L. (2017) The Antioxidant Activity of Quercetin in Water Solution. Biomimetics, 2, 9.

Anastas, P., Eghbali, N. (2010) Green Chemistry: Principles and Practice. Chem. Soc. Rev., 39, 301.

Arikibe, J. E., Lata, R., Kuboyama, K., Ougizawa, T., Rohindra, D. (2019) pH-Responsive Studies of Bacterial Cellulose /Chitosan Hydrogels Crosslinked with Genipin: Swelling and Drug Release Behaviour. Chemistry select, 4(34), 9915-9926.

Auta, R.; Adamus, G.; Kwiecien, M.; Radecka, I.; Hooley, P. (2017) Production and characterization of bacterial cellulose before and after enzymatic hydrolysis. Afr. J. Biotechnol., 16(10), 470-482.

Aydemir, N., Malmström, J., Travas-Sejdic, J. (2016) Conducting Polymer Based

Electrochemical Biosensors. Phys Chem Chem Phys., 28;18(12):8264-77.

Bancirova, M. (2015) Changes of the Quercetin Absorption Spectra in Dependence on Solvent. Chemistry Journal, Vol. 1, No. 2, pp. 31-34.

Basu, P., Saha, N., Saha, P. (2019) Swelling and rheological study of calcium phosphate filled bacterial cellulose-based hydrogel scaffold. J. Appl. Polym. Sci., 136, 48522.

Bawa, P., Pillay, V., Choonara, Y. E., du Toit, L. C. (2009) Stimuli-responsive polymers and their applications in drug delivery. Biomed. Mater., 4, 022001.

Behnaz, M., Davood, E. A., Atena, A. (2012) Quantitative analysis of quercetin in different parts of Capparis spinosa by HPLC. Ann Biol Res., 3(12), 5775-5778.

Bellamy, L.J. (1975) Infra-red spectra of complex molecules; Printed in Great Britain by Lowe & Brydone Ltd. Thetford, Norfolk, pp 1-420.

Botterhuis, N.E. (2008) Polymers in nanotechnology: molecular recognition and surface modification. Technische Universiteit Eindhoven.

Braun, D., Cherdron, H., Rehahn, M., Ritter, H., Voit, B. (2005) Polymer Synthesis: Theory and Practice Fundamentals, Methods, Experiments, Fourth Edition, Springer-Verlag Berlin Heidelberg, Printed in Germany.

Braun, D. (2009) Origins and development of initiation of free radical polymerization processes. International Journal of Polymer Science, 2009(1687-9422).

Brett, A. M. O., Ghica, M. E. (2003) Electrochemical Oxidation of Quercetin. Electroanalysis, 15, 22.

Bucatariu, S., Fundueanu, G., Prisacaru, I., Balan, M., Stoica, I., Harabagiu, V., Constantin, M. (2014) Synthesis and characterization of thermosensitive poly(N-isopropylacrylamide-co-hydroxyethylacrylamide) microgels as potential carriers for drug delivery. J Polym Res, 21:580, 12.

Cao, M. W., Wang, Y., Hu, X. Z., Gong, H. N., Li, R. H., Cox, H., Zhang, J., Waigh, T. A., Xu, H., Lu, J. R. (2019) Reversible thermoresponsive peptide-pnipam hydrogels for controlled drug delivery. Biomacromolecules, 20(9), 3601.

Cakir Hatir, P., Yalcin Capan, O. (2019) Comparison of Crosslinker Types and Initiation Systems of Thermoresponsive PNIPAM Hydrogels. Düzce Üniversitesi Bilim

ve Teknoloji Dergisi, 7(3), 1237 – 1248.

Carraher, Jr. C. E. (2003) Polymer Chemistry, Sixth Edition Revised and Expanded, Marcel Dekker, NEW YORK • BASEL.

Chouhan, R., Bajpai, A. (2009) Real time in vitro studies of doxorubicin release from PHEMA nanoparticles. Journal of Nanobiotechnology, 7:5.

Curcio, M., Cirillo, G., Parisi, O. I., Lemma, F., Picci, N., Puoci, F. (2012) Quercetin-Imprinted Nanospheres as Novel Drug Delivery Devices. Journal of Functional biomaterials., 3:269-282.

Czaja, W. K., Young, D. J., Kawecki, M., Brown, R. M. (2007) The future prospects of microbial cellulose in biomedical applications. Biomacromolecules, 8(1), 1.

Danaei, M., Dehghankhold, M., Ataei, S., Davarani, F. H., Javanmard, R., Dokhani, A., Khorasani, S., Mozafari, M. R. (2018) Impact of Particle Size and Polydispersity Index on the Clinical Applications of Lipidic Nanocarrier Systems. Pharmaceutics, 10, 57.

Davis, F., Higson, P. J. (2007) Polymers in biosensors. Biomedical Polymers, pp.174-196.

Das, S., Pandey, P., Mohanty, S., Nayak, S. K. (2017) Insight on castor oil based polyurethane and nanocomposites: recent trends and development. Plast Technol., 56 (14), 1556.

Duan, Y. (2014) Ultraviolet-Visible spectrum characterizations of Quercetin in aqueous ethanol solution with different pH values. Journal of Chemical and Pharmaceutical Research, 6(9):236-240.

Durkut, S., and Elcin, Y. M. (2019) Synthesis and characterization of thermosensitive poly (nvinyl caprolactam)-grafted-aminated alginate hydrogels. Macromolecular Chemistry and Physics, 221(2):1900412.

El-Ghazawy, R. A. M.; Farag, R. K.; Elsaeed, S. M.; Abde-Halim, E. D. A.; Yossef, M. A.; Toyor, W. E. (2014) Castor Oil Based Organogels: I. Synthesis, Swelling, and Network Parameters. J. Dısper. Scı.Technol., 35, 350.

Esa, F.; Tasirin, S. M.; Rahman, N. A. (2014) Overview of bacterial cellulose production and application. Agricul. Sci. Procedia., 2, 113.

Etchenausia, L., Alvarez, E. V., Forcadac, J., Savea, M., Taboada, P. (2019) Evaluation of cationic core-shell thermoresponsive poly(Nvinylcaprolactam)-based microgels as potential drug delivery nanocarriers. Mater. Sci. Eng. C., 104: 109871.

Fakirov, S. (2017) Fundamentals of Polymer Science for Engineers, First Edition, Published by Wiley-VCH Verlag GmbH&Co. K Ga A., Germany.

Fallahiarezoudar, E., Ahmadipourroudposht, M., Idris, A., Mohd, YN. (2015) A review of: Application of synthetic scaffold in tissue engineering heart valves. Materials Science and Engineering C. 48, 556–65.

Feng, Z., Lin, L., Yan, Z., Yu, Y. (2010) Dual responsive block copolymer micelles functionalized by nipam and azobenzene. Macromolecular Rapid Communications, 31(7), 640-4.

Frazar, E. M., Shah, R. A., Dziubla, T. D., Hilt, J. Z. (2019) Multifunctional temperature-responsive polymers as advanced biomaterials and beyond. J. APPL. POLYM. SCI, 137, 48770, 1-14.

Fundueanu, G., Constantin, M., Bucatariu, S., Ascenzi, P. (2017) pH/thermo-responsive poly(N-isopropylacrylamide-co-maleic acid) hydrogel with a sensor and an actuator for biomedical applications. Polymer, 117, 177-186.

Garcia-Valdez, O., Champagne, P., Cunningham, M. F. (2018) Graft Modification of Natural Polysaccharides via Reversible Deactivation Radical Polymerization. Prog. Polym. Sci., 76, 151.

Gao, W. H.; Chen, K.F.; Yang, R. D.; Yang, F.; Han, W. J. (2011) properties of bacterial cellulose and its influence on the physical properties of paper. BioResources., 6(1), 144-153.

Ge, J., Sun, L., Zhang, F.R., Zhang, Y., Shi, L.A., Zhao, H.Y., Zhu, H.W., Jiang, H.L., Yu, S.H., (2016) A stretchable electronic fabric artificial skin with pressure-, lateral strain-, and flexion-sensitive properties. Adv Mater., 28(4):722–8.

George, D., Maheswari, P. U., Begum, K. M. M. S. (2019) Synergic formulation of onion peel quercetin loaded chitosan-cellulose hydrogel with green zinc oxide nanoparticles towards controlled release, biocompatibility, antimicrobial and anticancer activity. International Journal of Biological Macromolecules 132, 784–794.

Goldberg, M., Langer, R., Jia, X. (2007) Nanostructured materials for applications in drug delivery and tissue engineering. J Biomater Sci Polym Ed.,18(3), 241-68.

Gutierrez, A. M.; Dziubla, T. D.; Hilt, J. Z. (2017) Recent advances on iron oxide magnetic nanoparticles as sorbents of organic pollutants in water and wastewater treatment. Rev. Environ. Health, 32, 111.

Hahm, J. (2011) Functional Polymers in Protein Detection Platforms: Optical, Electrochemical, Electrical, Mass-Sensitive, and Magnetic Biosensors. Sensors, 11, 3327-3355.

Hasan, S., (2015) A Review on Nanoparticles: their synthesis and types. Research Journal of Recent Sciences, Vol. 4(ISC-2014), 1-3.

Hatir, P. C., Cayli, G. (2019) Environmentally friendly synthesis and photopolymerization of acrylated methyl ricinoleate for biomedical applications. J. Appl. Polym. Sci., 47969, 1.

Hernandez, N. L. P., Bahú, J. O., Schiavon, M. I. R. B., Bonon, A. J., Benites, C. I., Jardini, A. L., Filho, R. M., Maciel, M. R. W. W. (2019) Correction to: (Epoxidized castor oil – citric acid) copolyester as a candidate polymer for biomedical applications. J. Polym. Res., 26, 149.

Hsieh, C.T., Liao, C.Y., Dai, N.T., Tseng, C.S., Yen, B.L., Hsu, S.H. (2018) 3D printing of tubular scaffolds with elasticity and complex structure from multiple waterborne polyurethanes for tracheal tissue engineering. Appl Mater Today, 12:330–41.

Huang, G., Gao, J., Hu, Z., St. John, J. V., Ponder, B. C., Moro, D. (2004) Controlled drug release from hydrogel nanoparticle networks. J. Control. Release, 94, 303.

Huang, H. J., Tsai, Y. L., Lin, S. H., Hsu, S. (2019) Smart polymers for cell therapy and precision medicine. Journal of Biomedical Science, 26:73.

Isikci Koca, E., Evrensel, C., Cayli, G., Cakir Hatir, P. (2017) Effect of plant oil-based crosslinker on drug release behaviour of hydrogels. Electric Electronics, Computer Science, Biomedical Engineerings' Meeting (EBBT), Istanbul, Turkey, pp. 1-4.

Isikci Koca, E., Bozdag, G., Cayli, G., Kazan, D., Cakir Hatir, P. (2019) Thermoresponsive hydrogels based on renewable resources. Journal of Applied Polymer

Science, 137, 48861.

Işikver, Y., and Saraydin, D., (2019) Stimuli responsive hydrogels:nipam/aam/ carboxylic acid polymers. ACTA CHEMICA IASI., 27:2, 155-184.

Kim, Y. J., Matsunaga, Y. T. (2017) Thermo-responsive polymers and their application as smart biomaterials. Mater. Chem. B, 5, 4307.

Klouda, L. (2015) Thermoresponsive hydrogels in biomedical applications: a seven-year update. European Journal of Pharmaceutics and Biopharmaceutics, 97, 338-349.

Komatsu, S., Asoh, T. A., Ishihara, R., Kikuchi, A. (2019) Fabrication of thermoresponsive degradable hydrogel made by radical polymerization of 2-methylene-1,3-dioxepane: Unique thermal coacervation in hydrogel. Polymer 179, 121633.

Krakovský, I., Kouřilová, H., Hrubovský, M., Labuta, J., Hanyková, L. (2019) Thermoresponsive double network hydrogels composed of poly (Nisopropylacrylamide) and polyacrylamide. European Polymer Journal, 116, 415–424.

Kucinska-Lipka, J., Gubanska, I., Janik, H. Z. (2015) Bacterial cellulose in the field of wound healing and regenerative medicine of skin: recent trends and future prospectives. Polym. Bull., 72, 2399.

Kunduru, K. R., Basu, A., Z, M. H., Domb, A. J. (2015) Castor oil based biodegradable polyesters. Biomacromolecules, 16, 2572.

Labusca, L., Herea, D.D., Mashayekhi, K. (2018) Stem cells as delivery vehicles for regenerative medicine-challenges and perspectives. World J Stem Cells., 10(5):43–56.

Lancaster, M.A., Renner, M., Martin, C.A., Wenzel, D., Bicknell, L.S., Hurles, M.E., Homfray, T., Penninger, J.M., Jackson, A.P., Knoblich, J.A. (2013) Cerebral organoids model human brain development and microcephaly. Nature, 501(7467):373–9.

Lanzalaco, S., Armelin, E. (2017) Poly (N-isopropylacrylamide) and Copolymers: A Review on Recent Progresses in Biomedical Applications. Gels, 3(4): 36.

Li, W., Li, J., Gao, J., Li, B., Xia, Y., Meng, Y., Yu, Y., Chen, H., Dai, J., Wang, H., Guo, Y. (2011) The fine-tuning of thermosensitive and degradable polymer micelles for enhancing intracellular uptake and drug release in tumors. Biomaterials, 32, 3832-3844.

Li, G., Nandgaonkar, A. G., Habibi, Y., Krause, W. E., Wei, Q., Lucia, L. A. (2017) An

environmentally benign approach to achieving vectorial alignment and high microporosity in bacterial cellulose/chitosan scaffolds. RSC Adv., 7, 13678.

Lin, D.; Lopez-Sanchez, P.; Li, R.; Li, Z. (2014) Production of bacterial cellulose by Gluconacetobacter hansenii CGMCC 3917 using only waste beer yeast as nutrient source. Bioresour. Technol., 151, 113.

Liu, Y., Zhang, K., Ma, J., Vancso, G. J. (2017) Thermoresponsive semi-ipn hydrogel microfibers from continuous fluidic processing with high elasticity and fast actuation. ACS Applied Materials & Interfaces, 9(1):901–908.

Liu, M., Song, X., Wen, Y., Zhu, J. L., Li, J. (2017) Injectable Thermoresponsive Hydrogel Formed by Alginateg-Poly(N-isopropylacrylamide) Releasing Doxorubicin-Encapsulated Micelles as Smart Drug Delivery System. ACS Appl. Mater. Interfaces, 9 (41).

Lu, Y., Zhuk, A., Xi, L., Liang, X., Kharlampieva, E., Sukhishvili, S. A. (2013) Tunable pH and temperature response of weak polyelectrolyte brushes: role of hydrogen bonding and monomer hydrophobicity. Soft Matter, 9, 5464.

Luo, C.; Dong, Q.; Qian, M.; Zhang, H. (2016) Thermosensitive polymer-modified gold nanoparticles with sensitive fluorescent properties. Chem. Phys. Lett., 664, 89.

Luo, MT., Li, H L., Huang,C., Zhang, HR., Xiong, L., Chen, SF., Chen, XD. (2018) Cellulose-Based Absorbent Production from Bacterial Cellulose and Acrylic Acid: Synthesis and Performance. Polymers, 10, 702.

Materska, M. (2008) Quercetin and its derivatives: chemical structure and bioactivity – a review. Pol. J. Food Nutr. Sci., 58(4): 407-413.

Mathew, A., Kurmvanshi, S., Mohanty, S., Nayak, S. K. (2018) Sustainable production of polyurethane from castor oil, functionalized with epoxy- and hydroxyl-terminated poly(dimethyl siloxane) for biomedical applications. J. Mater. Sci. Biomaterials., 53(5), 3119.

Montgomery, M., Ahadian, S., Davenport, H.L., Lo, R.M., Civitarese, R.A., Vanderlaan, R.D., Wu, J., Reis, L.A., Momen, A., Akbari, S., Pahnke, A., Li, R.K., Caldarone, C.A., Radisic, M. (2017) Flexible shape-memory scaffold for minimally invasive delivery of functional tissues. Nat Mater., 16(10):1038–46.

Nada, A. A., Arul, M. R., Ramos, D. M., Kroneková, Z., Mosnáček, J., Rudraiah, S., Kumbar, S. G. (2018) Bioactive polymeric formulations for wound healing. Polym Adv Technol., 29:6, 1815-1825.

Neto, F. N. M., Fialho, A. C. V., Moura, W. L., Rosa, A. G. F., Matos, J. M. E., Reis, F. S., Mendes, M. T. A., Sales, E. S. D. (2019) Castor polyurethane used as osteosynthesis plates:microstructural and thermal analysis. Polímeros., 29-2.

Odian, G. (2004) Principles of polymerization. Fourth Edition, A JOHN WILEY & SONS, INC., PUBLICATION.

Onaciu, A., Munteanu, R. A., Moldovan, A. I., Moldovan, C. S., and Neagoe, I. B. (2019) Hydrogels based drug delivery synthesis, characterization and administration. Pharmaceutics, 11:432.

Pabuccuoğlu, S. K. POLİMER KİMYASI -4. https://docplayer.biz.tr/45013582-Polimer-kimyasi-4-prof-dr-saadet-k-pabuccuoglu.html. 28.04.2020

Pa'e, N., Salehudin, M. H., Hassan, N. D., Marsin, A. M., Muhamad, I. I. (2018) Thermal Behavior of Bacterial Cellulose Based Hydrogels with Other Composites and Related Instrumental Analysis. Polymers and Polymeric Composites: A Reference Series; Springer International Publishing AG: New York City; Vol. 25.

Pakade, V. E., Molefe, E. D., Tavengwa, N. T. (2017) Quantitative determination of trace concentrations of quercetin from prickly pear skin complex sample extracts by application of molecularly imprinted polymers. Journal of Environmental Chemical Engineering, 5, 1186-1195.

Park, J. H., Jang, J. W., Sim, J. H., Kim, I. J., Lee, D. J., Lee, Y. H., Park, S. H., and Kim, H. D. Hindawi (2019) Preparation and properties of thermoresponsive p(n-isopropylacrylamide-co-butylacrylate) hydrogel materials for smart windows. INT J POLYM SCI., 3824207, 7.

Pattanashetti, N. A., Heggannavar, G. B., Kariduraganavar, M. Y. (2017) Smart Biopolymers and Their Biomedical Applications. Procedia Manufacturing, 12, 263 – 279.

Pavun, L., Đurđević, P., Jelikić-Stankov, M., Đikanović, D., Ćirić, A., Uskoković-Marković, S. (2014) Spectrofluorimetric determination of quercetin in pharmaceutical

dosage forms. Macedonian Journal of Chemistry and Chemical Engineering, Vol. 33, No. 2, pp. 209–215.

Peng, B.Y., Dubey, N.K., Mishra, V.K., Tsai, F.C., Dubey, R., Deng, W.P., Wei, H.J., (2018) Addressing stem cell therapeutic approaches in pathobiology of diabetes and its complications. J Diabetes Res., 2018:7806435.

Petrusic, S., Jovancic, P., Lewandowski, M., Giraud, S., Grujic, S., Ostojic, S., Bugarski, B., Koncar, V. (2013) Synthesis, characterization and drug release properties of thermosensitive poly(N-isopropylacrylamide) microgels. J. Mater. Sci., 48, 7935.

Polymers, Classification of Polymers, https://www.toppr.com/guides/chemistry/polymers/classification-of-polymers/ 28.04.2020

Polymers - Types, Classification, Properties, and Uses of Polymers, https://byjus.com/jee/polymers/ 28.04.2020

Polymer Properties Database, https://polymerdatabase.com/polymer%20chemistry/radical%20mechanism.html 25.03.2020

Pool, H., Quintanar, D., Figueroa, J. D., Mano, C. M., Bechara, J. E. H., God´ınez, L. A., Mendoza, S. (2012) Antioxidant Effects of Quercetin and Catechin Encapsulated into PLGA Nanoparticles. Journal of Nanomaterials, 12 pp.

Prior, L. R. (2003) Fruits and vegetables in the prevention of cellular oxidative damage. Am J Clin Nutr., 78(suppl):570–8.

Ramelow, U. A., Pingili, S. (2010) Synthesis of ethylene glycol dimethacrylate-methyl methacrylate copolymers, determination of their reactivity ratios, and a study of dopant and temperature effects on their conductivities. Polymers, 2, 265-285.

Razmara, R. S., Daneshfar, A., Sahraei, R. (2010) Solubility of quercetin in water + methanol and water + ethanol from (292.8 to 333.8) K. J. Chem. Eng. Data, 55, 3934-3936.

Roy, S. G., Banerjee, S., De, P. (2016) Cationic Polymerization of Nonpolar Vinyl Monomers for Producing High Performance Polymers. Reference Module in Materials

Science and Materials Engineering.

Su, J., Yang, Y., Chen, Z., Zhou, J., Liu, X., Fang, Y., Cui, Y. (2019) Preparation and performance of thermosensitive poly(N-isopropylacrylamide) hydrogels by frontal photopolymerization. Polym Int, 68:10, 1673-1680.

Qureshi, D., Nayak, S. K., Maji, S., Anis, A., Kim, D., and Pal, K. (2019) Environment sensitive hydrogels for drug delivery applications. European Polymer Journal, 120: 109220.

Salmiah, I., Azizan, A., Nor, S. M. (2015) Synthesis and characterization of castor oil based polyurethane for potential application as host in polymer electrolytes. Bull. Mater. Sci., 38 (5), 1155.

Salmiah, I., Azizan, A., Nor, S. M. (2015) Characterization of Novel Castor Oil-Based Polyurethane Polymer Electrolytes. Polymers, 7, 747.

Schulz, D. N., Patil, A. O. (1998) Functional Polymers: An Overview, ACS Symposium Series; American Chemical Society: Washington, DC.

Singh, D., Wang, S.B., Xia, T., Tainsh, L., Ghiassi-Nejad, M., Xu, T., Peng, S., Adelman, R.A., Rizzolo, L.J. (2018) A biodegradable scaffold enhances differentiation of embryonic stem cells into a thick sheet of retinal cells. Biomaterials, 154:158–68.

Singh, A., Elisseeff, J. (2010) Biomaterials for stem cell differentiation. J Mater Chem., 20(40):8832–47.

Sponchioni, M., Palmiero, U. C., Moscatelli, D. (2019) Thermo-responsive polymers: Applications of smart materials in drug delivery and tissue engineering. Materials Science & Engineering C, 102, 589–605.

Tan, A. C. W., Polo-Cambronell, B. J., Provaggi, E., Ardila-Suârez, C., Ramirez-Caballero, G. E., Baldovino-Medrano, V. G., Kalaskar, D. M. (2017) Design and development of low cost polyurethane biopolymer based on castor oil and glycerol for biomedical applications. Biopolymers., 109(2), 23078.

Tang, S., Bhandari, R., Delaney, S. P., Munson, E. J., Dziubla, T. D., Hilt, J. Z. (2017) Synthesis and characterization of thermally responsive N-isopropylacrylamide hydrogels copolymerized with novel hydrophobic polyphenolic crosslinkers. Materials

Today Communications, Volume 10, Pages 46-53.

Tang, S., Floy, M., Bhandari, R., Sunkara, M., Morris, A. J., Dziubla, T. D., Hilt, J. Z. (2017) Synthesis and Characterization of Thermoresponsive Hydrogels Based on N-Isopropylacrylamide Crosslinked with 4,4'-Dihydroxybiphenyl Diacrylate. ACS Omega, 2, 8723.

Uscátegui, Y. L., Díaz, L. E., Valero, M. F. (2019) In vitro and in vivo biocompatibility of polyurethanes synthesized with castor oil polyols for biomedical devices. J. Mater. Res., 34(4), 519.

Uscátegui, Y. L., Díaz, L. E., Gómez-Tejedor, J. A., Vallés-Lluch, A., Vilariño-Feltrer, G., Serrano, M. A., Valero, M. F. (2019) Candidate Polyurethanes Based on Castor Oil (Ricinus communis), with Polycaprolactone Diol and Chitosan Additions, for Use in Biomedical Applications. Molecules, 24, 237.

Vihola, H., Laukkanen, A., Valtola, L., Tenhu, H., Hirvonen, J. (2005) Cytotoxicity of thermosensitive polymers poly (N-isopropylacrylamide), poly (N-vinylcaprolactam) and amphiphilically modified poly (N-vinylcaprolactam). Biomaterials, 26(16), 3055-3064.

Wang, J., Zhao, X. H. (2016) Degradation kinetics of fisetin and quercetin in solutions

affected by medium pH, temperature and co-existing proteins. J. Serb. Chem. Soc. 81 (3) 243–253.

Wang, L.; Lian, W.; Yao, H.; Liu, H. (2015) Multiple-Stimuli Responsive Bioelectrocatalysis Based on Reduced Graphene Oxide/Poly(N-isopropylacrylamide) Composite Films and its Application in the Fabrication of Logic Gates. ACS Appl. Mater. Interfaces., 7, 5168.

Wang, M., Guo, L., Sun, H. (2018) Manufacturing Technologies for Biomaterials. The University of Hong Kong, Pokfulam, Hong Kong.

Wang, Y., Yang, Nç, Wang, D., He, Y., Chen, Li., Zhao, Y. (2018) Poly (MAH-β-cyclodextrin-co-NIPAAm) hydrogels with drug hosting and thermo/pH-sensitive for controlled drug release. Polymer Degradation and Stability, 147, 123–131.

Wang, Q., Asoh, T. A., Uyama, H. (2018) Rapid uniaxial actuation of layered bacterial cellulose/poly (N-isopropylacrylamide) composite hydrogel with high mechanical

strength. RSC Adv., 8, 12608.

Wang, X., Xu, K., Yao, H., Chang, L., Wang, Y., Li, W., Zhao, Y., Qin, J. (2018) Temperature-Regulated Aggregation-Induced Emissive Self-Healable Hydrogel for Controlled Drug Delivery. Polymer Chemistry, 9 (38).

Ward, M. A., Georgiou, T. K. (2011) Thermoresponsive polymers for biomedical applications. Polymers, 3, 1215-1242.

Wilems, T. S., Lu, X., Kurosu, Y., Kahn, Z., Lim, H. J., Callahan, L. A. S. (2017) Effects of free radical initiators on polyethylene glycol dimethacrylate hydrogel properties and biocompatibility. Journal of Biomedical Materials Research Part A 105 (11).

Wong, C. S.; Badri, K. H. (2012) Chemical Analyses of Palm Kernel Oil-Based Polyurethane Prepolymer. Materials Sciences and Applications (MSA)., 3, 78-86.

Xu, G., Li, B., Wang, T., Wan, J., Zhang, Y., Huang, J., Shen, Y. (2018) Enhancing the anti-ovarian cancer activity of quercetin using a self-assembling micelle and thermosensitive hydrogel drug delivery system. RSC Adv., 8, 21229.

Zarrintaj, P., Urbanska, A., Gholizadeh, S. S., Goodarzi, V., Saeb, M. R., Mozafari, M. (2018) A facile route to the synthesis of anilinic electroactive colloidal hydrogels for neural tissue engineering applications. Journal of Colloid and Interface Science, 516.

Zhang, Y., Fu, C., Li, Y., Wang, K., Wang, X., Wei, Y., Tao, L. (2016) Synthesis of an injectable, self-healable and dual responsive hydrogel for drug delivery and 3d cell cultivation. Polymer Chemistry, 8 (3).

Zhao, F., Yao, D., Guo, R., Deng, L., Dong, A., Zhang, J. (2015) Nanomater. (Basel, Switzerland). Composites of polymer hydrogels and nanoparticulate systems for biomedical and pharmaceutical applications, 5, 2054.

CURRICULUM VITAE

Address	Beylikdüzü / ISTANBUL
GSM	(+90) 506 939 0319
E-mail	elif.isikci@gmail.com

Personal Information

Sex	Female
Date of Birth	18/11/1989
Marital Status	Married
Nationality	Turkish
Driving License	B

Education

- **Doctorate** — **Marmara University – Istanbul/Turkey**
  Department of Bioengineering – 2014 – …
  (thesis subject : Smart Polymer Nanostructures from Renewable Resources for Biomedical Applications)

- **Postgraduate** — **Ege University – Izmir/Turkey**
  Department of Bioengineering – 2012 – 2014
  (thesis subject : Developing New *Bacillus* Formulations For Control of Mosquitos)

- **University** — **Ege University – Izmir/Turkey**
  Department of Bioengineering – 2008 – 2012
  (thesis subject : Production of Cholesterol Lowering Agents from Fungal Microorganisms)

- **High School** — **Gonen Anatolian High School**
  Gonen- Balıkesir/Turkey 2003 – 2007

Work Experience

- **03/2014 – Working** — **Istanbul Arel University / Istanbul**
  Research Asistant

Faculty of Engineering and Architecture, Department of Biomedical Engineering

Publications

- **Isikci Koca, E**., Bozdag, G., Cayli, G., Kazan, D., and Cakir Hatir, P., 2020 "Thermoresponsive hydrogels based on renewable resources", *Journal of Applied Polymer Science*, 137:28, 48861. *DOI: 10.1002/app.48861*.

- Goksel Duru, D, **Isikci Koca, E**., 2019. Assessment of Electrophysiological Findings during Mental Workload in the Effect of Physical Performance, *Academic Platform Journal of Engineering and Science*, 7:3-389-397 pp.

Projects

- ERANET-"Nanofabricated Nanocomposite Nanobioactive and Nanofunctional replacements of tympanic membrane as advanced drug delivery and regenerative platforms", "EUROPEAN INNOVATIVE RESEARCH & TECHNOLOGICAL DEVELOPMENT PROJECTS IN NANOMEDICINE" (EURONANOMED III), Bursiyer, (01.04.2018-continues).
- MARMARA BAP-"Smart Polymer Nanostructures from Renewable Resources for Biomedical Applications", Marmara University Project No. FEN-C-DRP-170118-0011, Araştırmacı, (17.01.2018-continues).

Symposiums

- 2nd Eurasia Biochemical Approaches & Technologies (2. EBAT) Congress, 26-29 October 2019, Antalya/TURKEY – (Oral presentation) – "Investigation of Biocompatibility of Castor Oil and Bacterial Cellulose Based Thermoresponsive Hydrogels".
- 2ND INTERNATIONAL EURASIAN CONFERENCE ON BIOLOGICAL AND CHEMICAL SCIENCES (EURASIANBIOCHEM 2019) 28-29 th June, 2019 Ankara/TURKEY – (Oral presentation) – "Synthesis and Characterization of Castor Oil and Bacterial Cellulose based Thermoresponsive Hydrogels**".**
- Medical Technologies Congress, TIPTEKNO'17 12-14 th October 2017, Trabzon/TURKEY – (Oral presentation) – " Relationship between Mental Workload and Photoplethysmography in the Effect of Physical Performance"
- The Scientific Meeting on Electrical-Electronics & Biomedical Engineering and Computer Science in 2017 (EBBT'2017) 20-21 th April 2017, Istanbul/TURKEY – (Oral presentation) – "Comparative Multiple Sclerosis Lesion Segmentation in Magnetic Resonance Images".
- The Scientific Meeting on Electrical-Electronics & Biomedical Engineering and Computer Science in 2017 (EBBT'2017) 20-21 th April 2017, Istanbul/TURKEY – (Oral presentation) – "Effect of Plant Oil-Based Crosslinker on Drug Release Behaviour of Hydrogels".
- The Scientific Meeting on Electrical-Electronics & Biomedical Engineering and Computer Science in 2016 (EBBT'2017) 26-27 th April 2016, Istanbul/TURKEY – (Oral presentation) – " Analysis of the Relationship Between Maximum Volume of Oxygen Consumption and Electrophysiological Measurements".
- The Scientific Meeting on Electrical-Electronics & Biomedical Engineering and Computer Science in 2016 (EBBT'2017) 26-27 th April 2016, Istanbul/TURKEY – (Oral presentation) – "Synthesis of Thermoresponsive Hydrogel for Controlled Release of Quercetin".
- Medical Technologies Congress, TIPTEKNO'15 15-18 th October 2015, Bodrum/TURKEY – (Oral presentation)-" Extraction of Multiple Sclerosis Lesions in MR Images Based onActive Contours".